NASA TN D-1518

TECHNICAL NOTE

D-1518

LONGITUDINAL AERODYNAMIC CHARACTERISTICS AT MACH NUMBERS FROM 0.40 TO 1.10 OF A BLUNTED RIGHT-TRIANGULAR PYRAMIDAL LIFTING REENTRY CONFIGURATION EMPLOYING VARIABLE-SWEEP WING PANELS

By Bernard Spencer, Jr.

Langley Research Center
Langley Station, Hampton, Va.

NATIONAL AERONAUTICS AND SPACE ADMINISTRATION
WASHINGTON
March 1963

Cadet

SINGLE COPY ONLY

NATIONAL AERONAUTICS AND SPACE ADMINISTRATION

TECHNICAL NOTE D-1518

LONGITUDINAL AERODYNAMIC CHARACTERISTICS AT MACH NUMBERS FROM 0.40 TO 1.10 OF A BLUNTED RIGHT-TRIANGULAR PYRAMIDAL LIFTING REENTRY CONFIGURATION EMPLOYING VARIABLE-SWEEP WING PANELS

By Bernard Spencer, Jr.

SUMMARY

An investigation has been conducted in the Langley 7- by 10-foot transonic tunnel at Mach numbers from 0.40 to 1.10 on a right-triangular pyramidal-type reentry configuration employing variable wing sweep as a means of increasing lift and lift-drag ratio at subsonic speeds. Various means of longitudinal control were also tested in conjunction with the range of wing-panel sweep at a Mach number of 0.40.

The results indicated that reducing the sweep of the wing panels from 80° to 0° at a Mach number of 0.40 increased the maximum lift-drag ratio of the basic configuration from 2.55 to 5.65 and increased the lift-curve slope from 0.0195 to 0.0565 with little or no change in the low-lift stability level for the configuration with all controls off.

The configuration having 30° or 40° sweep, however, provided the highest lift coefficient for the maximum angle-of-attack range of the investigation. Wing-panel leading-edge sweep angles below 30° indicated stalling and rapid losses in lift coefficient occurring at moderate angles of attack.

Comparison of the longitudinal control characteristics of a high and low horizontal tail and a trailing-edge flap control indicated the highest values of control effectiveness for the high-positioned horizontal tail. Use of the trailing-edge flap control provided trim conditions throughout the angle-of-attack range.

INTRODUCTION

Configurations designed for atmospheric reentry or cruise at hypersonic speeds with capability of low-speed landings, by virtue of their basic design requirements, present poor performance characteristics in the landing phase of flight. Since aerodynamic heating during reentry is of prime importance, the

configurations are designed from hypersonic aerodynamic considerations with the result that the landing configurations have both low lift coefficients and low lift-drag ratios.

One such configuration representing good qualities from aerodynamic heating considerations is a highly swept right triangular pyramid with a conical ridge line. (See ref. 1.) This type of configuration has shown satisfactory longitudinal and lateral stability characteristics from hypersonic to low subsonic speeds. (See refs. 2 to 9.) Low values of lift and maximum lift-drag ratio at subsonic speeds indicate high landing velocities and high sinking rates may be expected. However, because of the body planform of these pyramid-type configurations, the use of variable-sweep wing panels to improve subsonic lift and lift-drag ratios appears promising, since these wing panels could be well shielded during the reentry phase of flight on the upper surface of the configuration and deployed at subsonic speeds. The use of variable sweep has been shown to increase greatly both maximum lift and lift-drag ratios at subsonic speeds on various supersonic design configurations without large changes in longitudinal stability level with changes in wing-panel sweep. (See ref. 10.)

The purpose of the present investigation was to provide information at subsonic and transonic speeds on the use of variable wing sweep on the right-triangular-pyramid lifting reentry configuration previously mentioned.

Various types of longitudinal controls were also tested at the low Mach numbers in conjunction with the various wing-panel sweep positions. These controls included low- and high-position horizontal-tail controls, deployable from the underside of the model, and an extendible trailing-edge flap, located at the upper edge of the model base.

SYMBOLS

All data presented herein are referenced to the wind-axis system, and all coefficients are nondimensionalized with respect to the projected planform area and ridge line length of the configuration with wing panels folded 80°. The moment reference point was located 9.50 inches ahead of the model base, as presented in reference 8. Symbols used in this paper are defined as follows:

A aspect ratio, b^2/S

b configuration span when wing panels are folded and $\Lambda_{LE} = 80°$, in.

C_D drag coefficient, $\frac{\text{Drag}}{qS}$

C_L lift coefficient, $\frac{\text{Lift}}{qS}$

C_{L_α} lift-curve slope, per deg

C_m pitching-moment coefficient, $\frac{\text{Pitching moment}}{qSc}$

C_{m_Δ} control effectiveness parameter, $\frac{(C_m \text{ at } i_t \text{ or } \delta_f = n) - (C_m \text{ at } i_t \text{ or } \delta_f = 0^o)}{n}$

$\partial C_m/\partial C_L$ longitudinal stability parameter

c model ridge line, in.

i_t horizontal-tail deflection (positive when trailing edge is down) referenced to body upper surface, deg

L/D lift-drag ratio

$(L/D)_{max}$ maximum untrimmed lift-drag ratio

M Mach number

n integer

q dynamic pressure, lb/sq in.

S reference area, sq in.

X,Y wing panel coordinates

α angle of attack of model upper surface, deg

Γ_h drag flap (positive for outer edge moving forward) referenced to plane of model base, deg

δ_f trailing-edge flap deflection (positive when trailing edge is down) referenced to body upper surface, deg

Λ_{LE} wing-panel leading-edge sweep, deg

Subscripts:

max maximum

trim trimmed condition

MODEL

The basic configuration of the present investigation was considered as the configuration having wing panels folded 80°. Geometric characteristics of this

model were nearly identical to that of reference 8 and are presented in figure 1. Photographs of the model mounted in the Langley 7- by 10-foot transonic tunnel with the wing panels at 80°, 40°, and 20° sweep are presented in figures 2(a), 2(b), and 2(c), respectively.

Geometry of the swept-wing panels are presented in figure 1(a). Longitudinal and vertical ordinates were measured along the wing-panel reference chord. This panel was constructed in such a way that the leading-edge radius was the same as the leading-edge radius of the basic model and provided a continuous leading edge when the wing panels are completely retracted ($\Lambda_{LE} = 80°$). The airfoil section of the wing panel is constant across the span and the ordinates are presented in the table of figure 1(a).

Geometric characteristics of the longitudinal controls are presented in figure 1(b). The horizontal tails were 0.125-inch flat plates and were mounted 0.98 inch (high tail) below the body upper surface and 2.58 inches (low tail) below the body upper surface. Both tails at 0° incidence were parallel with the body upper surface. These tails were considered as retractable-type controls which could be deployed from the underside of the body. The trailing-edge flap was also 0.125-inch flat plate and was mounted on the upper surface. The drag flaps were located on the model base; the deflections being referenced to the model base. These flaps were also 0.125-inch flat plates.

TESTS AND CORRECTIONS

The present investigation was conducted in the Langley 7- by 10-foot transonic wind tunnel at Mach numbers from 0.40 to 1.10 corresponding to a range of average test Reynolds numbers, based on the basic-model reference chord from 5.04×10^6 to 12.60×10^6. The model was sting supported and forces and moments were measured by use of a six-component internally mounted strain-gage balance. The model was tested through an angle-of-attack range from -1° to approximately 25° at zero sideslip angle.

Corrections to the angle of attack due to sting and balance bending under load have been applied to the data. No corrections for base pressure have been applied to the data, since the configuration was considered as a gliding, unpowered vehicle. Representative base-pressure coefficient variation with angle of attack and Mach number may be obtained from reference 8 on an identical model.

PRESENTATION OF RESULTS

The basic data for configurations investigated are presented in the following figures:

DISCUSSION

Basic longitudinal aerodynamic characteristics of the various combinations of longitudinal controls and wing-panel sweeps are presented in figures 3 to 18 and a summary of the lift-drag characteristics, longitudinal aerodynamic parameters, and control characteristics is presented in figures 19 to 24. Most of the discussion is confined to these summary figures except for pertinent observations to be noted from the basic data.

Extending the wing panels from the 80° fully retracted position to 0° leading-edge sweep results in large increases in lift coefficient throughout the angle-of-attack range, the maximum C_L occurring for the configuration having $\Lambda_{LE} = 40^\circ$ (M = 0.40). (See fig. 3(a).) A lift coefficient of approximately 1.24

at the maximum angle of attack was realized from the configuration having the wing panel swept back 30° to 40°; this result indicated an increase in lift coefficient of 0.46 compared with the fully retracted wing-panel configuration. Lift-coefficient changes from 0.07 for the 80° sweptback wing to 0.33 for the 0° sweep configuration at $\alpha = 0°$ are also realized because of the camber of the variable-sweep panel; however, rapid losses in C_L were noted for wing-panel sweeps below 40° at moderate angles of attack. Large reductions in drag due to lift with little effect on minimum drag due to reduction of the sweep of the wing panels are also noted at a Mach number of 0.40.

Effects of Wing-Panel Sweep on Lift-Drag Ratio

For the configuration with all controls retracted, the variation of lift-drag ratio with increasing lift coefficient at various subsonic Mach numbers is presented as figure 19. An increase in $(L/D)_{max}$ from approximately 2.55 at a C_L of 0.35 to 5.65 at a C_L of 0.50 is noted in reducing the sweep of the wing panel from 80° to 0° at the lowest Mach number (M = 0.40). Increasing the Mach number from 0.40 to 0.60 results in losses in $(L/D)_{max}$ for the 0° sweep condition below the $(L/D)_{max}$ realized from the 20° sweep configuration. Summary of the effects of increasing Mach number on the configurations at various wing-panel sweeps (fig. 20) indicate rapid losses in $(L/D)_{max}$ for the low and moderate sweep configurations as the Mach number is increased beyond the critical Mach number of the relatively thick wing. The loss in $(L/D)_{max}$ with increasing Mach number is accompanied by losses in C_{L_α} and losses of stability in the low-lift range. Comparison of the low-lift stability level for the 0° and 80° sweep configurations indicates an increase from approximately -0.015 ($\Lambda_{LE} = 0°$; M = 0.40) to approximately -0.04 ($\Lambda_{LE} = 80°$; M = 1.10). Reducing the sweep of the wing panels from 80° to 0° at low subsonic speeds therefore provides large increases in $(L/D)_{max}$ and C_{L_α} with only a slight reduction in stability level relative to the 80° sweep M = 1.10 configuration.

Although the highest values of lift coefficient occur for the configurations having $\Lambda_{LE} = 40°$ (M = 0.40), the configuration having $\Lambda_{LE} = 0°$ would be a more desirable configuration from the standpoint of change in stability level between the high Mach number (M = 1.2), 80° sweptback configuration and the low-speed (M = 0.40), wing-panel-extended configuration. Improvements in maximum lift coefficient for the low sweep $\Lambda_{LE} = 0°$ configuration may be possible by use of wing leading-edge flaps or alterations in airfoil section. Data for the basic configuration ($\Lambda_{LE} = 80°$) at M = 1.20 were obtained from reference 8.

Characteristics of Various Longitudinal Controls at Low Mach Number

Longitudinal aerodynamic characteristics at a Mach number of 0.40 for the high horizontal tail, low horizontal tail, and trailing-edge flap control for various wing-panel sweeps are presented in figures 4, 5, and 6, respectively.

Control characteristics noted for the three types of longitudinal controls are summarized in figures 16, 17, and 18 for wing-panel sweeps of 80°, 40°, and 0°, respectively. The addition of the high horizontal tail to the configurations is seen to increase the lift at the maximum angle of attack tested and to increase the angle of attack at which loss of lift occurs for the lower wing-panel sweep configurations. (See fig. 6.) Slight increases in stability level and more linear variations of pitching-moment coefficient with increasing lift coefficient are also noted from addition of the high horizontal tail for the range of wing-panel sweep. (See fig. 18.) Addition of the low horizontal tail to the configuration (figs. 5 and 18) indicated similar results with regard to linearizing the pitching-moment variations with lift coefficient for the range of wing-panel sweeps. However, only slight increases in lift coefficient at the maximum angle of attack were realized by addition of the low horizontal tail. The addition of the trailing-edge flap control to the basic configurations had little or no effect on the overall longitudinal aerodynamic characteristics for the various wing-panel sweeps presented. (See figs. 6 and 18.)

The variation of L/D with C_L for each of the longitudinal controls employed for various wing-panel sweeps is presented in figures 21 and 22, the effects of the addition of the longitudinal controls on $(L/D)_{max}$ for the range of wing-panel sweeps being presented in figure 24. The addition of the high horizontal tail provided slight increases in $(L/D)_{max}$ for the configuration having the wing panel in either the low (Λ_{LE} = 0° to 20°) or high (Λ_{LE} = 60° to 80°) sweep range, reductions in $(L/D)_{max}$ being noted for the intermediate sweep positions, whereas the addition of the low horizontal tail reduced $(L/D)_{max}$ for the range of sweeps except for the fully retracted wing (Λ_{LE} = 80°). The addition of the trailing-edge flap control also indicated slight reductions in $(L/D)_{max}$ throughout the range of wing-panel sweep.

Longitudinal trim characteristics associated with deflection of the high and low horizontal tails and trailing-edge flap control are presented in figures 7 to 14. Comparison of the trim characteristics for high and low horizontal tails for various wing-panel sweeps indicate higher trim lift coefficients for a given deflection of -10° on the low horizontal tails, primarily because of the larger increase in low-lift stability level noted from addition of the high horizontal tail. (See figs. 7 to 11.) The higher horizontal tail however gives higher values of control effectiveness C_{m_Δ} throughout the range of wing-panel sweep. (See fig. 23.) Deflection of the trailing-edge flap control provided trim conditions to the maximum lift obtained for both the 80° and 0° wing-panel sweep conditions. (See figs. 12 and 14.) Considerably lower values of control effectiveness are noted from deflection of the trailing-edge control as compared with either the high or low horizontal tail for the range of wing-panel sweeps. (See fig. 23.) Variations in $(L/D)_{trim}$, $C_{L_{trim}}$, and α_{trim} with increasing wing-panel sweep and for constant control deflection are presented in figure 23 for the high and low horizontal tails and trailing-edge flap control. The large reductions in $C_{L_{trim}}$ and α_{trim} occurring in the moderate sweep range (Λ_{LE} = 20° to Λ_{LE} = 60°) for each control may be attributed to the large increases in low-lift stability level noted for the intermediate wing-panel sweeps. (See also fig. 24.)

Longitudinal aerodynamic characteristics associated with deployment of a drag flap from the base of the model as a braking device with the wing panel folded ($\Lambda_{LE} = 80^\circ$) are presented in figure 15; the effects of drag flap deflection on L/D are presented in figure 22. Deflection of this device from the streamwise position ($\Gamma_h = 0^\circ$) indicates large increases in drag coefficient and slight increases in lift coefficient while producing relatively large displacement in nose-down pitching moment. This device apparently has little value unless employed in combination with an additional control to provide trim conditions. Large reductions in $(L/D)_{max}$ are noted from high deflection of this surface (fig. 22) in the low and moderate lift-coefficient range, only slight reductions being noted for low deflection of this flap.

The variation of the longitudinal aerodynamic parameters C_{L_α}, $(L/D)_{max}$, and $\partial C_m/\partial C_L$ with increasing wing-panel sweep are presented in figure 24 for various configurations tested at a Mach number of 0.40. As previously noted for the configurations with controls off, decreasing the wing-panel sweep from 80° to 0° indicates increases in C_{L_α} from approximately 0.0195 to 0.0565, increases in $(L/D)_{max}$ from 2.55 to approximately 5.65, and little or no change in low-lift longitudinal stability level between the 80° and 0° wing-panel sweep position. Addition of the trailing-edge flap control at 0° deflection provided little or no effect on $\partial C_m/\partial C_L$, and only a slight reduction in C_{L_α} in the moderate wing-panel sweep range ($\Lambda_{LE} = 50^\circ$ to $\Lambda_{LE} = 20^\circ$). Addition of either the high or low horizontal tails generally provided slight increases in C_{L_α} throughout the range of sweep. Large increases in low-lift longitudinal stability level for the 80° sweep condition are noted from addition of either the low or high horizontal tail; thereby, the favorable effect of little change in longitudinal stability level between the 0° and 80° sweep positions noted for the configuration without control on or with trailing-edge flap control was reduced.

CONCLUDING REMARKS

An investigation has been conducted in the Langley 7- by 10-foot transonic tunnel at Mach numbers from 0.40 to 1.10 on a right-triangular pyramidal-type reentry configuration employing variable wing sweep as a means of increasing lift and lift-drag ratio at subsonic speeds. Various means of longitudinal control were also tested in conjunction with the range of wing-panel sweep at a Mach number of 0.40.

The results indicated that reducing the sweep of the wing panels from 80° to 0° at a Mach number of 0.40 increased the maximum lift-drag ratio of the basic configuration from 2.55 to 5.65 and increased the lift-curve slope from 0.0195 to 0.0565 with little or no change in the low-lift stability level for the configuration with all controls off.

The configuration having 30° or 40° sweep, however, provided the highest lift coefficient for the maximum angle-of-attack range of the investigation. Wing-panel

leading-edge sweep angles below 30° indicated stalling and rapid losses in lift coefficient occurring at moderate angles of attack.

Comparison of the longitudinal control characteristics of a high and low horizontal tail and a trailing-edge flap control indicated the highest values of control effectiveness for the high-positioned horizontal tail. Use of the trailing-edge flap control provided trim conditions throughout the angle-of-attack range investigated.

Langley Research Center,
National Aeronautics and Space Administration,
Langley Station, Hampton, Va., September 17, 1962.

REFERENCES

1. Cooper, Morton, and Stainback, P. Calvin: Influence of Large Positive Dihedral on Heat Transfer to Leading Edges of Highly Swept Wings at Very High Mach Numbers. NASA MEMO 3-7-59L, 1959.

2. Paulson, John W.: Low-Speed Static Stability and Control Characteristics of a Model of a Right Triangular Pyramid Reentry Configuration. NASA MEMO 4-11-59L, 1959.

3. Cooper, Morton, and Gunn, Charles R.: Pressure Measurements on a Hypersonic Glide Configuration Having 79.5° Sweepback and 45° Dihedral at a Mach Number of 4.95. NASA TM X-223, 1959.

4. Mayo, Edward E.: Static Longitudinal Stability Characteristics of a Blunted Glider Reentry Configuration Having 79.5° Sweepback and 45° Dihedral at a Mach Number of 6.2 and Angles of Attack up to 20°. NASA TM X-222, 1959.

5. Whitcomb, Charles F., and Foss, Willard E., Jr.: Static Stability and Control Characteristics of Two Large-Dihedral Right Triangular Pyramid Lifting Reentry Configurations at a Mach Number of 3.05. NASA TM X-295, 1960.

6. Ware, George M.: Low-Subsonic-Speed Static Stability of Right-Triangular-Pyramid and Half-Cone Lifting Reentry Configurations. NASA TN D-646, 1961.

7. Olstad, Walter B., Mugler, John P., Jr., and Cahn, Maurice S.: Static Longitudinal and Lateral Stability Characteristics of a Right Triangular Pyramidal Lifting Reentry Configuration at Transonic Speeds. NASA TN D-655, 1961.

8. Mugler, John P., Jr., and Olstad, Walter B.: Static Longitudinal Aerodynamic Characteristics at Transonic Speeds of a Blunted Right Triangular Pyramidal Lifting Reentry Configuration for Angles of Attack up to 110°. NASA TN D-797, 1961.

9. Wornom, Dewey E., and Olstad, Walter B.: Static Longitudinal Aerodynamic Characteristics of a Right Triangular Pyramidal Lifting Reentry Configuration at Mach Numbers of 3.00, 4.50, and 6.00 for Angles of Attack up to 56°. NASA TM X-675, 1962.

10. Polhamus, Edward C., and Hammond, Alexander D.: Aerodynamic Research Relative to Variable-Sweep Multimission Aircraft. Ch. II of Compilation of Papers Summarizing Some Recent NASA Research on Manned Military Aircraft. NASA TM X-420, 1960, pp. 13-38.

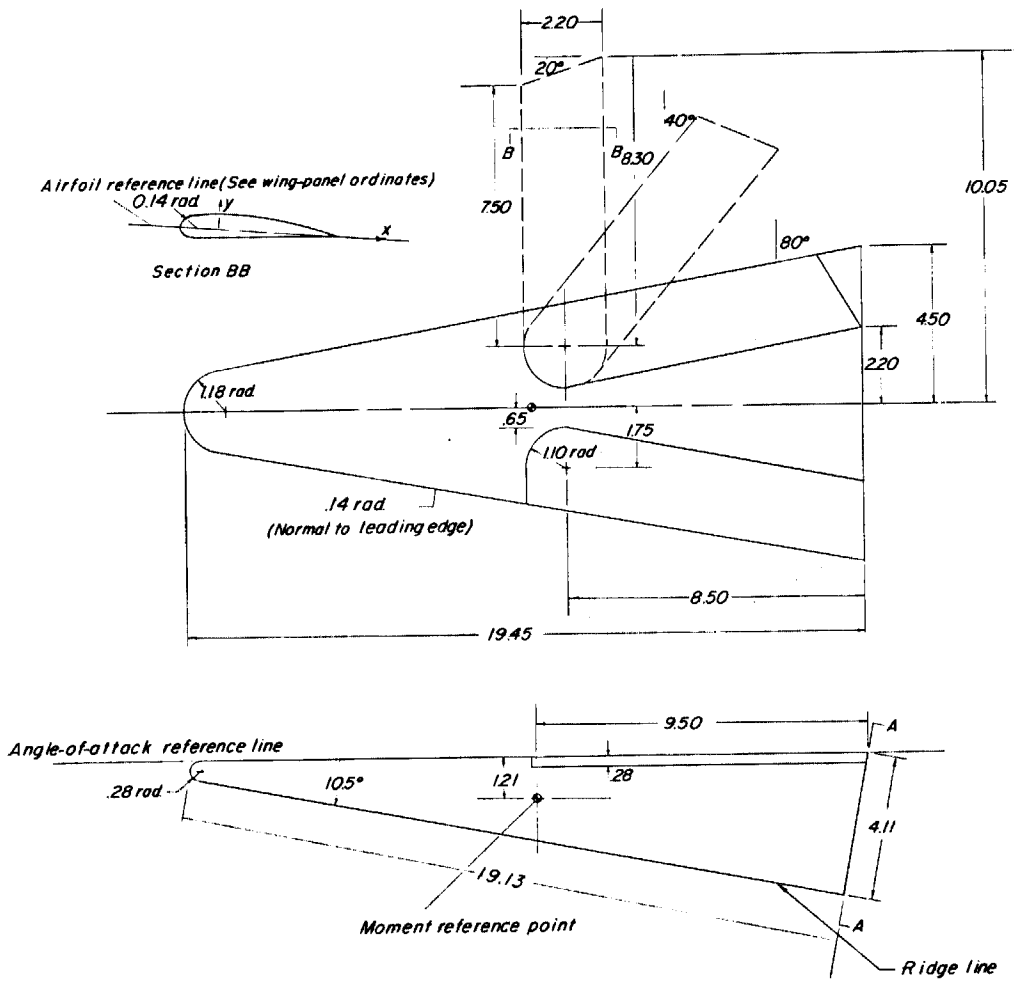

Basic model

$\Lambda_{LE} = 80°$

$A = .843$

$b = 9.00$ in.

$S = 96.20$ in.^{2}

$c = 19.13$ in.

ORDINATES FOR AIRFOIL (Measured from reference chord line)

Upper surface ordinates	
x, in.	y, in.
0	0
.01957	.08607
.04450	.12951
.09687	.16702
.15085	.20020
.20568	.22592
.31700	.26292
.42966	.28661
.54508	.30051
.65687	.30684
.88467	.30092
1.10845	.27716
1.33150	.24114
1.55357	.19515
1.77450	.14048
1.99408	.07745
2.10327	.04268
2.21169	0

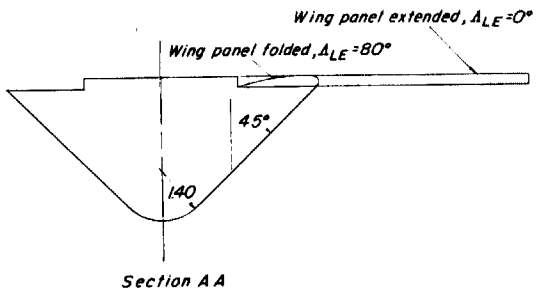

(a) Characteristics of the various wing-panel sweeps on the basic configuration.

Figure 1.- Geometric characteristics of models. All linear dimensions are in inches.

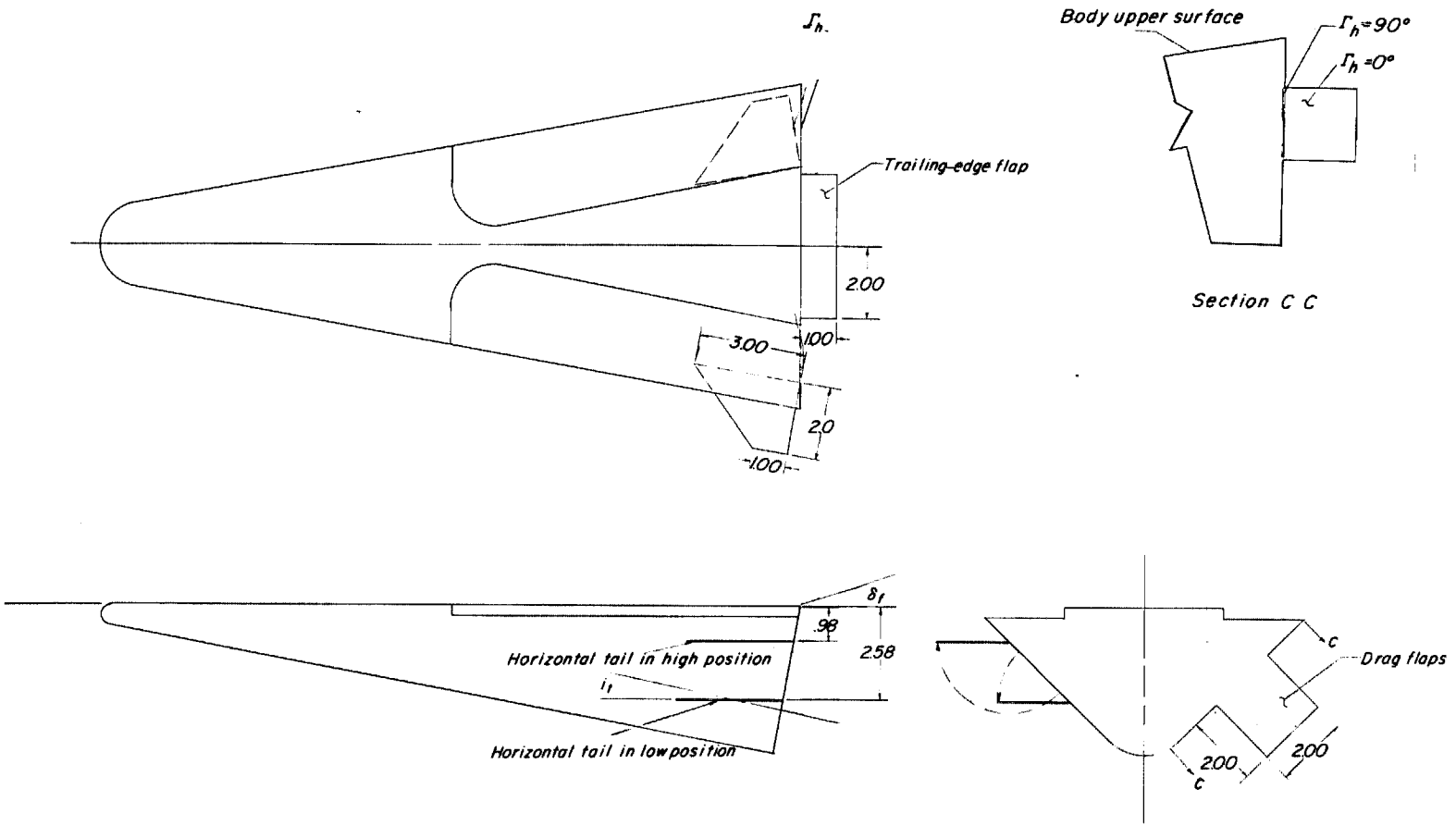

(b) Geometry of various controls used.

Figure 1.- Concluded.

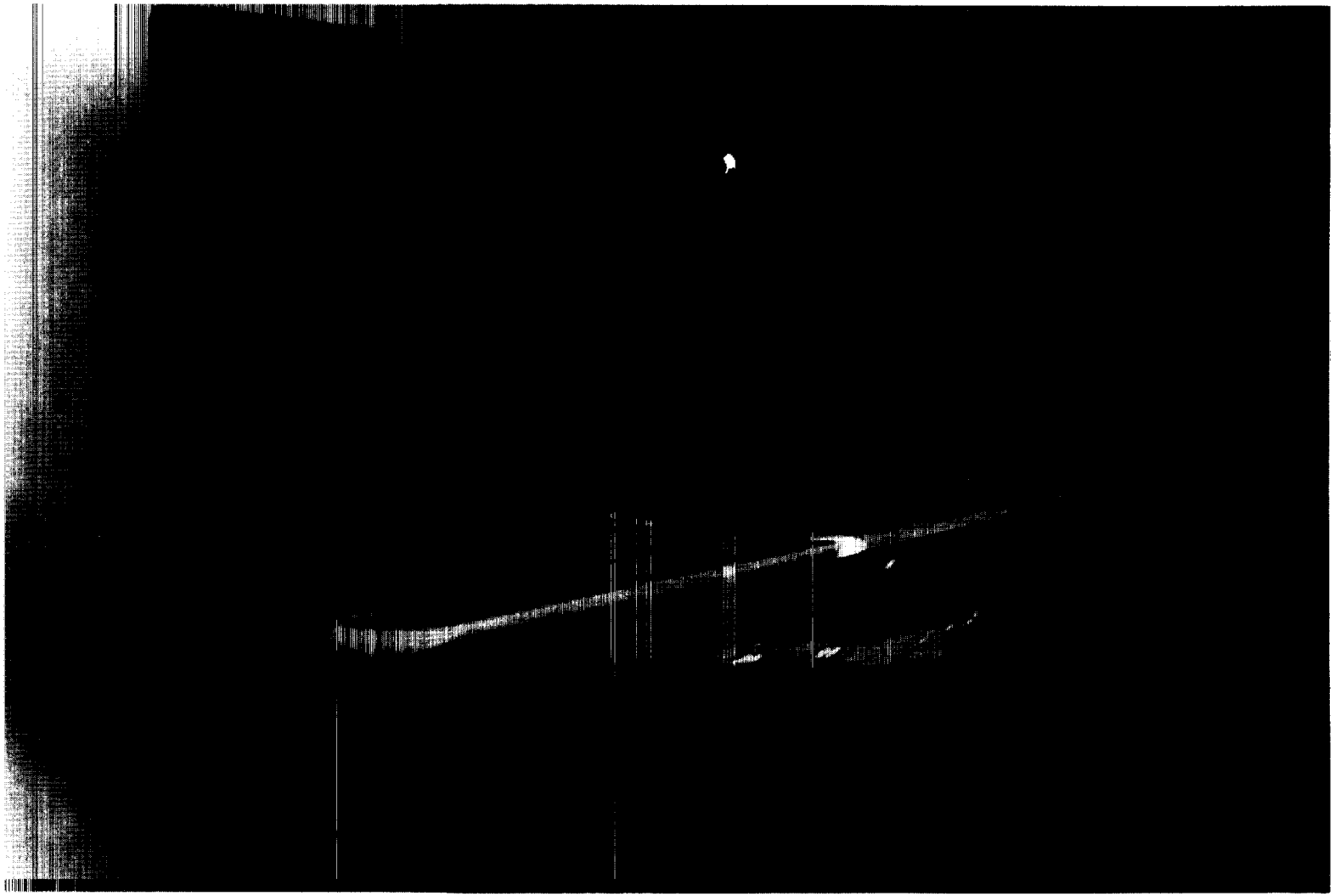

(a) $\Lambda_{LE} = 80^{\circ}$. L-61-8780

Figure 2.- Photographs of the basic configuration with various wing-panel sweeps mounted in the Langley 7- by 10-foot transonic wind tunnel. i_t = Off; δ_f = Off.

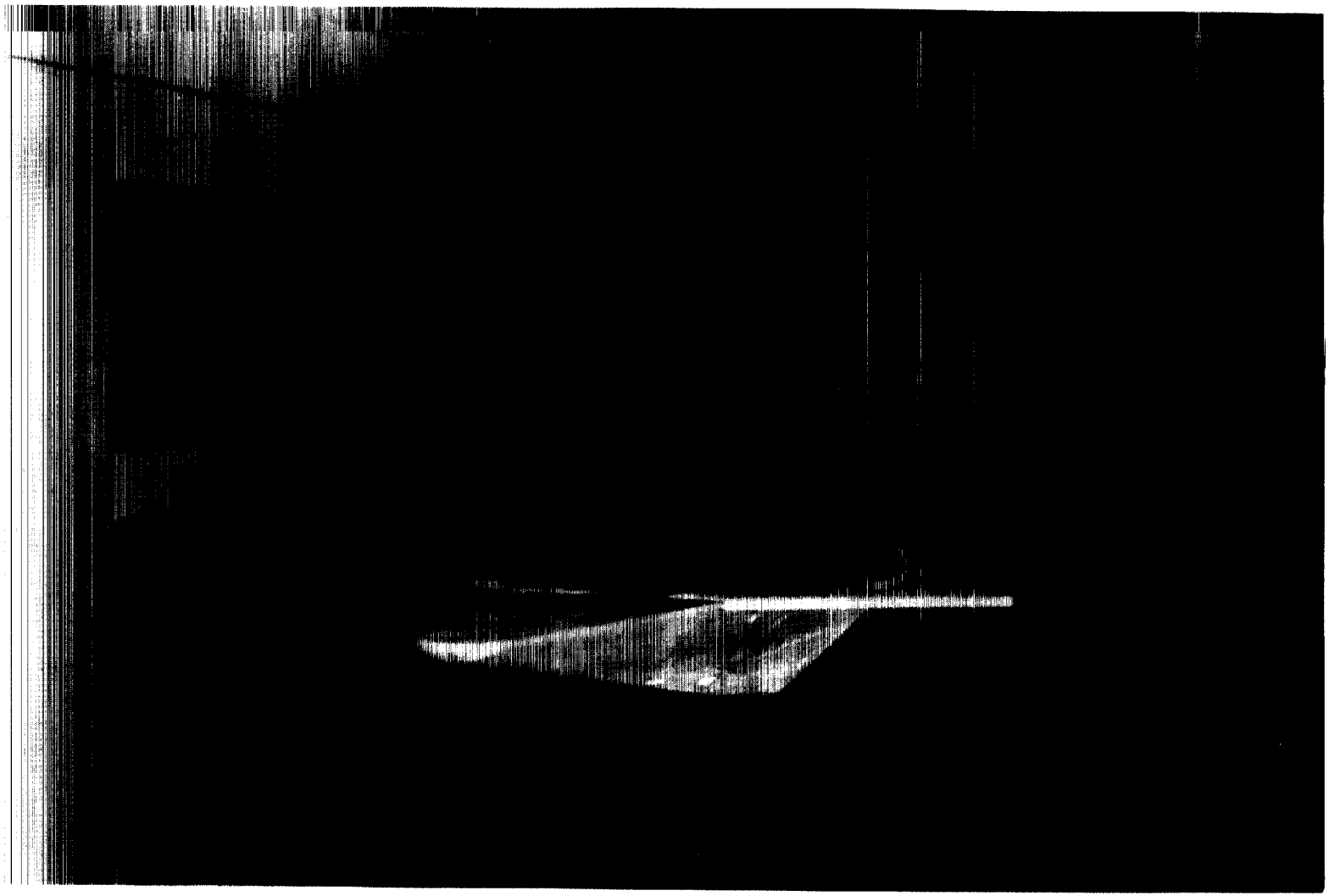

(b) $\Lambda_{LE} = 40^{\circ}$. L-61-8781

Figure 2.- Continued.

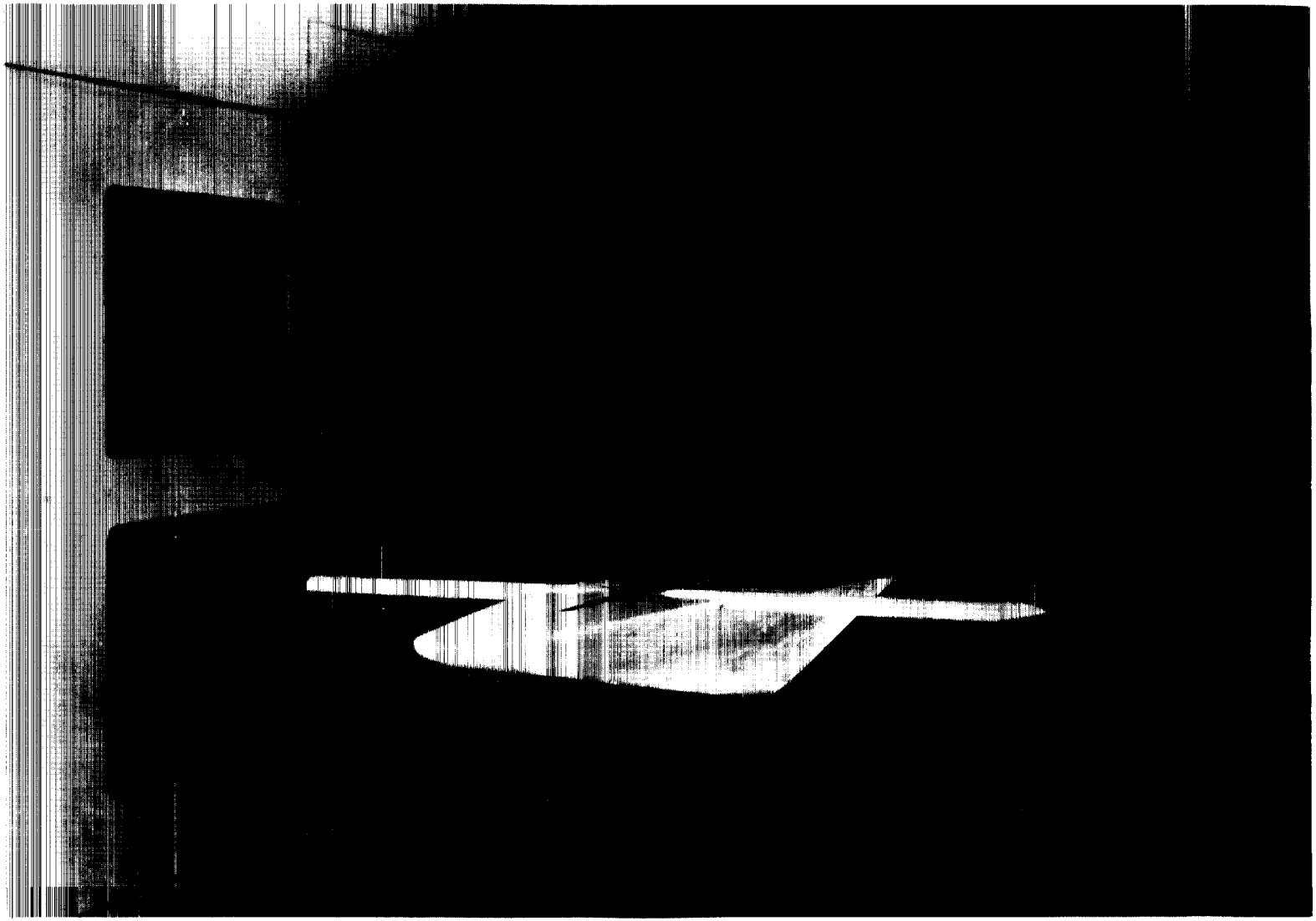

(c) $\Lambda_{LE} = 0^{\circ}$. L-61-8782

Figure 2.- Concluded.

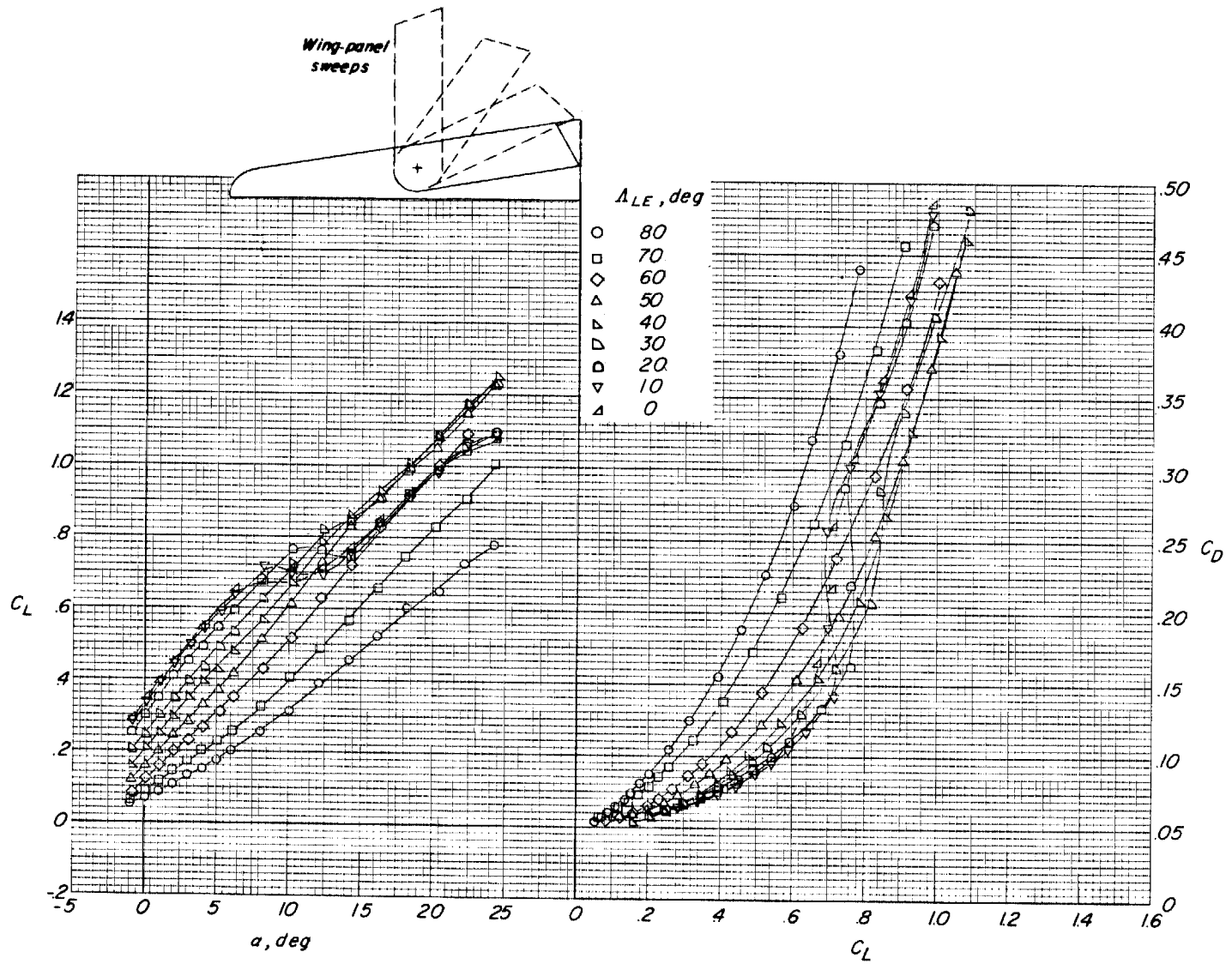

(a) M = 0.40.

Figure 3.- The effects of wing-panel sweep on the longitudinal aerodynamic characteristics of the basic configuration at various Mach numbers. All longitudinal controls off.

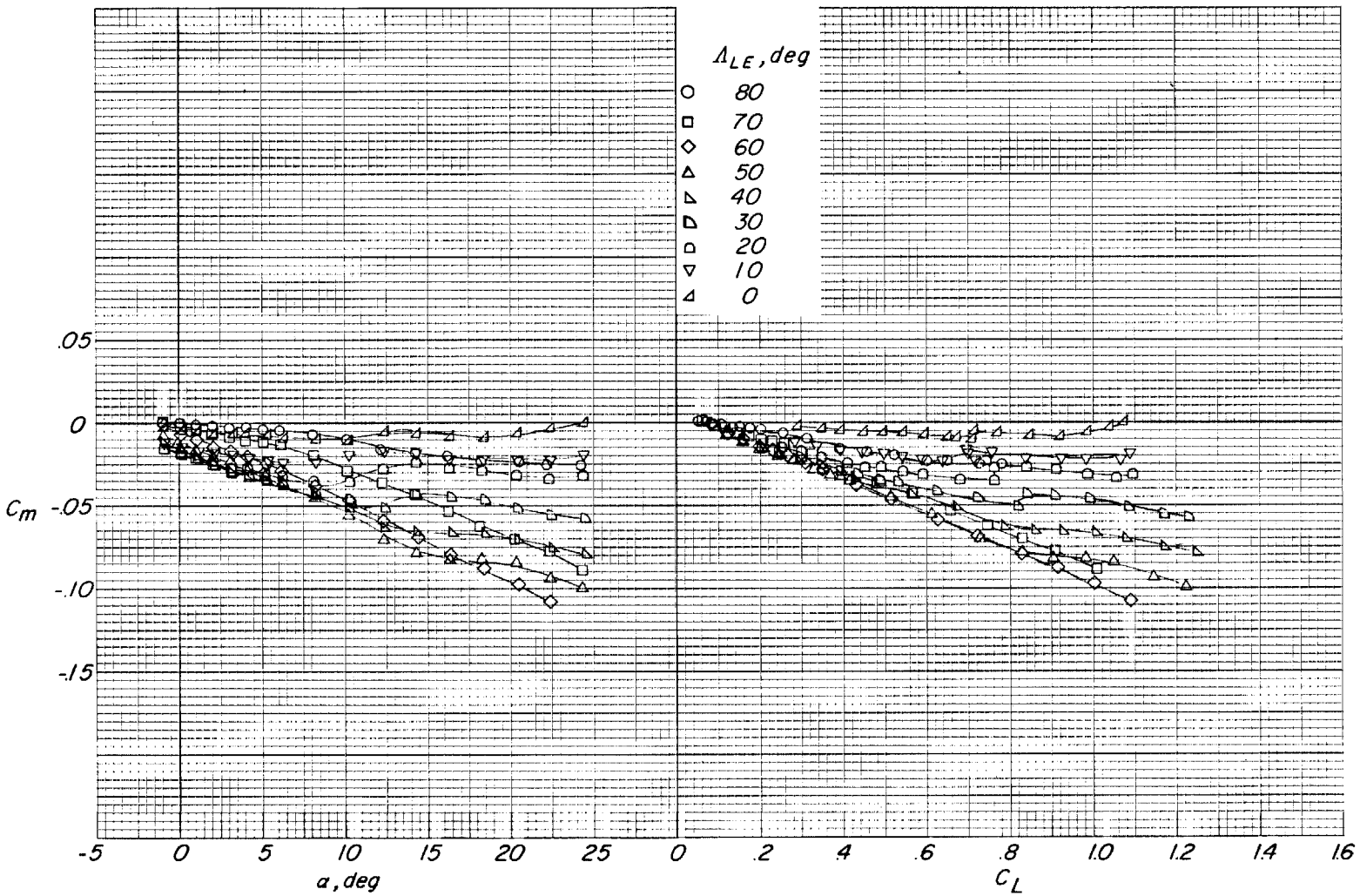

(a) M = 0.40. Concluded.

Figure 3.- Continued.

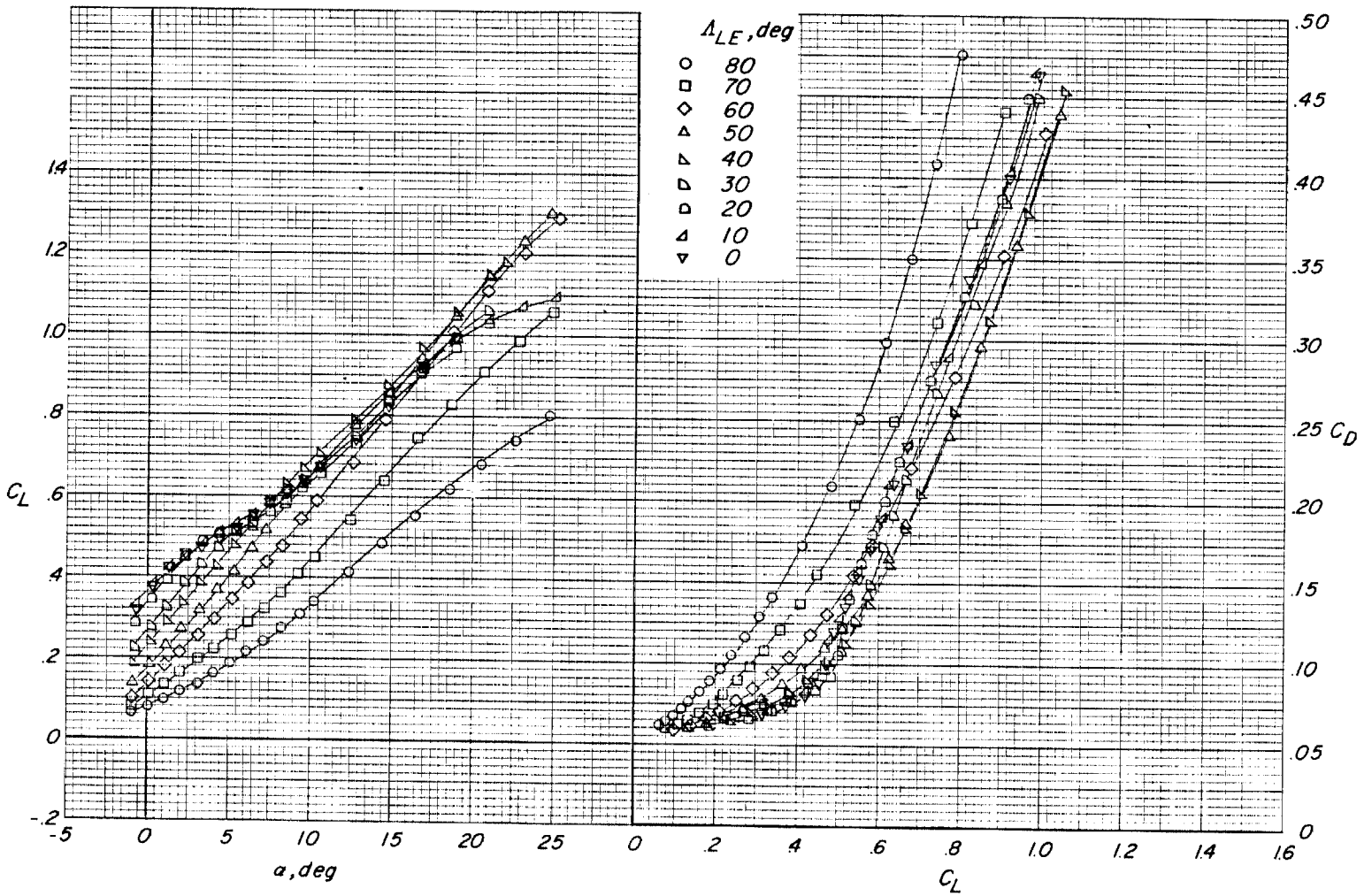

(b) M = 0.60.

Figure 3.- Continued.

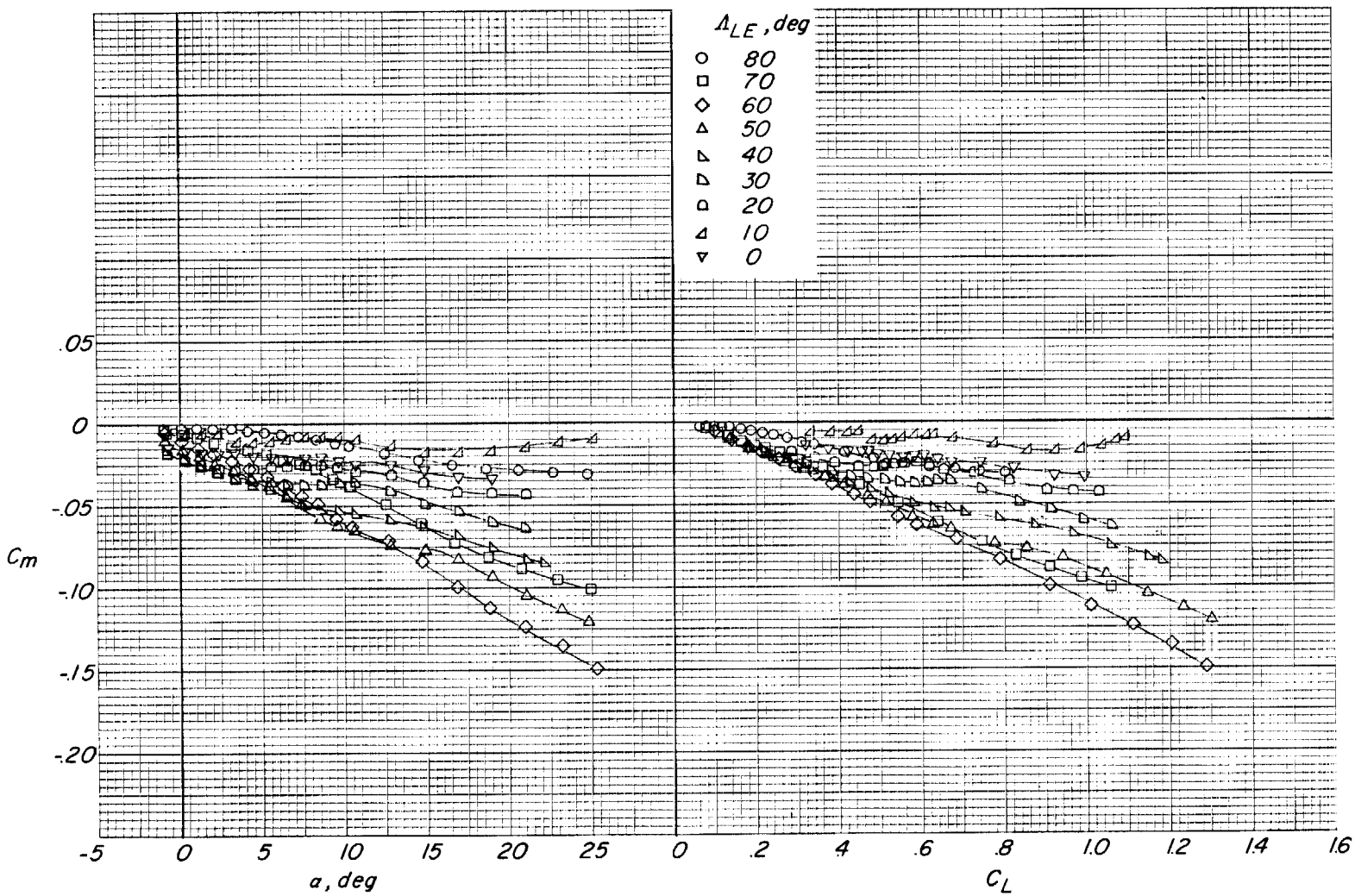

(b) M = 0.60. Concluded.

Figure 3.- Continued.

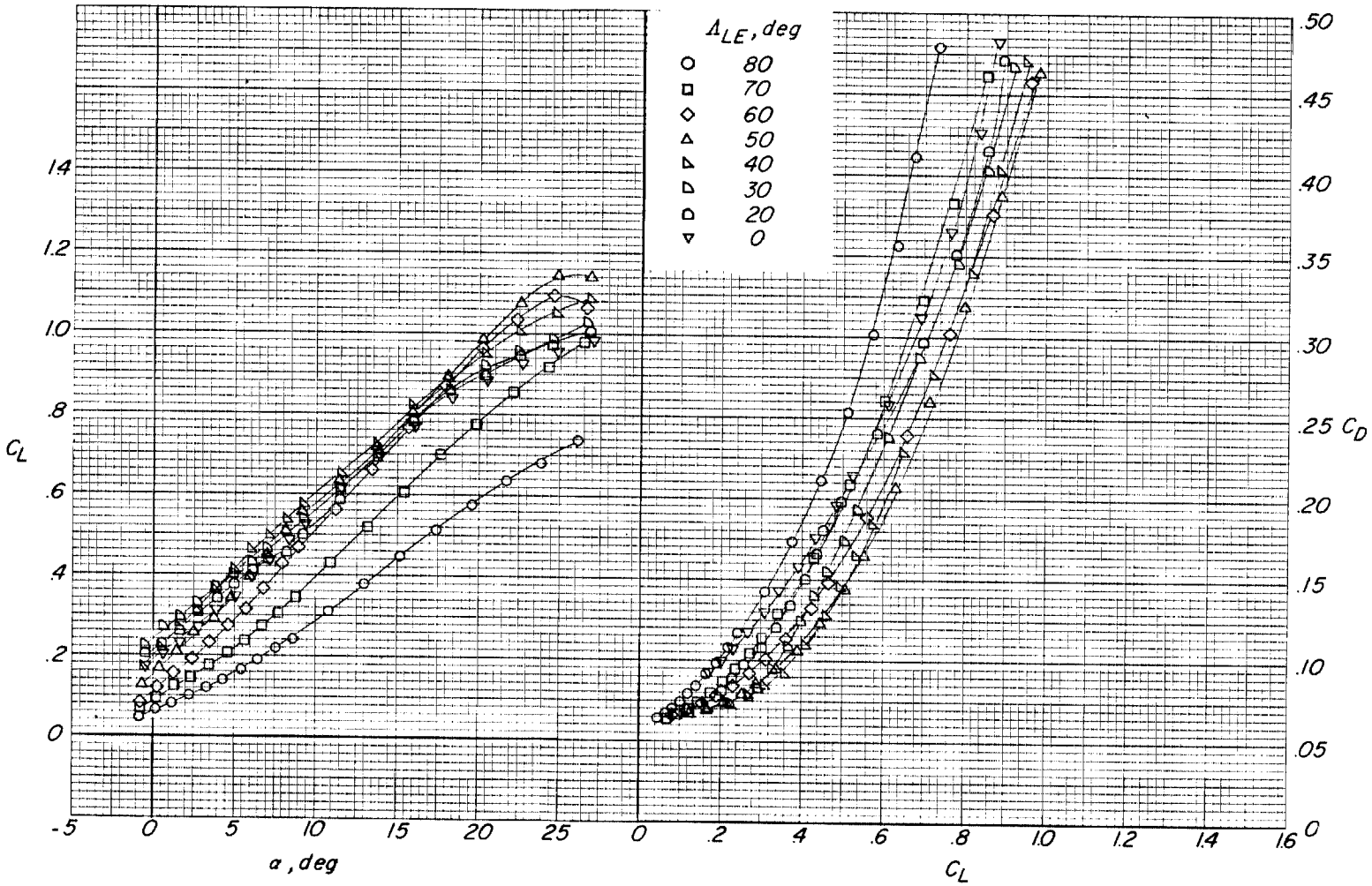

(c) M = 0.70.

Figure 3.- Continued.

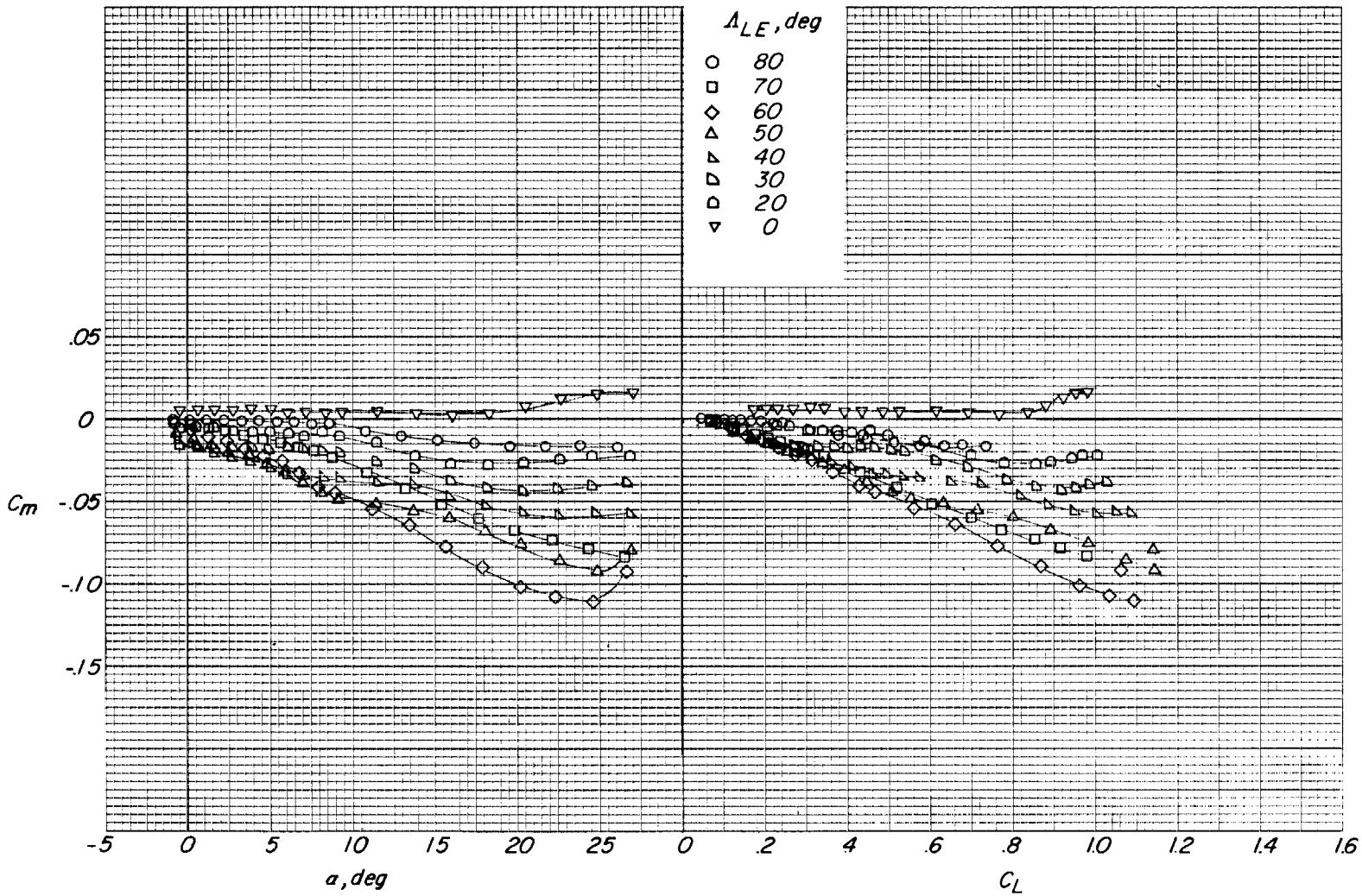

(c) M = 0.70. Concluded.

Figure 3.- Continued.

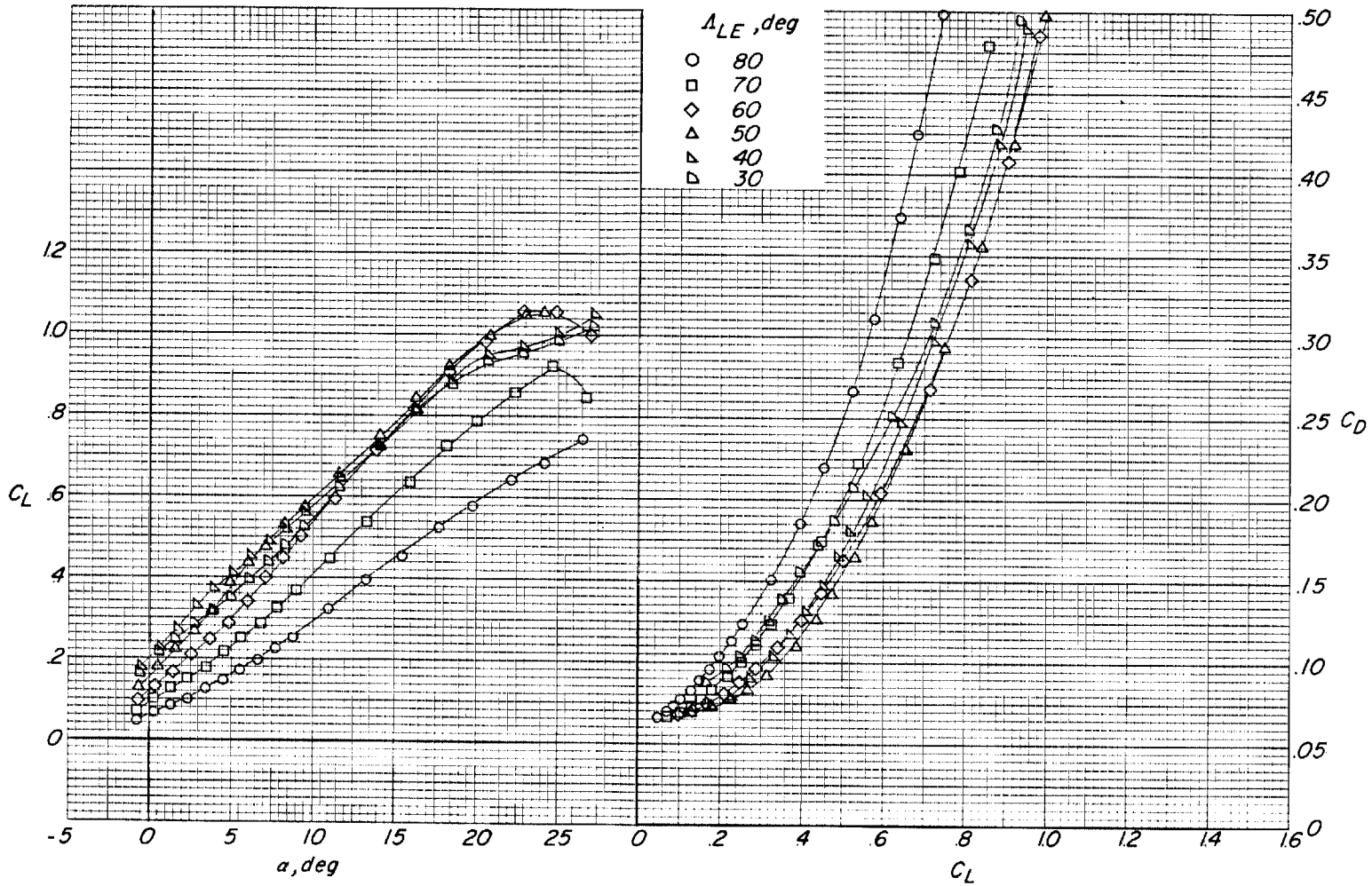

(d) M = 0.80.

Figure 3.- Continued.

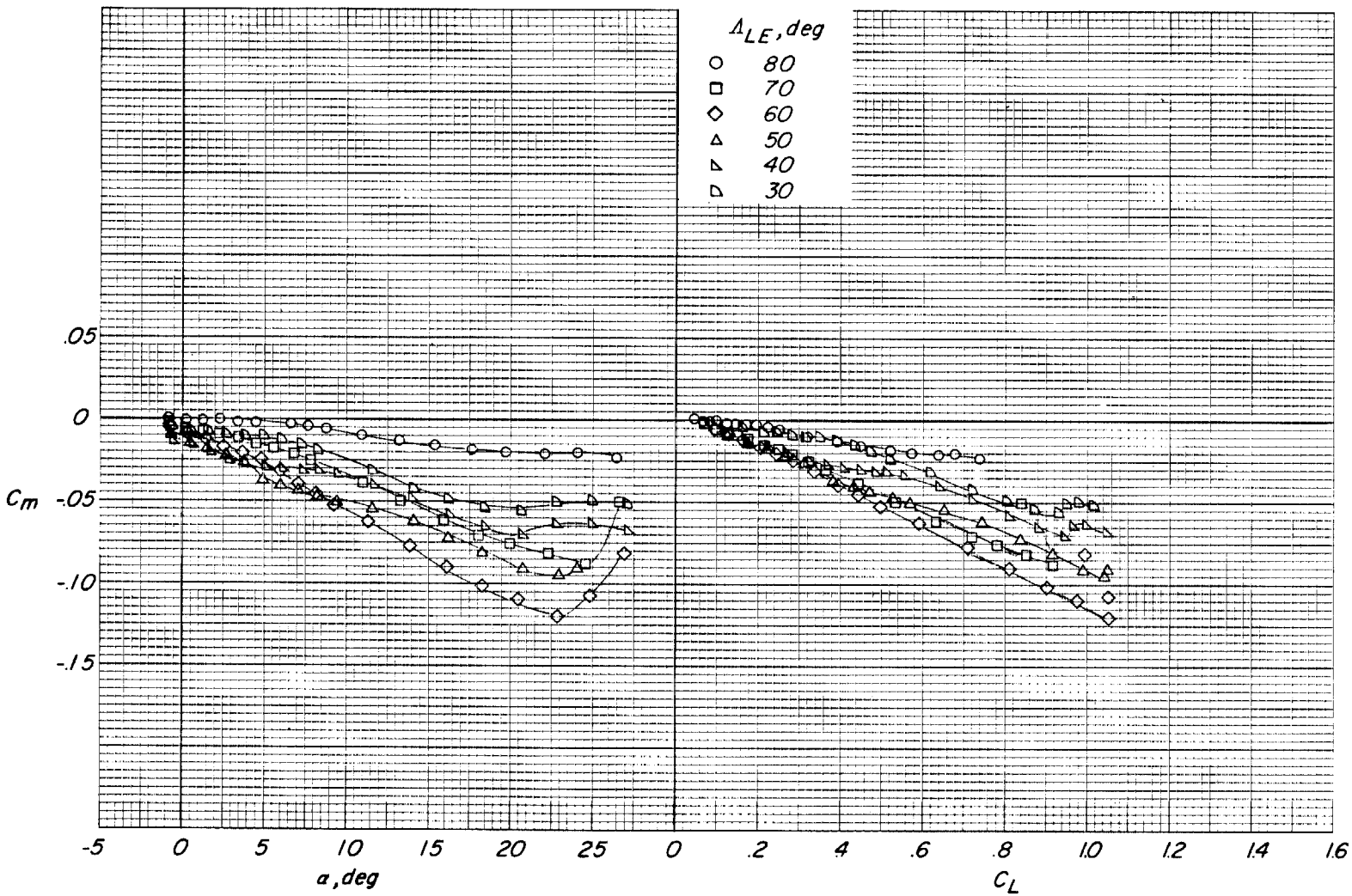

(d) M = 0.80. Concluded.

Figure 3.- Continued.

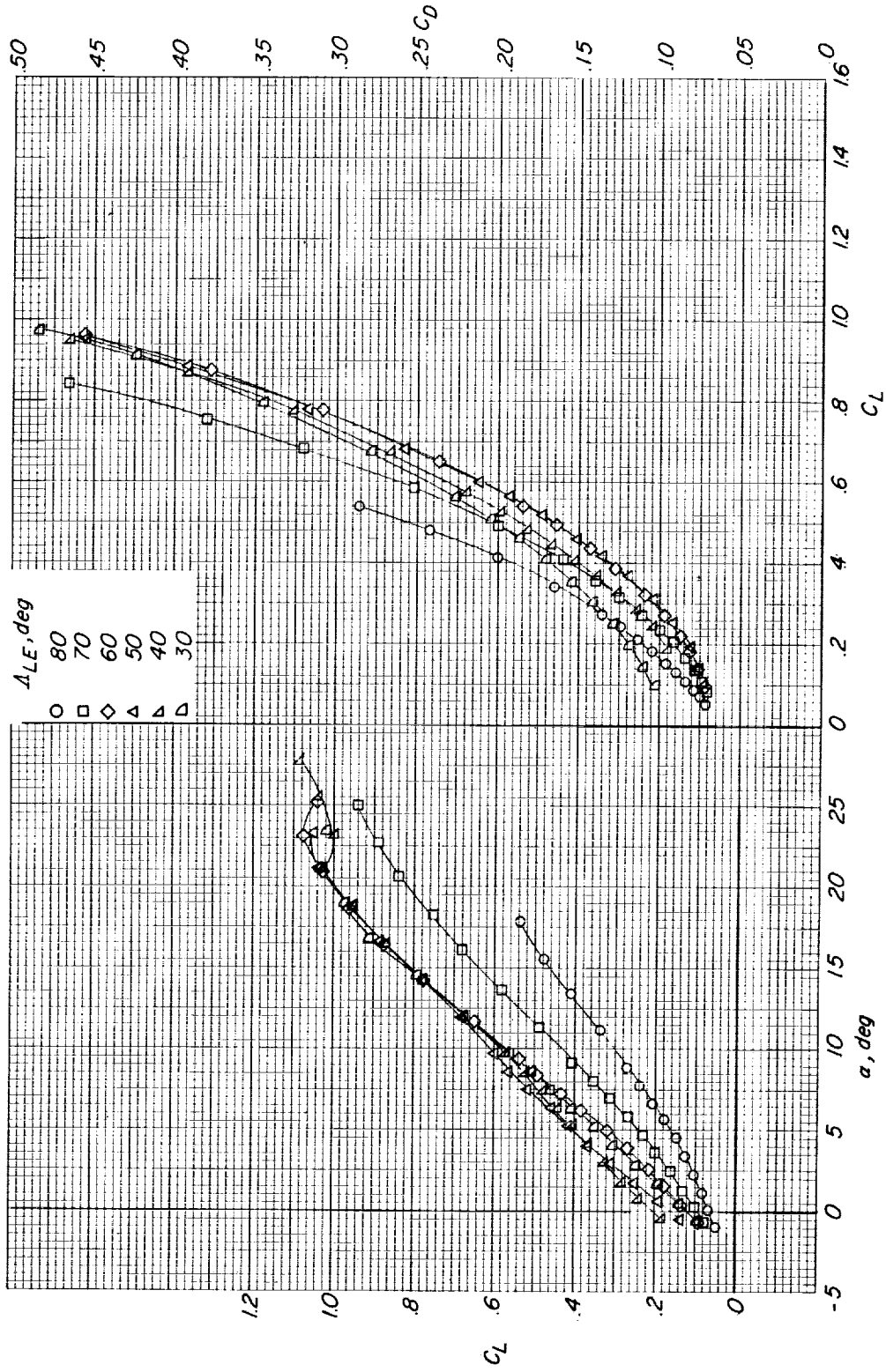

(e) M = 0.90.

Figure 3.- Continued.

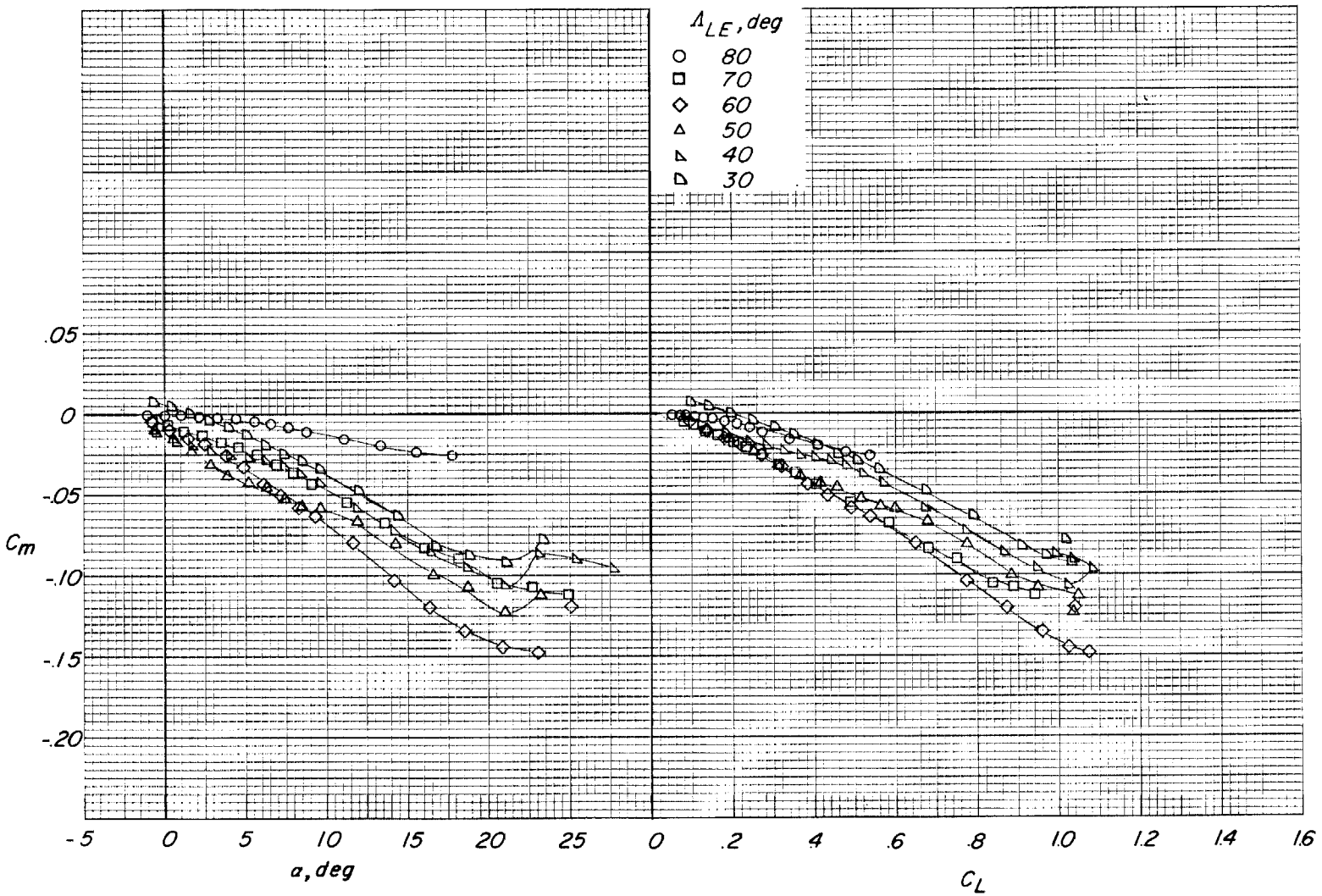

(e) M = 0.90. Concluded.

Figure 3.- Continued.

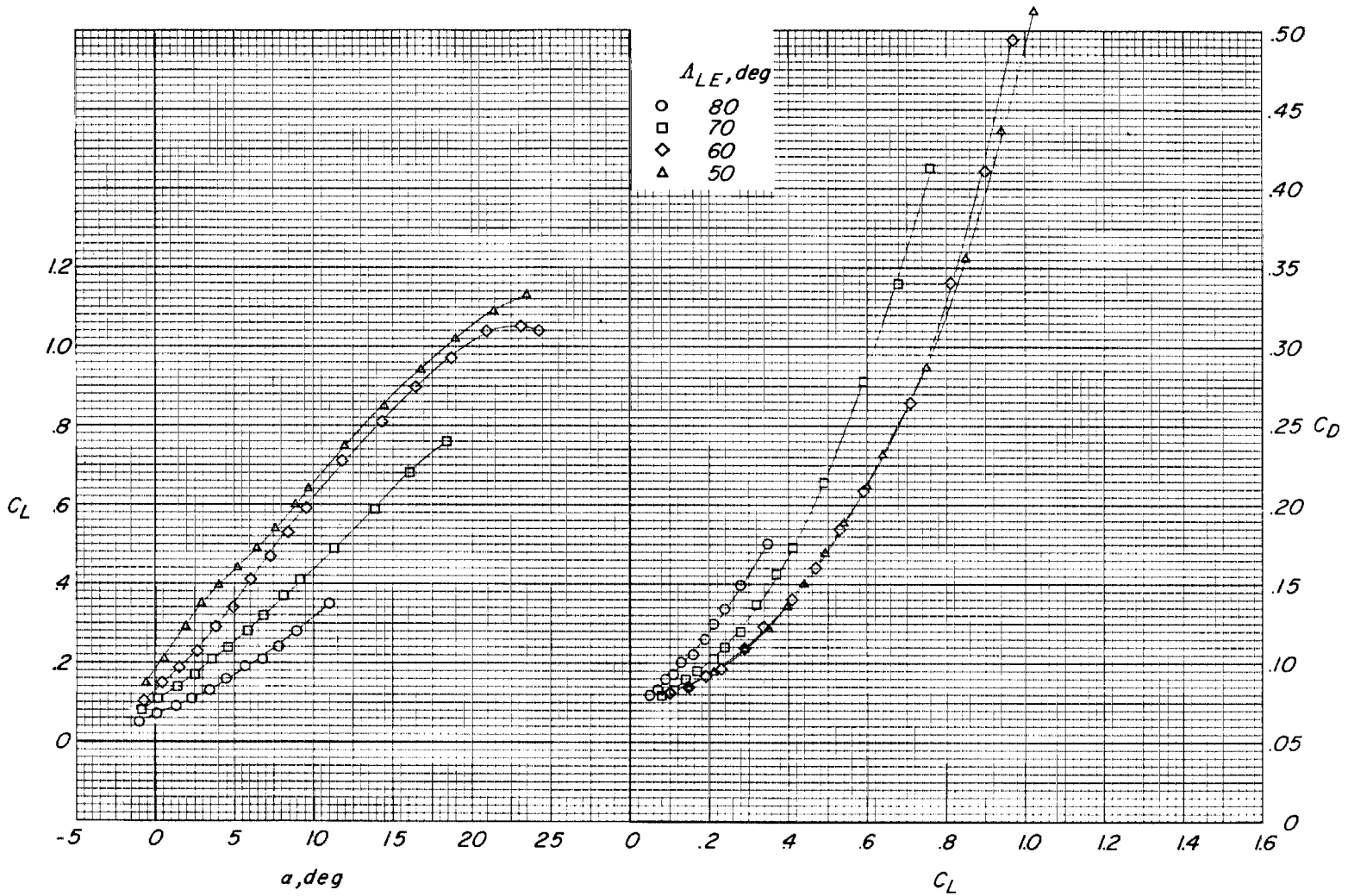

(f) M = 0.95.

Figure 3.- Continued.

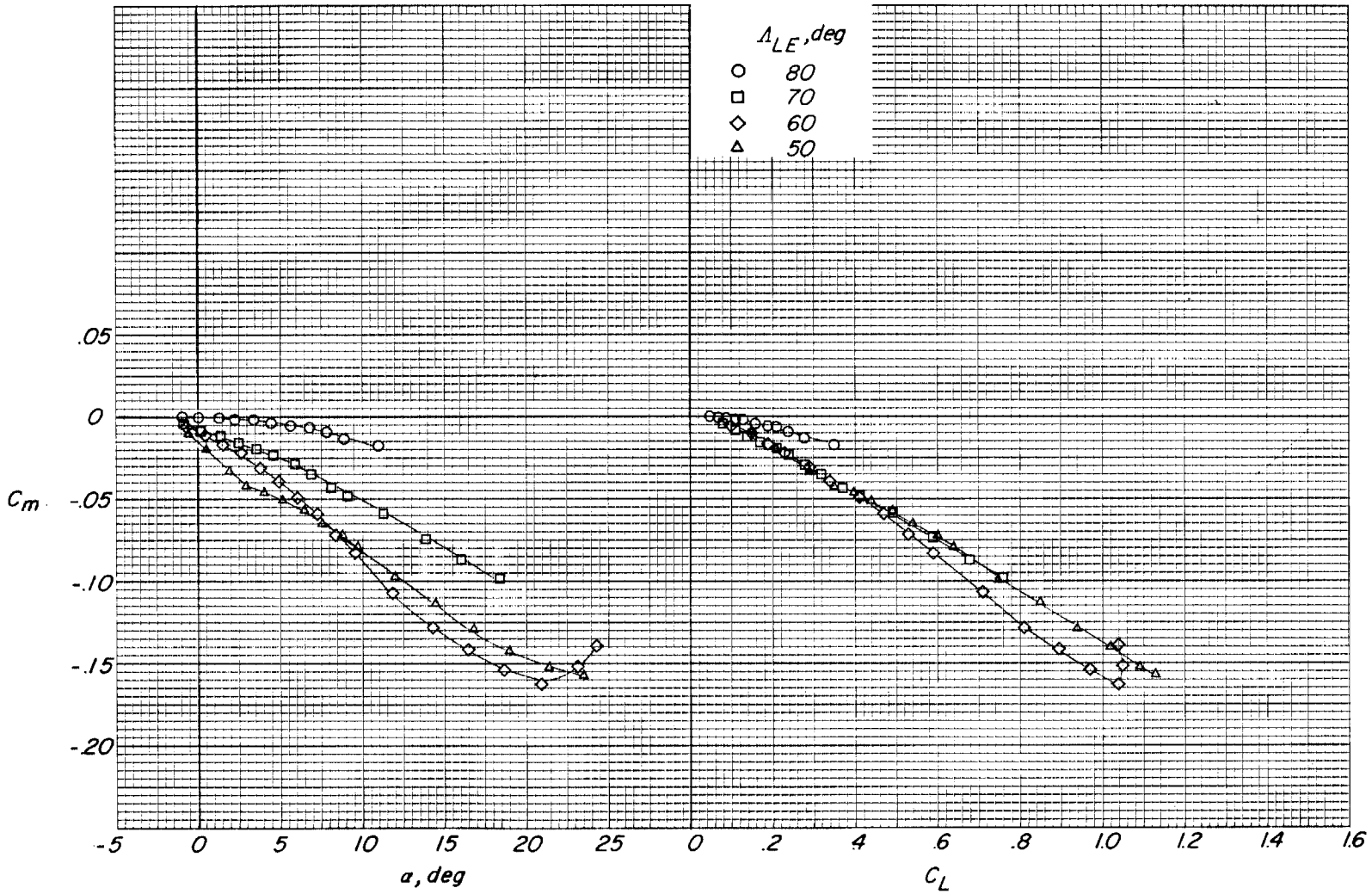

(f) M = 0.95. Concluded.

Figure 3.- Continued.

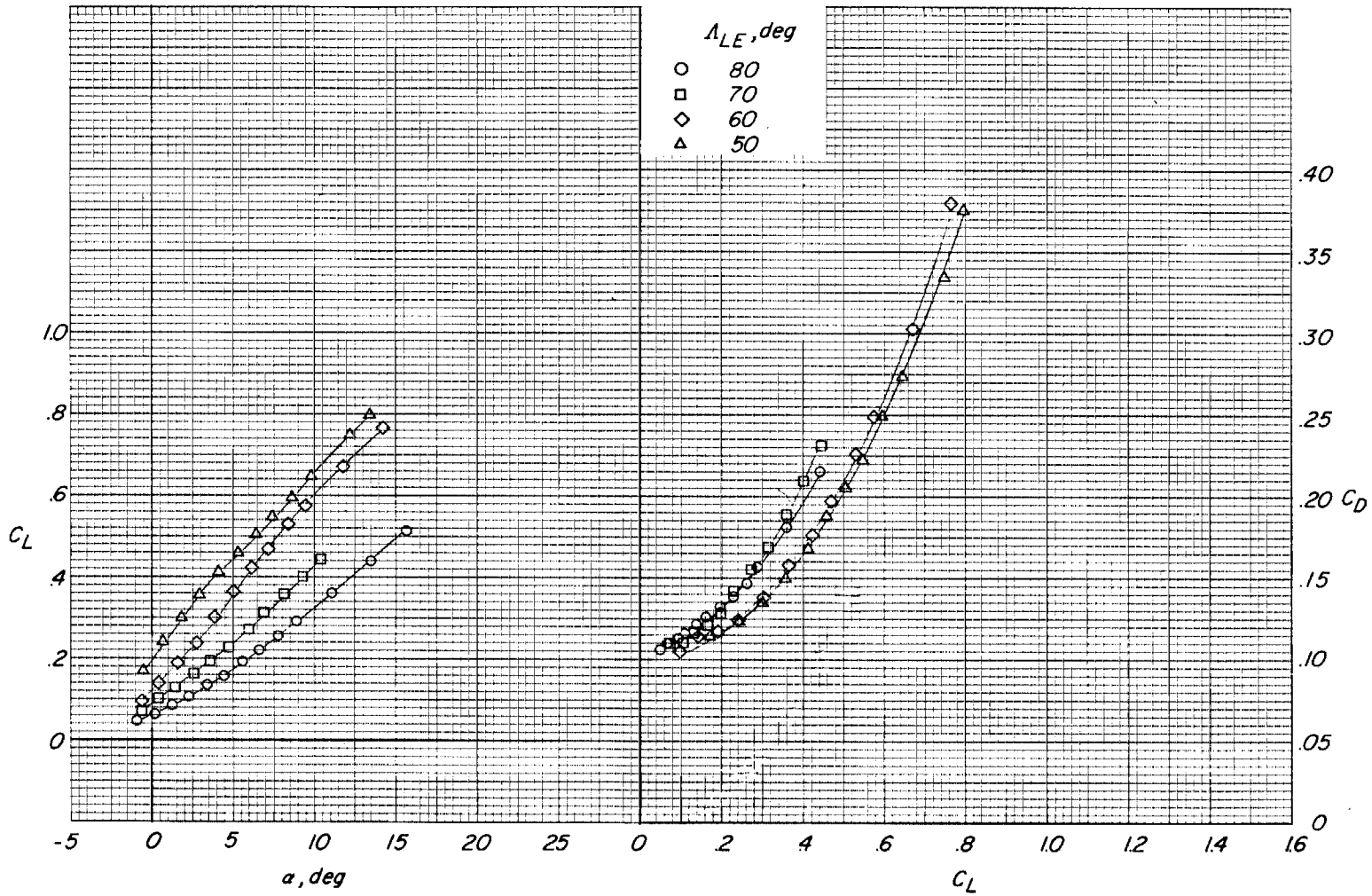

(g) M = 1.00.

Figure 3.- Continued.

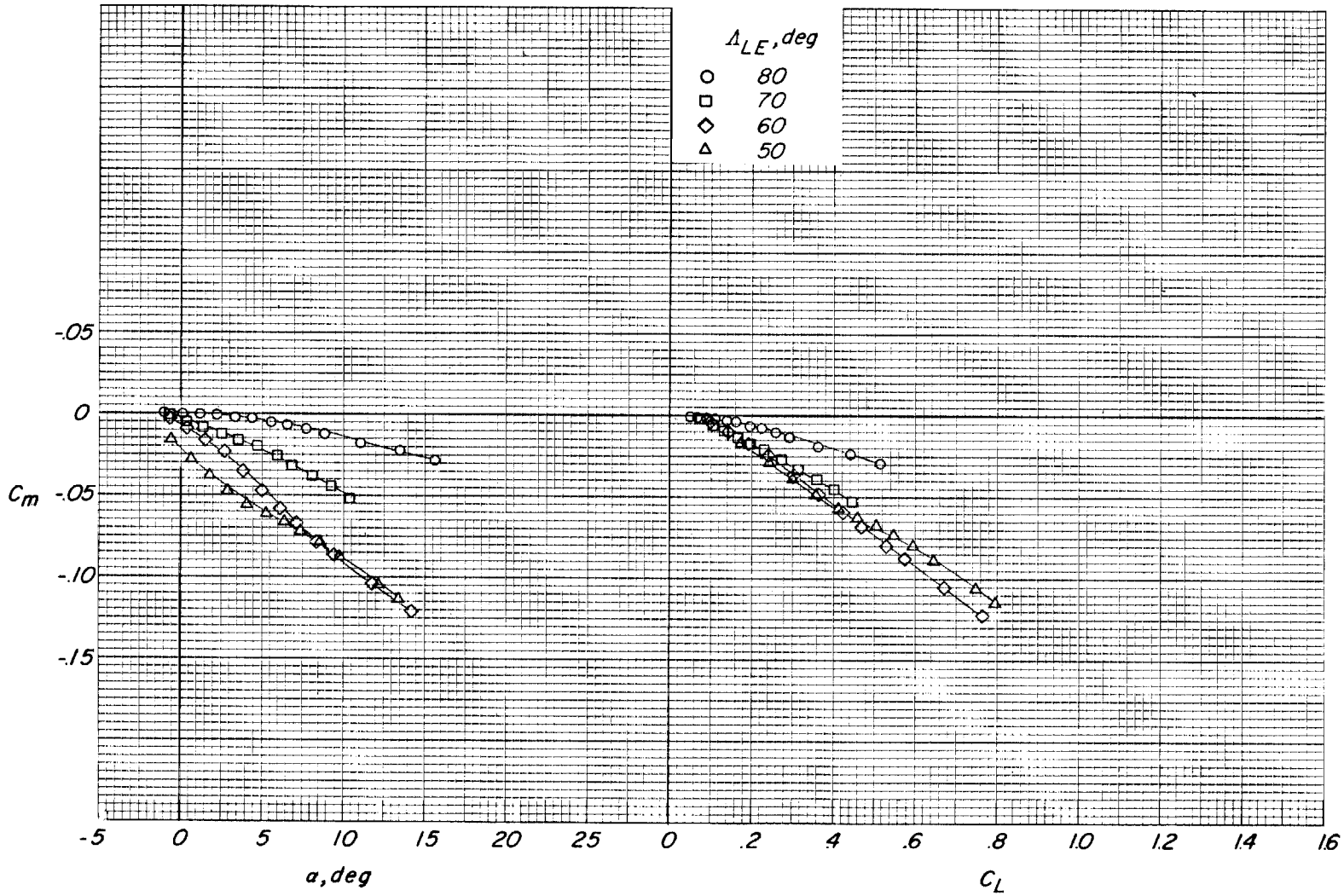

(g) M = 1.00. Concluded.

Figure 3.- Continued.

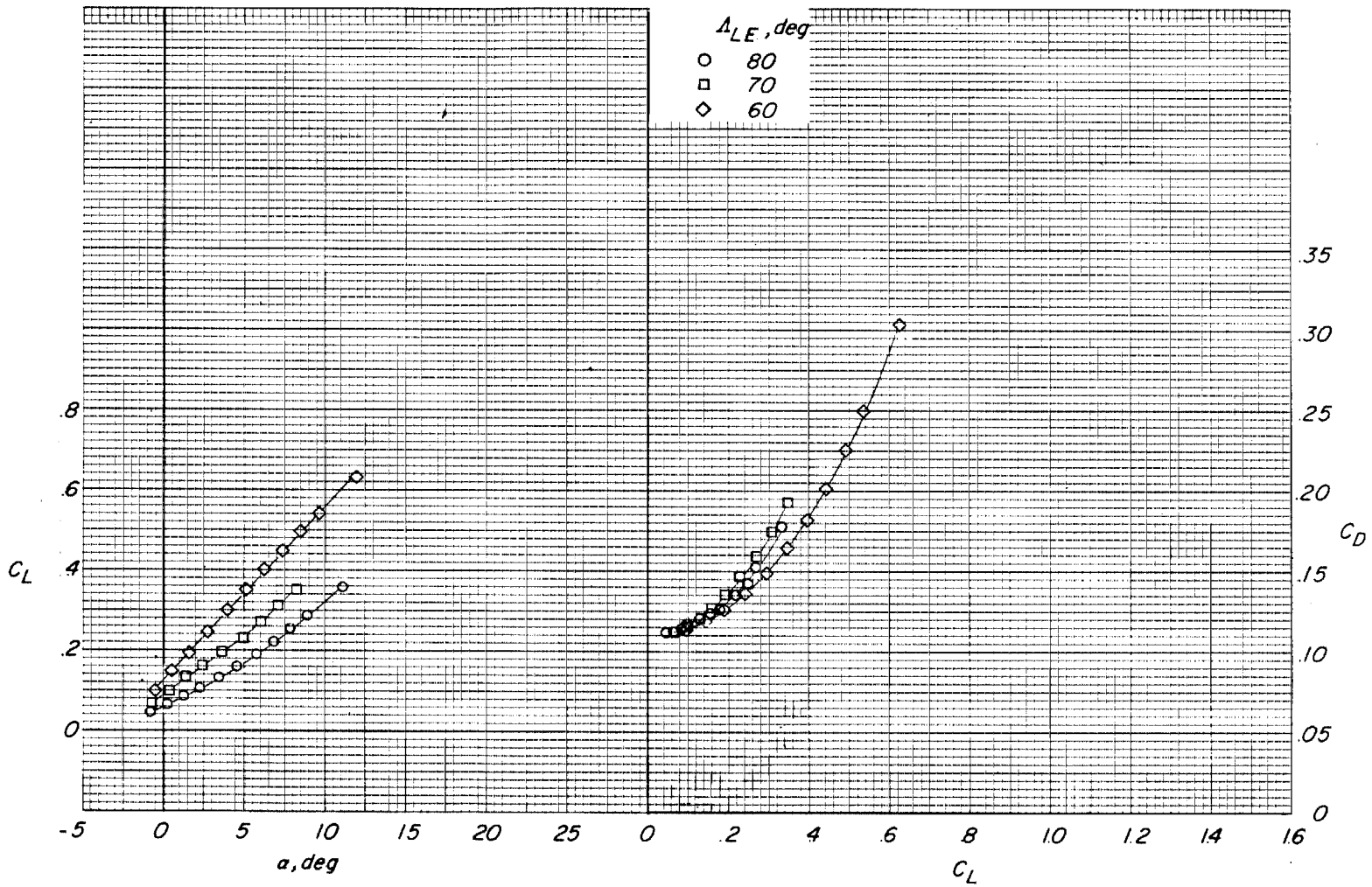

(h) M = 1.10.

Figure 3.- Continued.

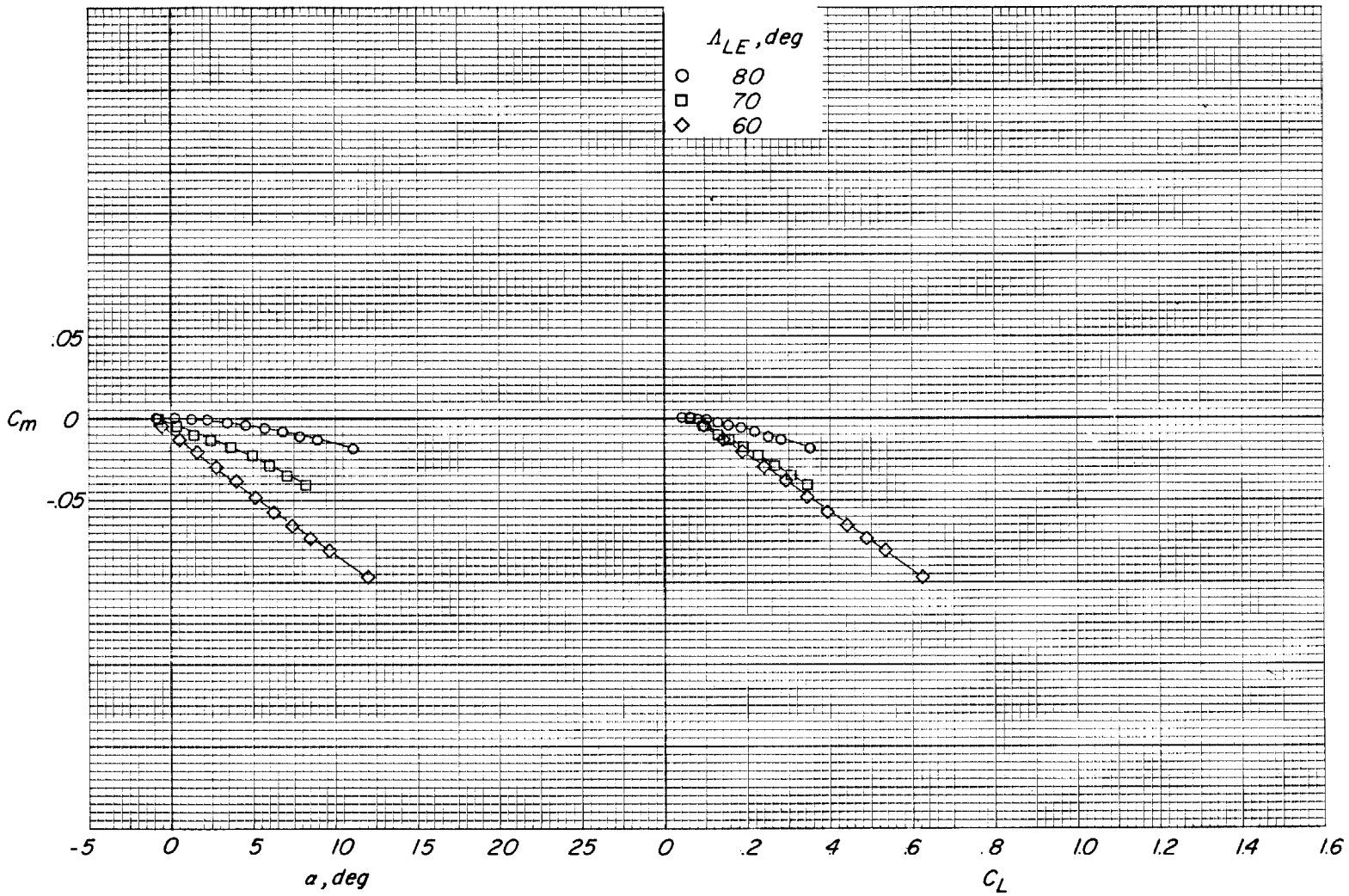

(h) M = 1.10. Concluded.

Figure 3.- Concluded.

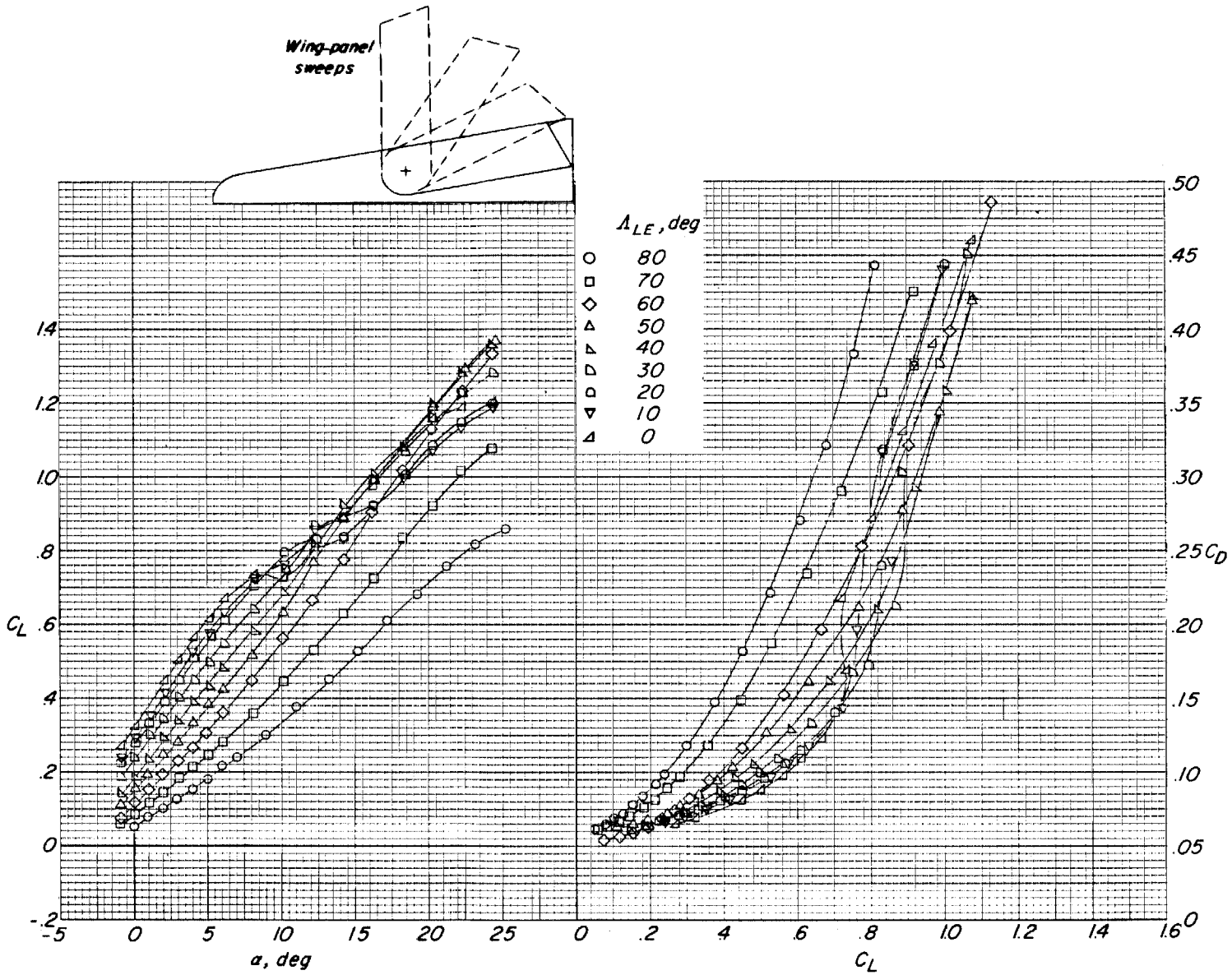

Figure 4.- The effects of wing-panel sweep on the longitudinal aerodynamic characteristics of the configuration having the horizontal tail on in the high position. $i_t = 0^o$; δ_f = Off; M = 0.40.

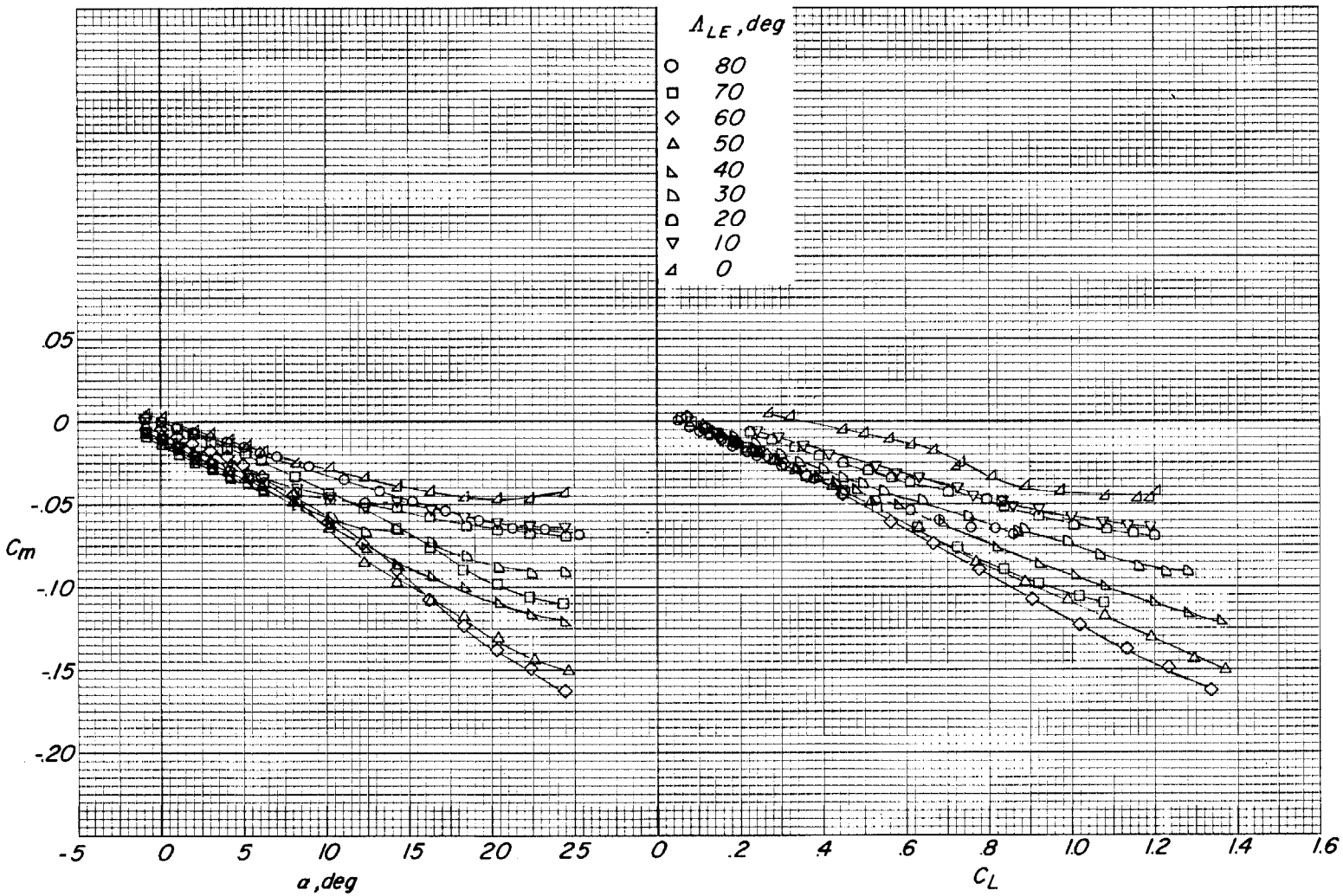

Figure 4.- Concluded.

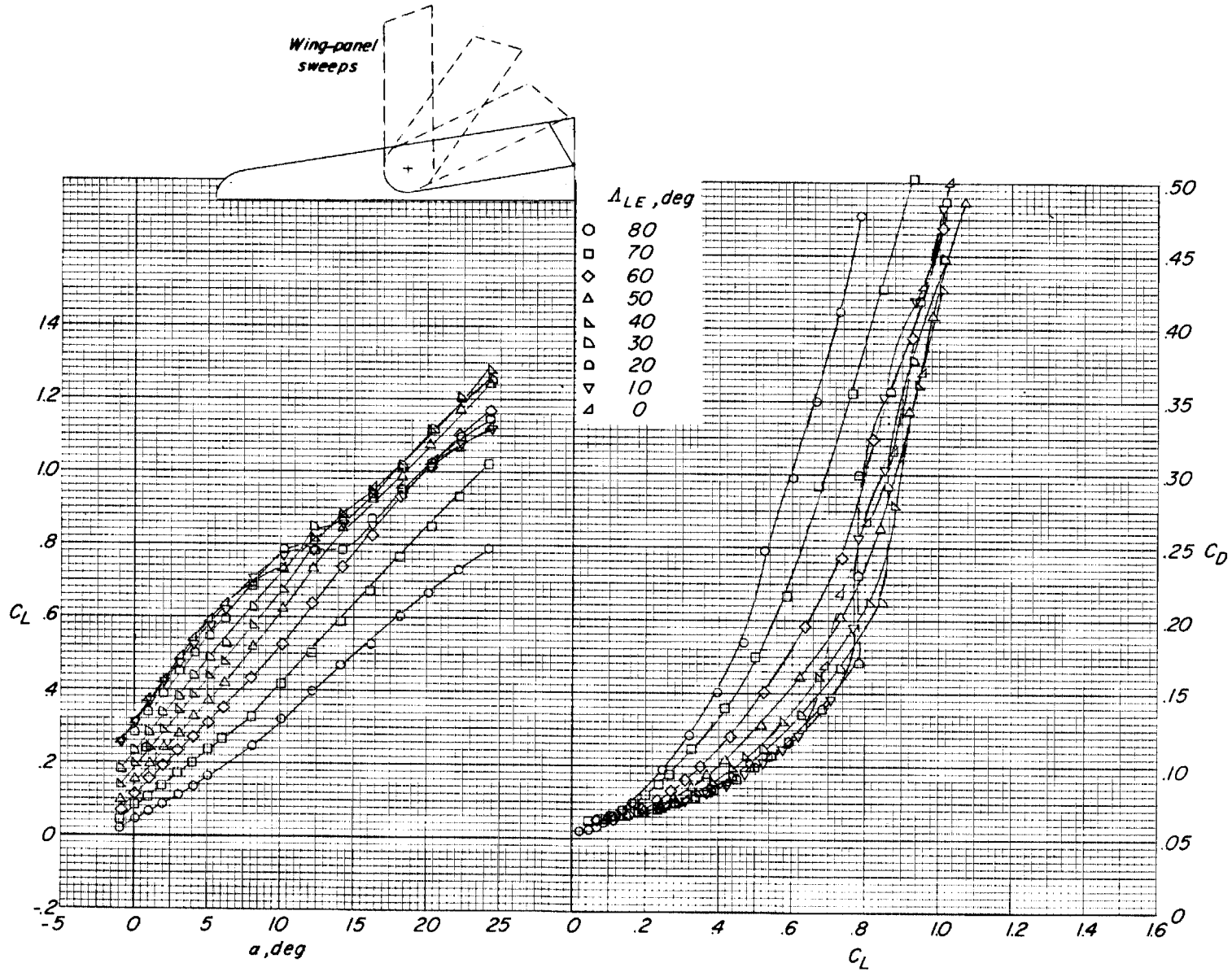

Figure 5.- The effects of wing-panel sweep on the longitudinal aerodynamic characteristics of the configuration having the horizontal tail on in the low position. $i_t = 0^o$; M = 0.40; δ_f = 0ff.

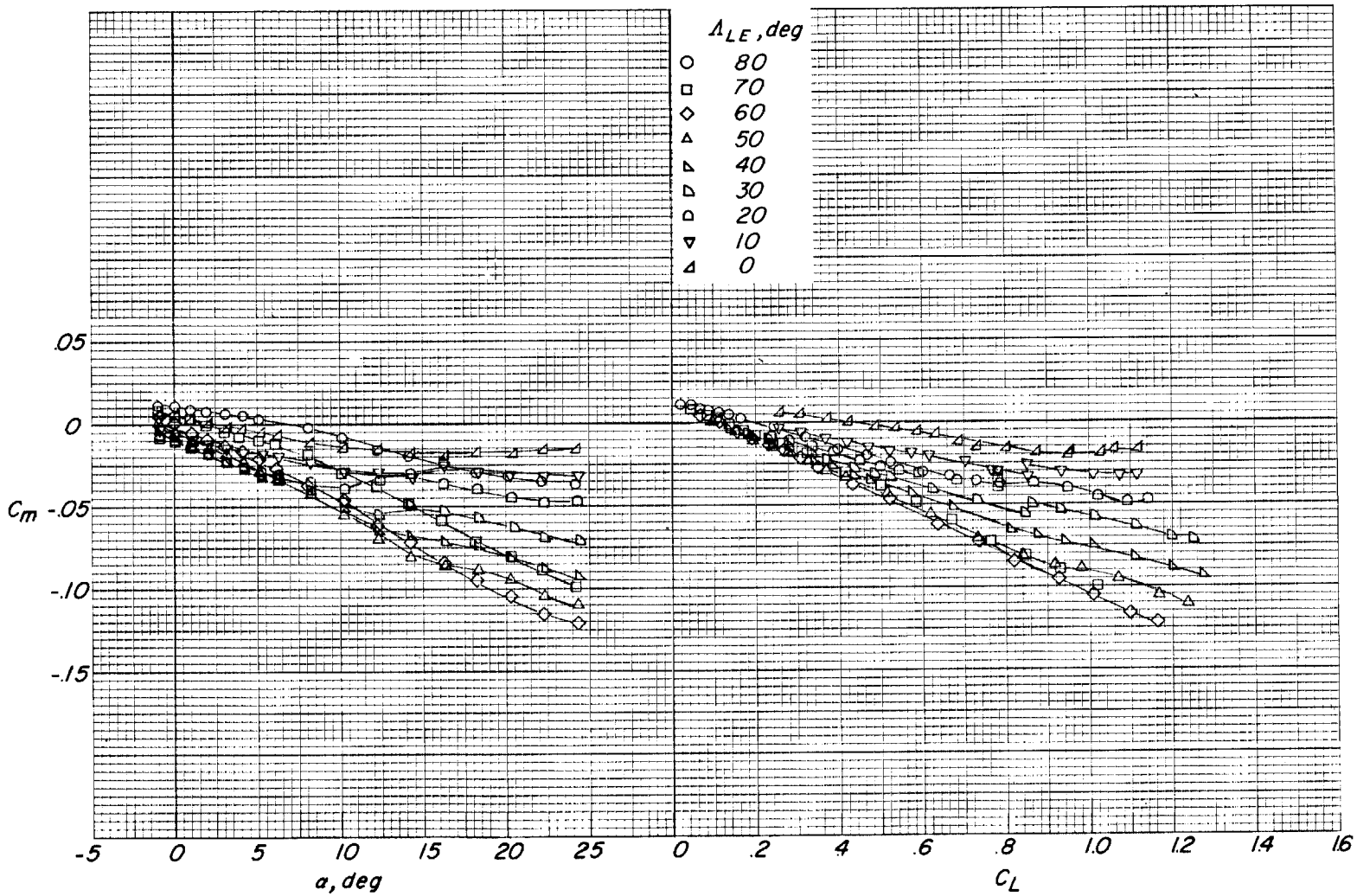

Figure 5.- Concluded.

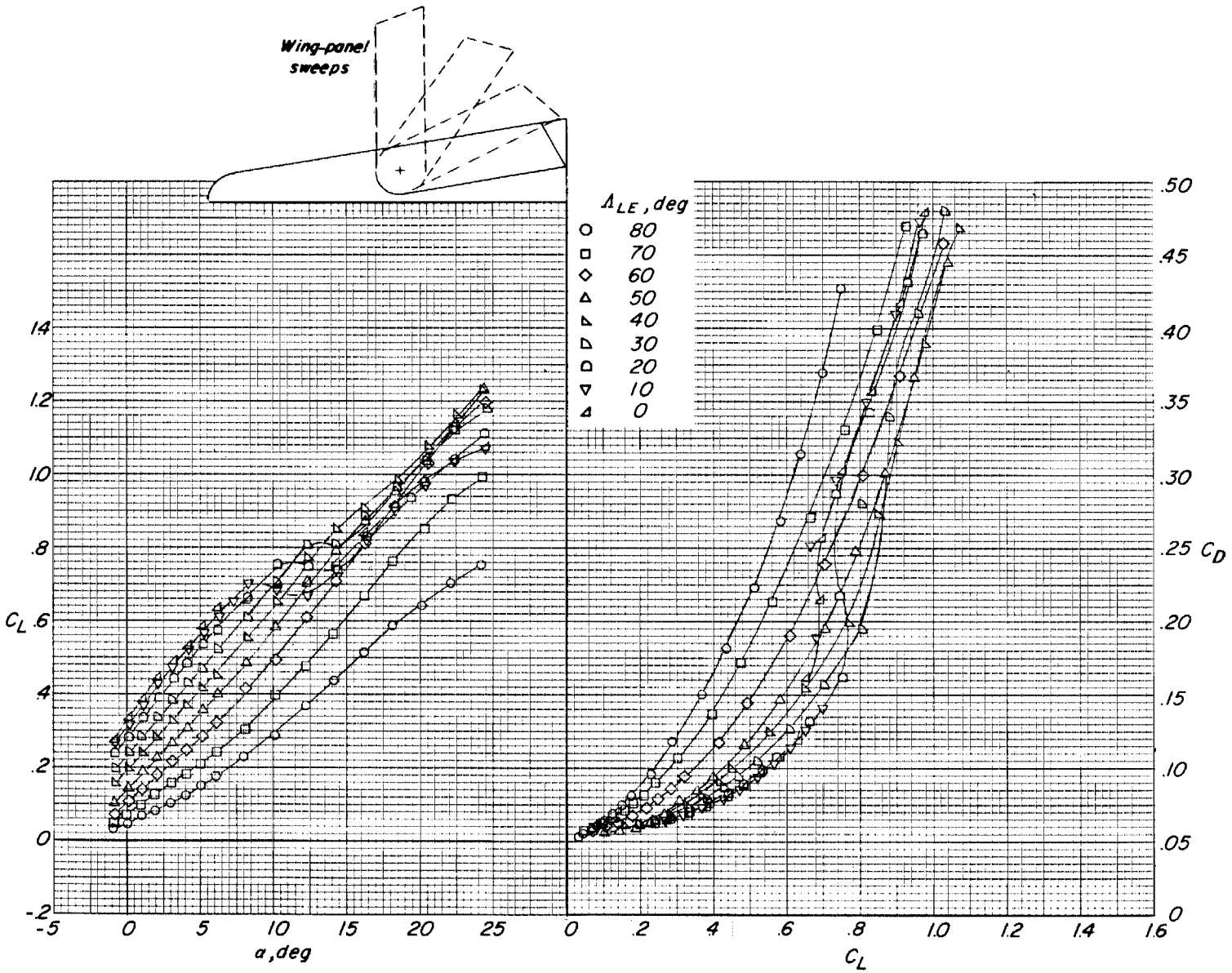

Figure 6.- The effects of wing-panel sweep on the longitudinal aerodynamic characteristics of the configuration having a trailing-edge flap extended. Horizontal tail off; M = 0.40; $\delta_f = 0^o$.

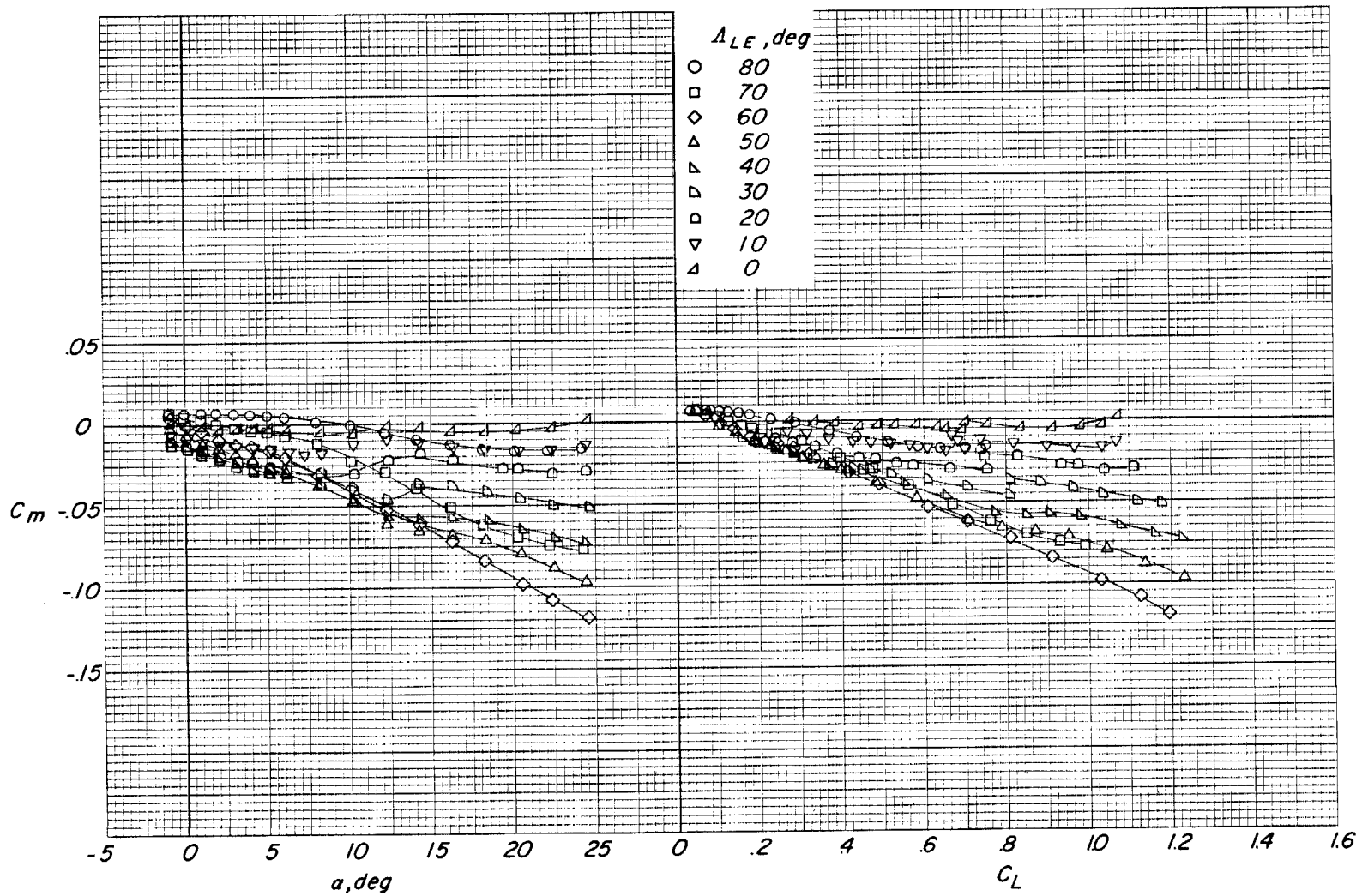

Figure 6.- Concluded.

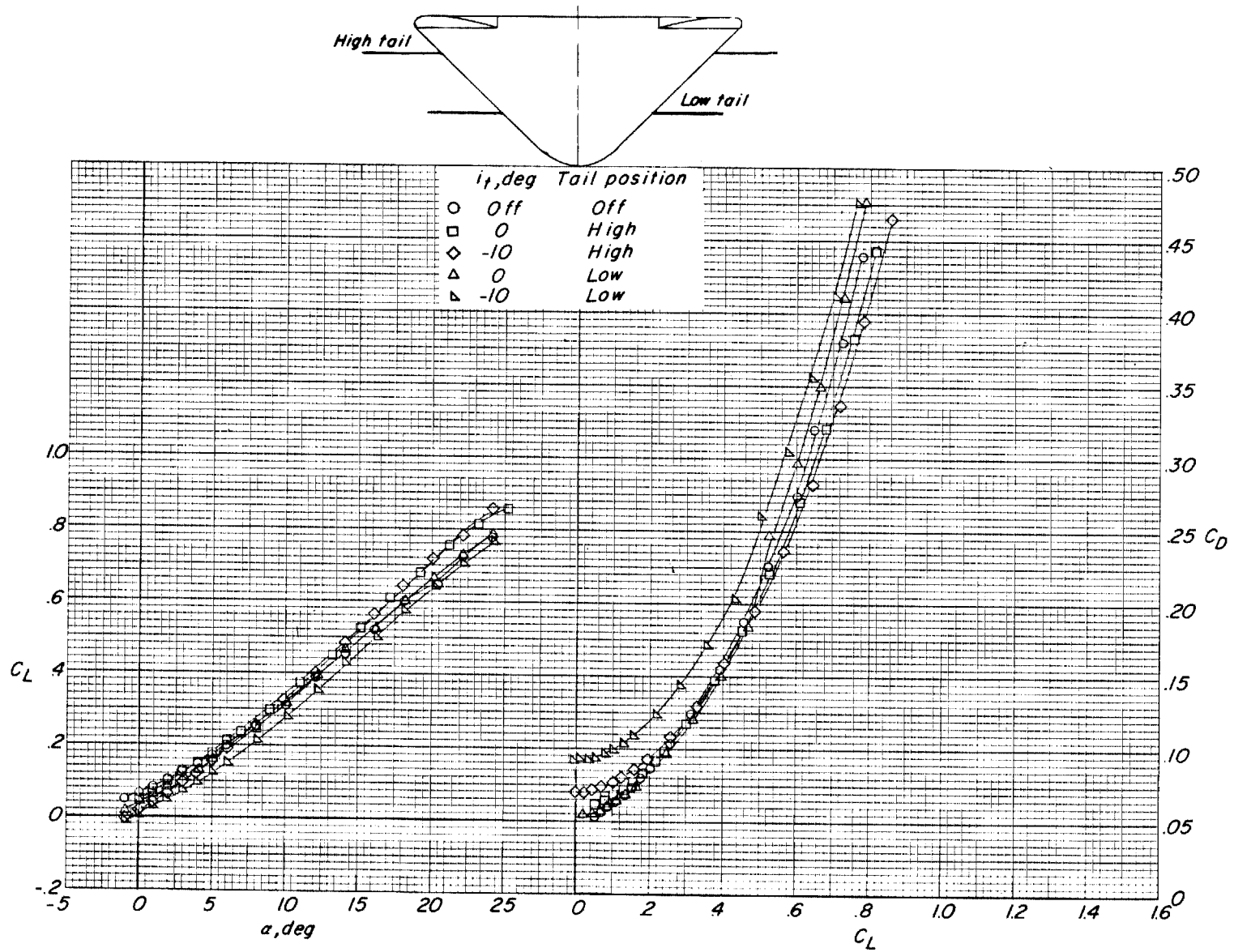

Figure 7.- The effects of horizontal-tail location and deflection on the longitudinal aerodynamic characteristics of the configuration having the wing panel swept back 80°. δ_f = Off; M = 0.40.

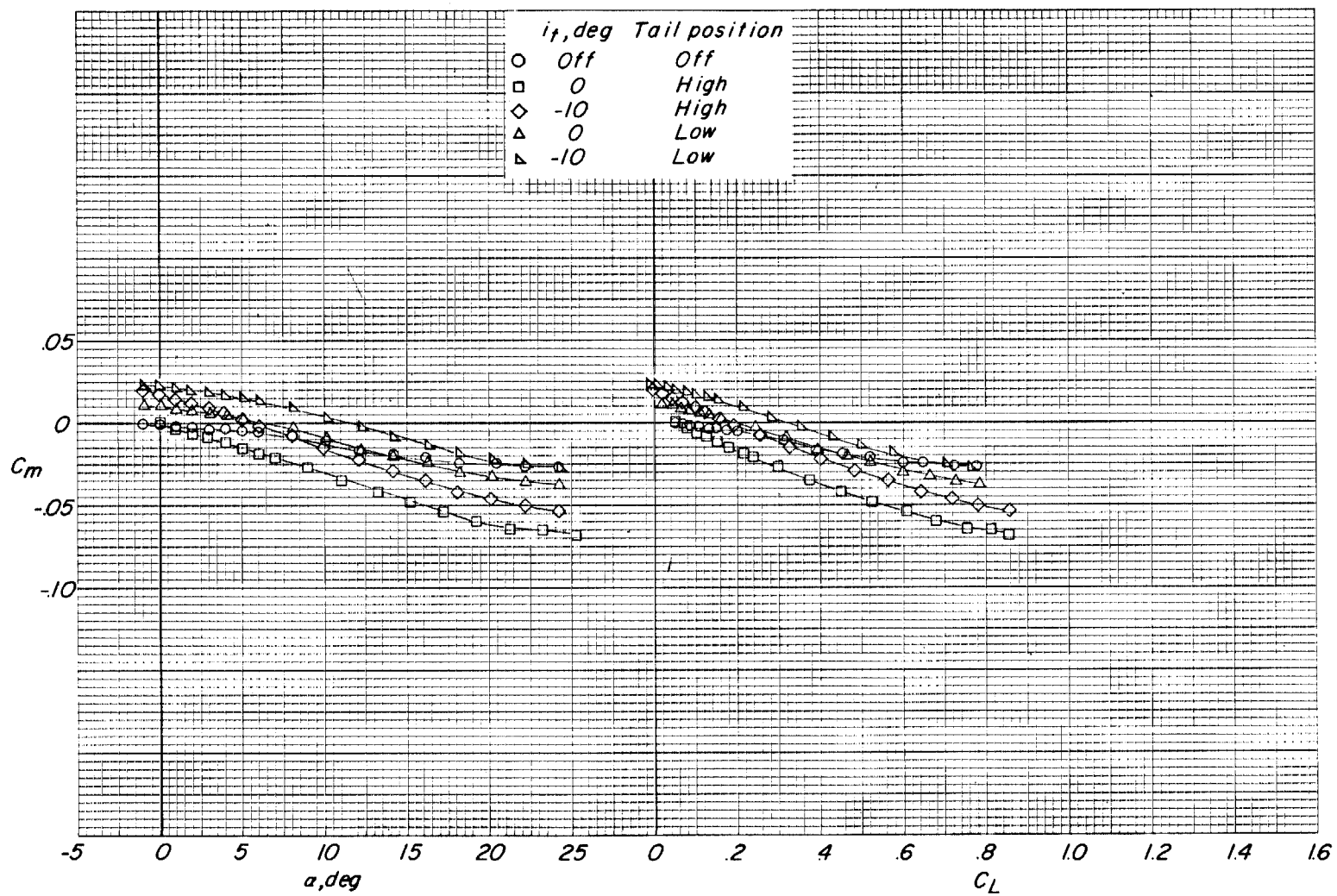

Figure 7.- Concluded.

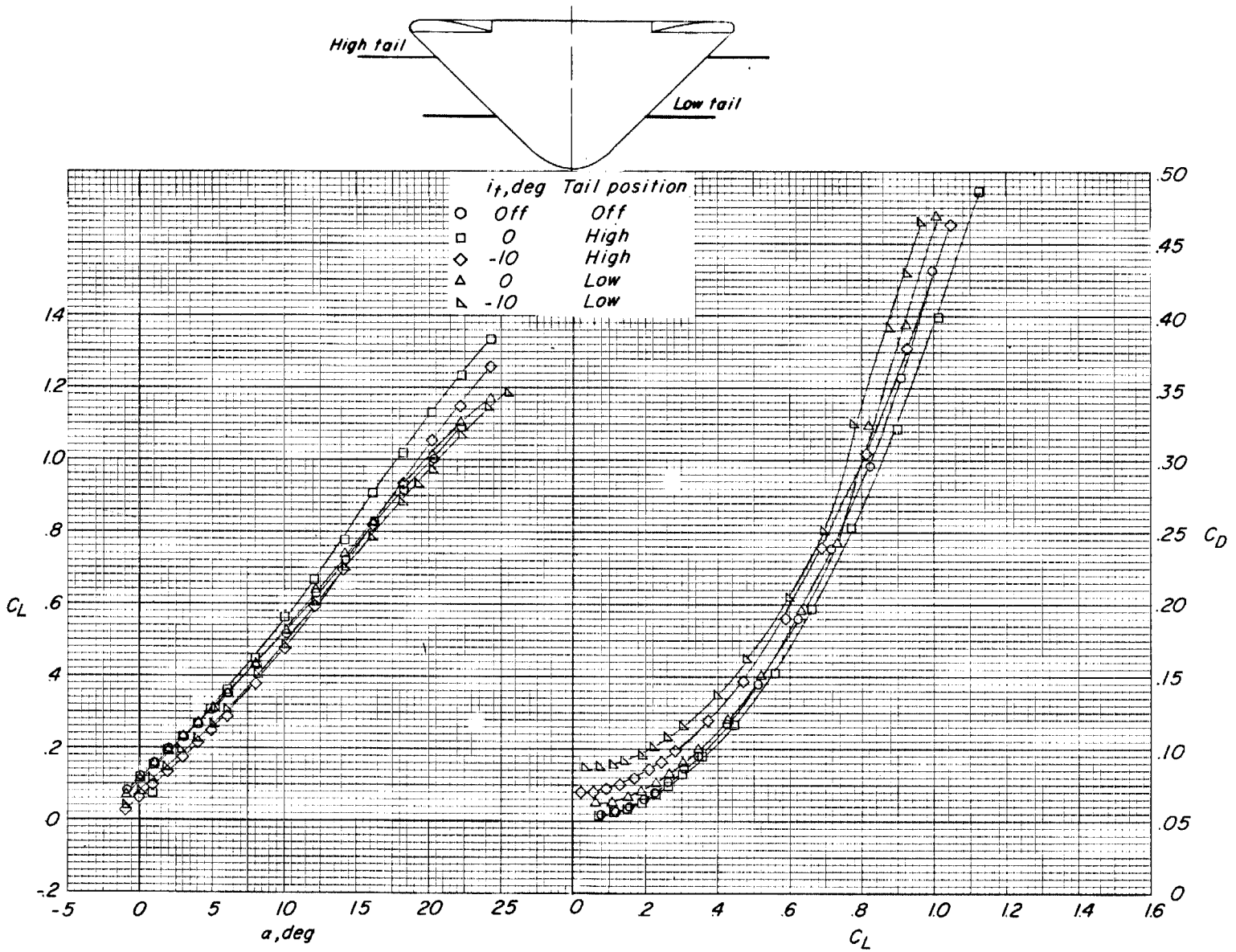

Figure 8.- The effects of horizontal-tail location and deflection on the longitudinal aerodynamic characteristics of the configuration having the wing panel swept back 60°. δ_f = Off; M = 0.40.

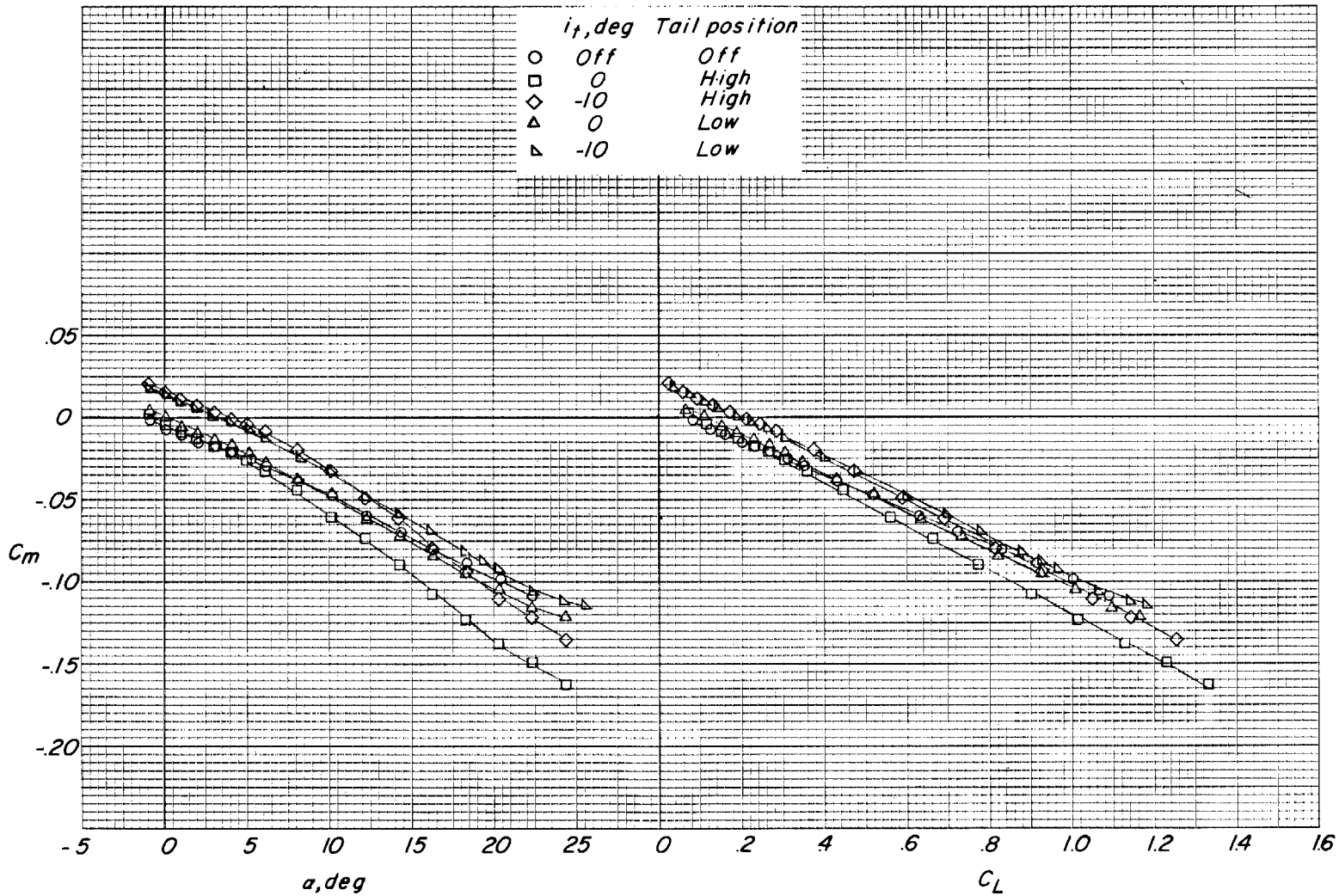

Figure 8.- Concluded.

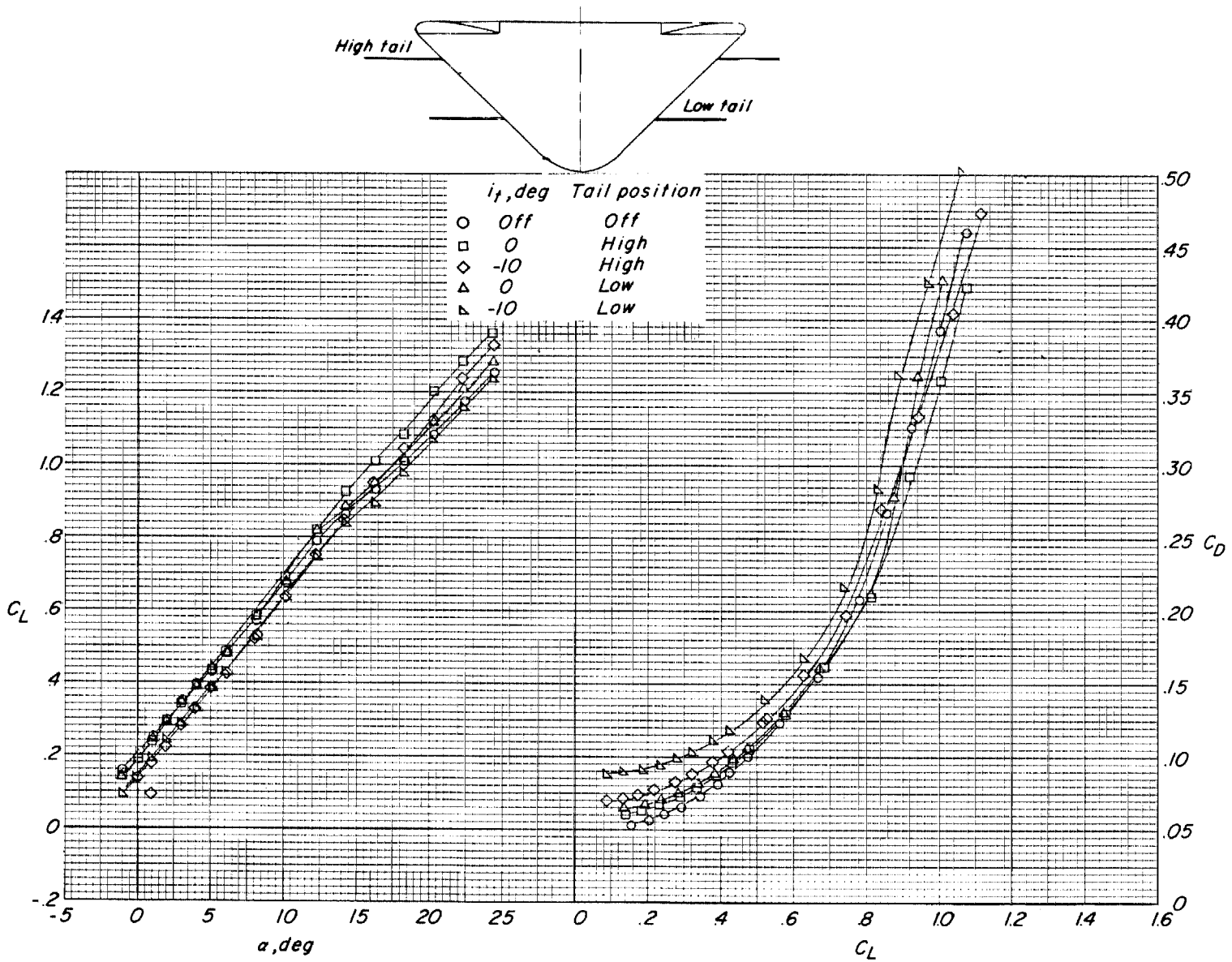

Figure 9.- The effects of horizontal-tail location and deflection on the longitudinal aerodynamic characteristics of the configuration having the wing panel swept back 40°. δ_f = Off; M = 0.40.

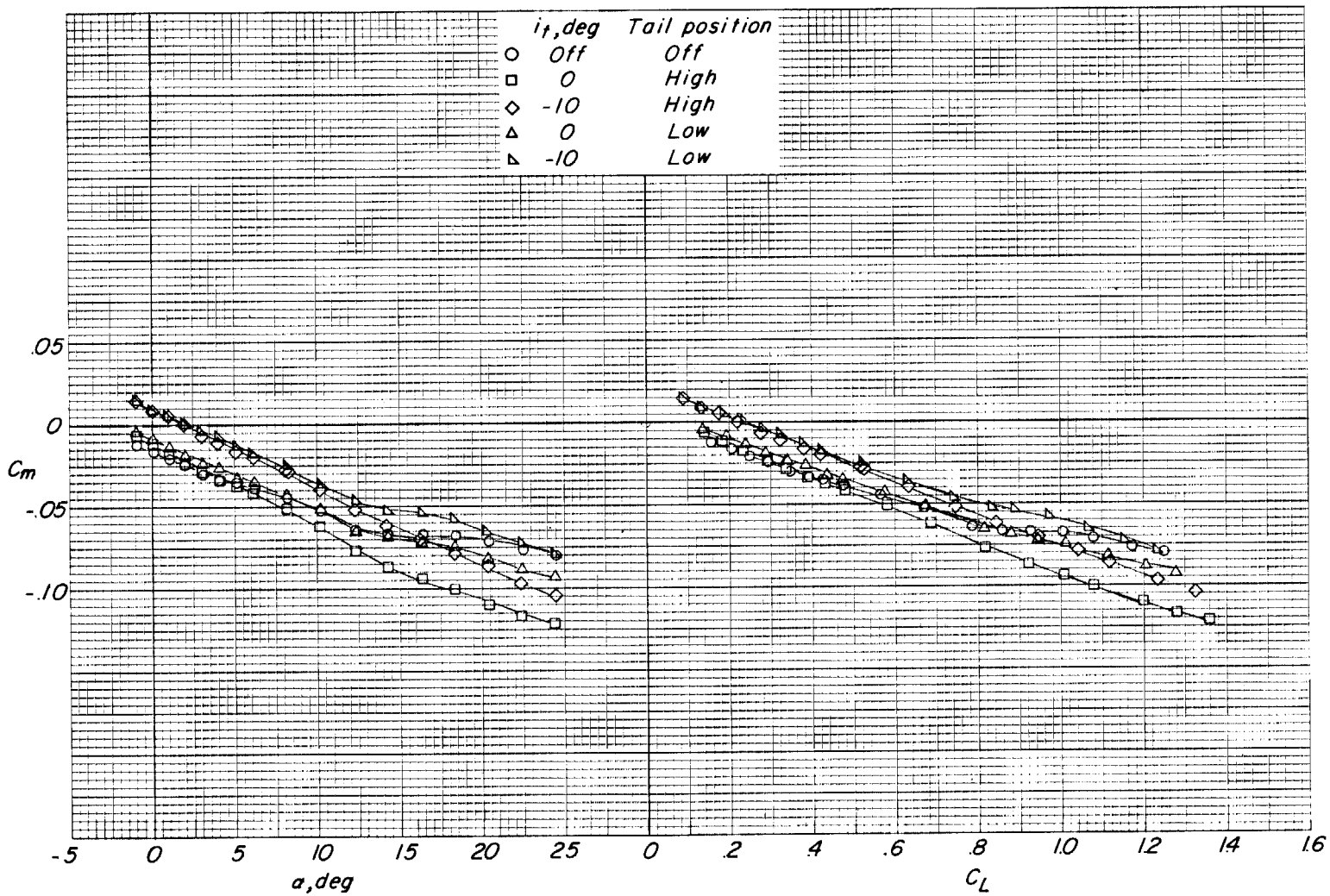

Figure 9.- Concluded.

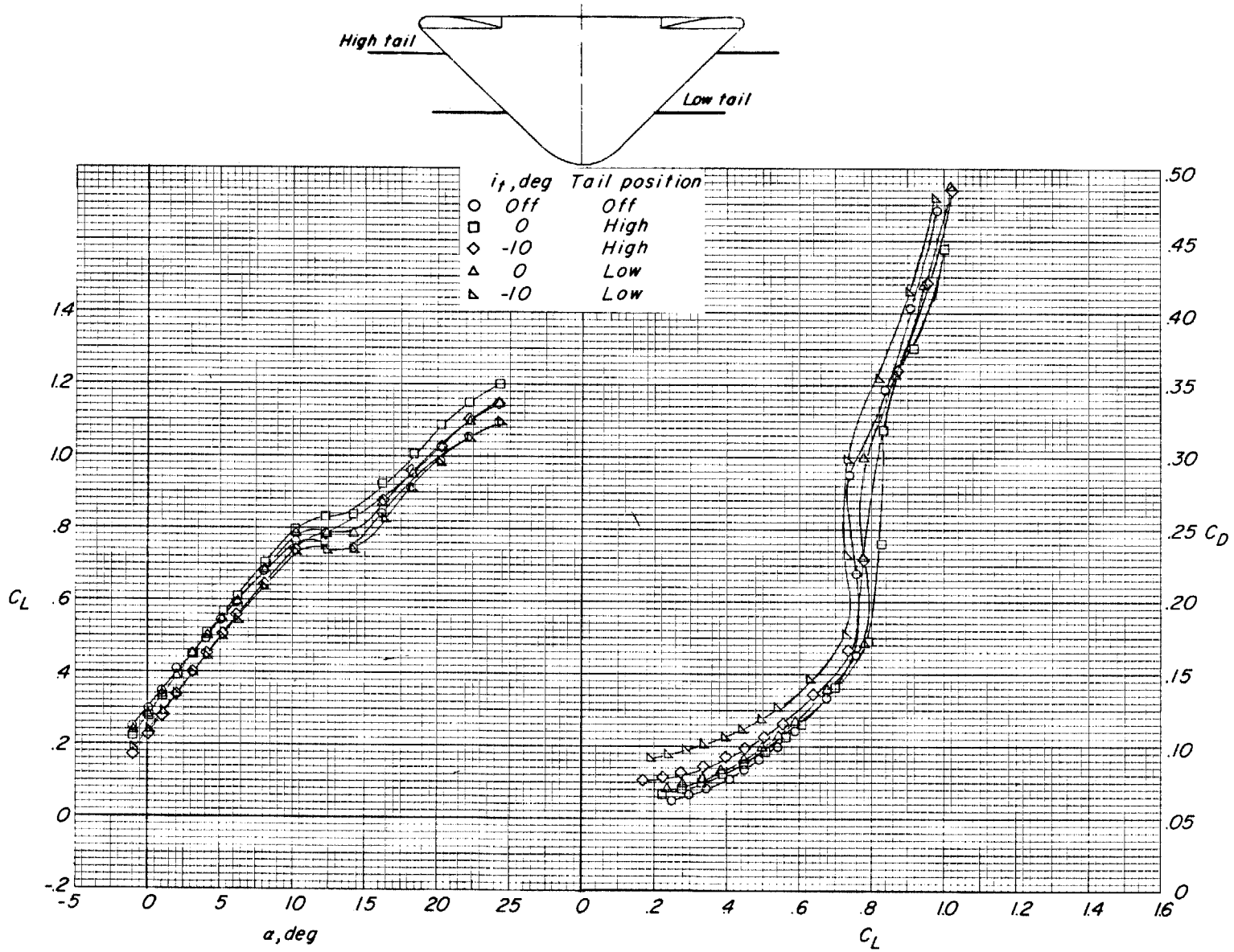

Figure 10.- The effects of horizontal-tail location and deflection on the longitudinal aerodynamic characteristics of the configuration having the wing panel swept back 20°. δ_f = Off; M = 0.40.

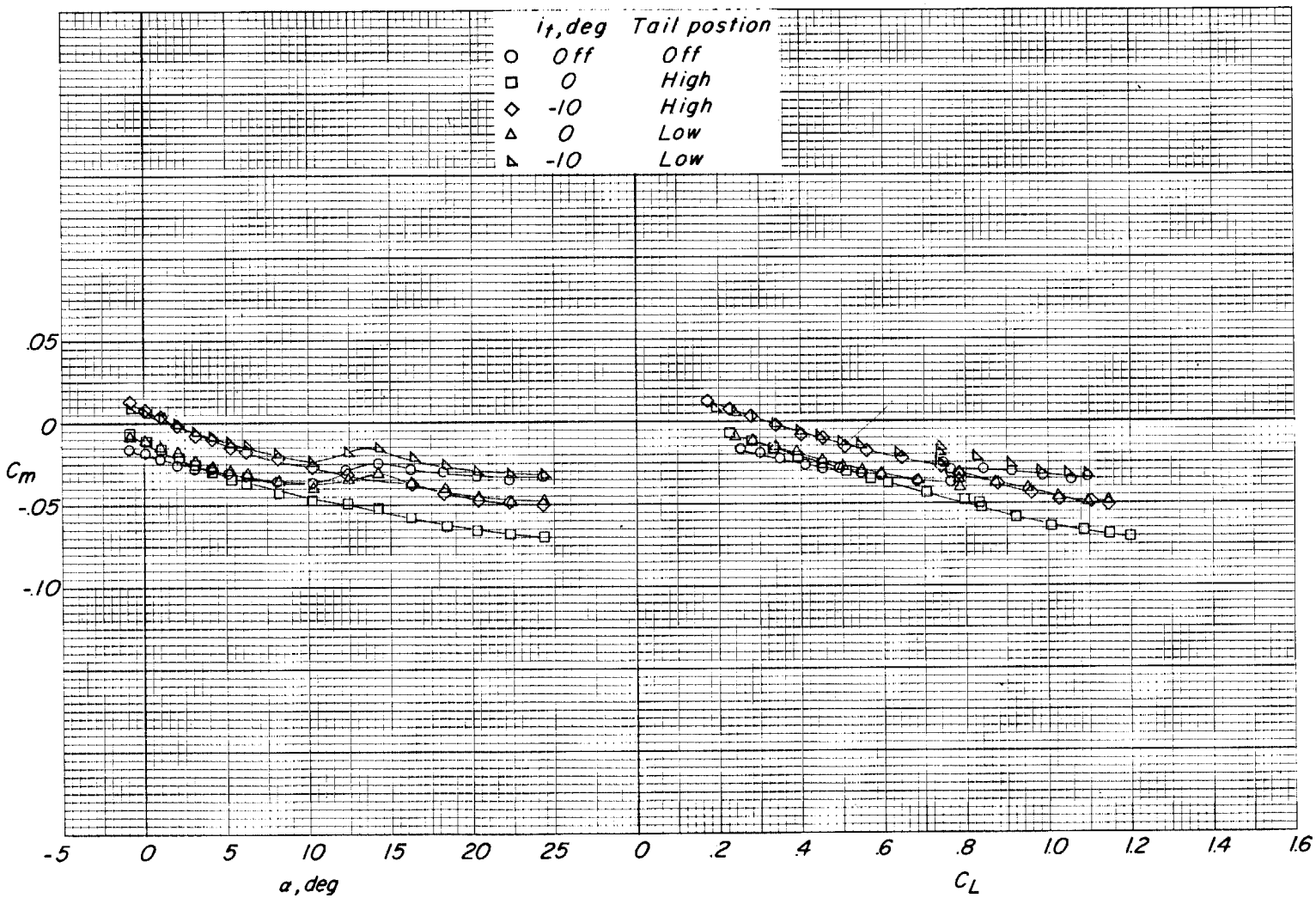

Figure 10.- Concluded.

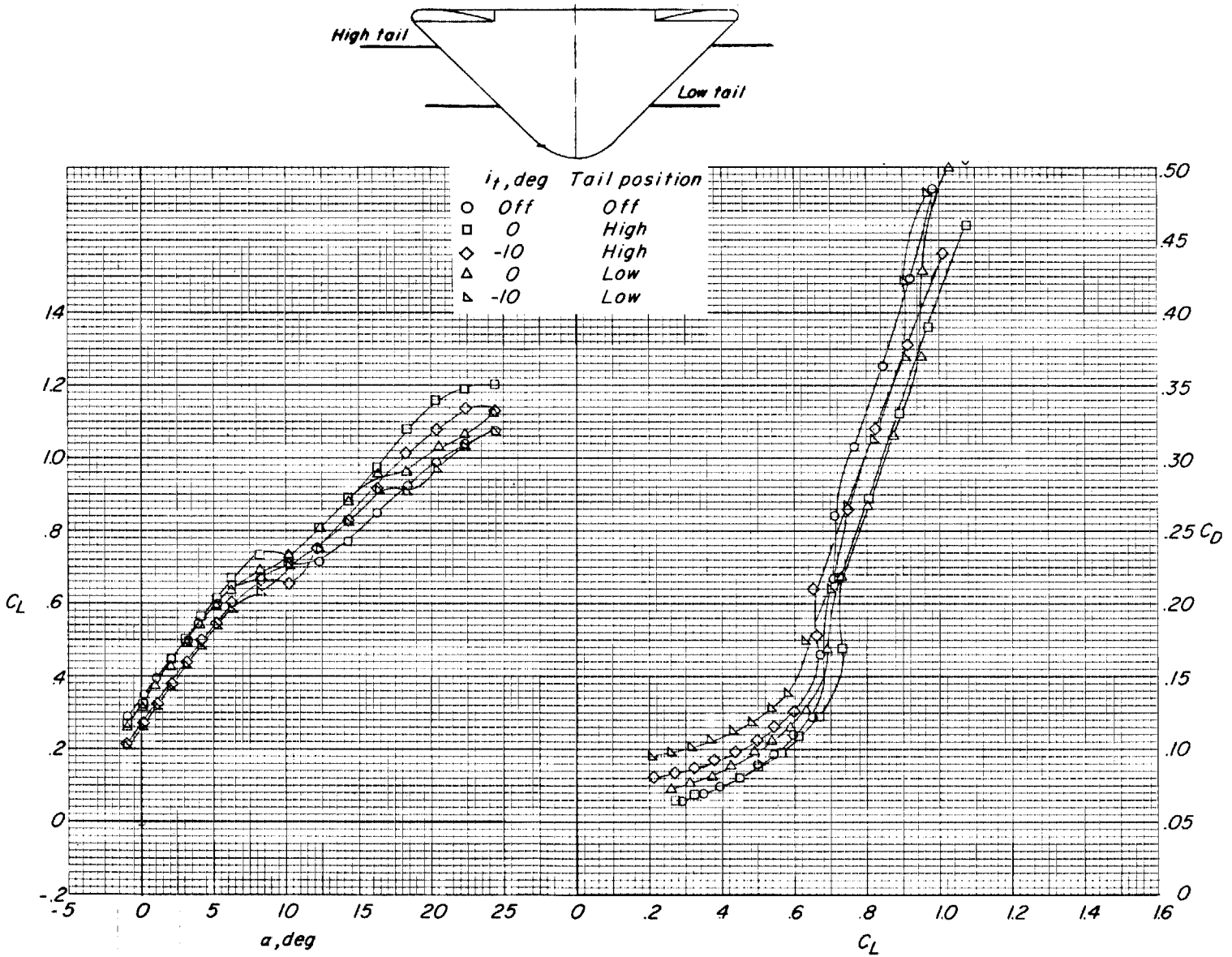

Figure 11.- The effects of horizontal-tail location and deflection on the longitudinal aerodynamic characteristics of the configuration having the wing panel at 0° of sweep. δ_f = Off; M = 0.40.

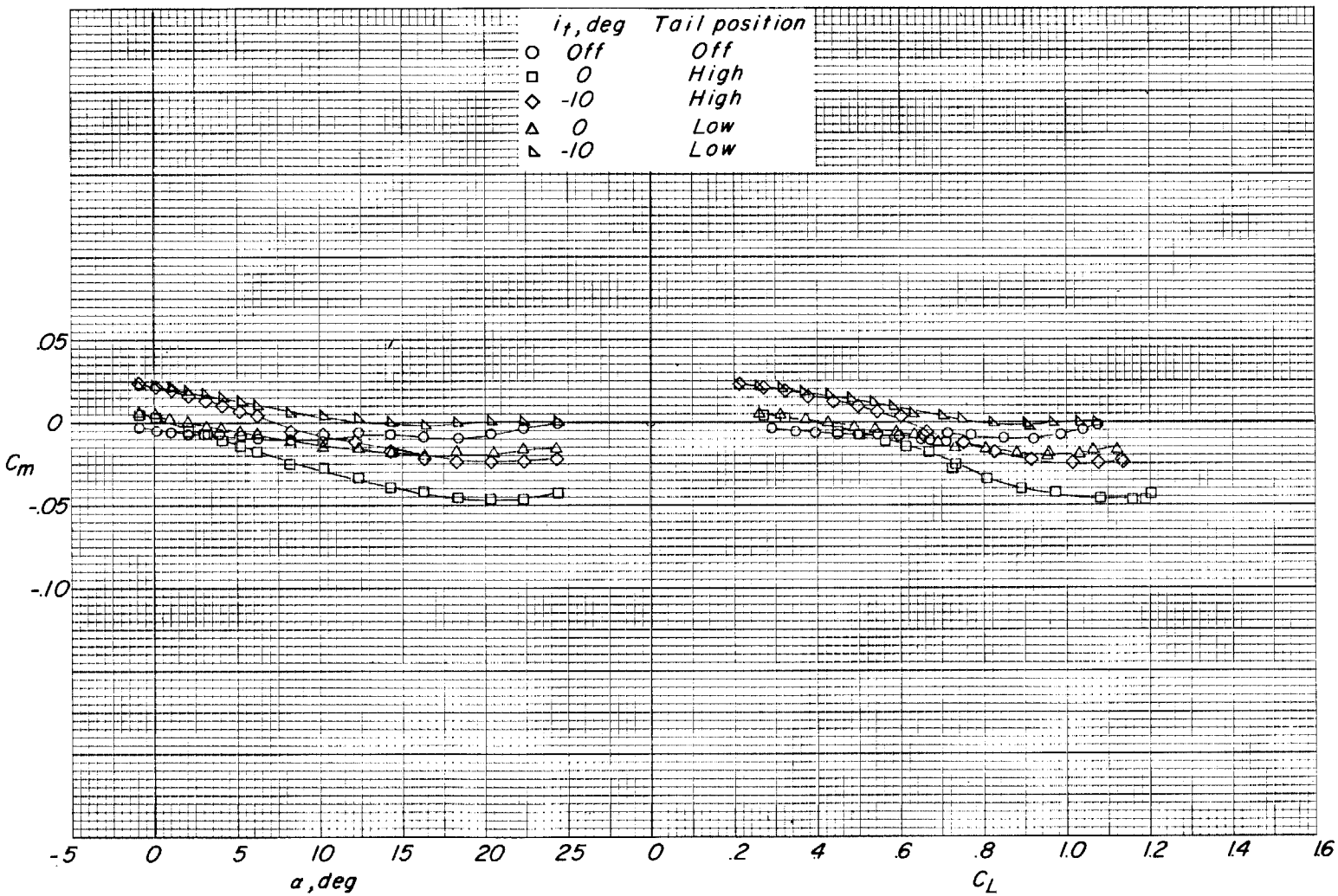

Figure 11.- Concluded.

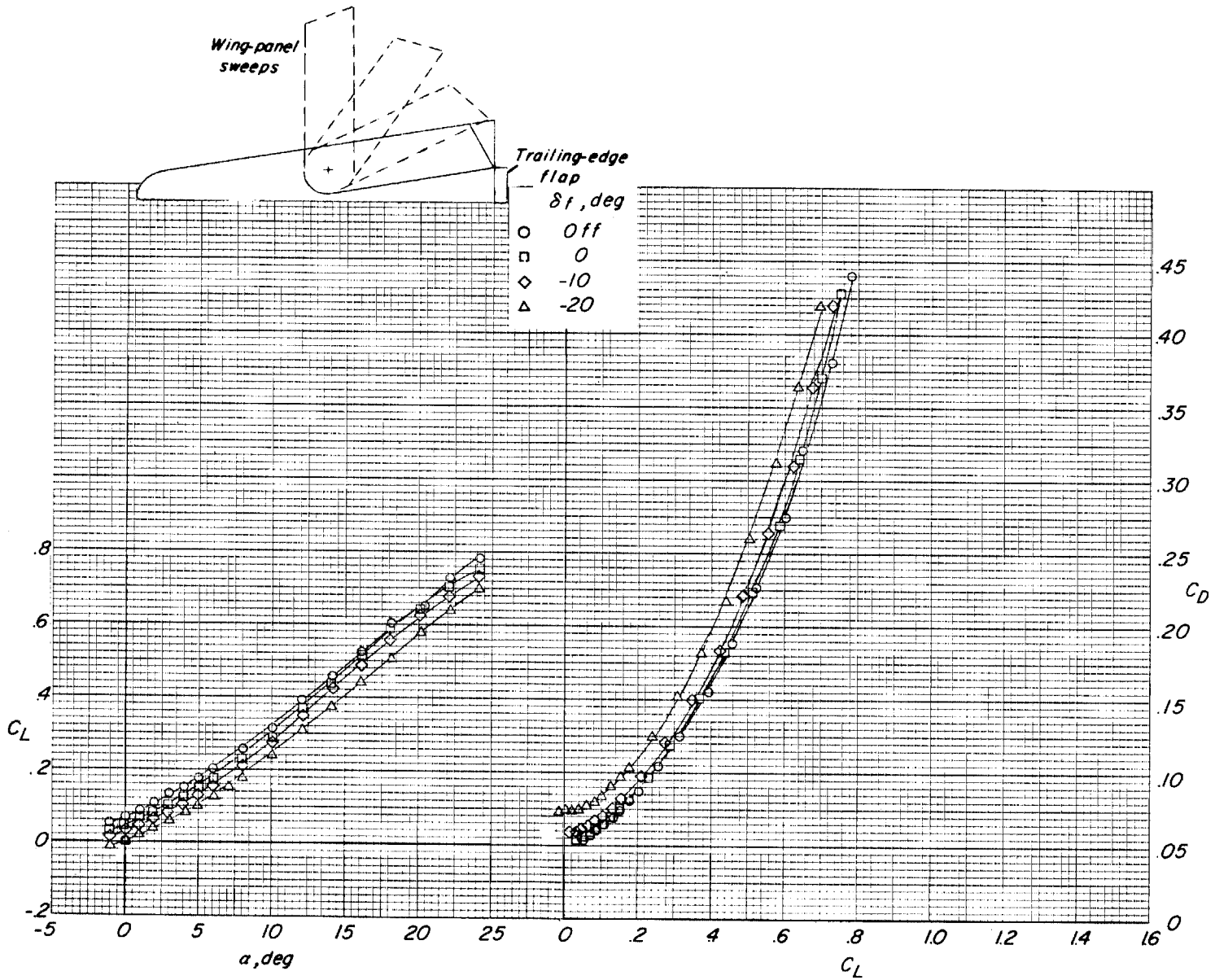

Figure 12.- The effects of the addition and deflection of a trailing-edge flap located at the base of the basic configuration on the longitudinal aerodynamic characteristics of the configuration having the wing panel swept back 80°. i_t = Off; M = 0.40.

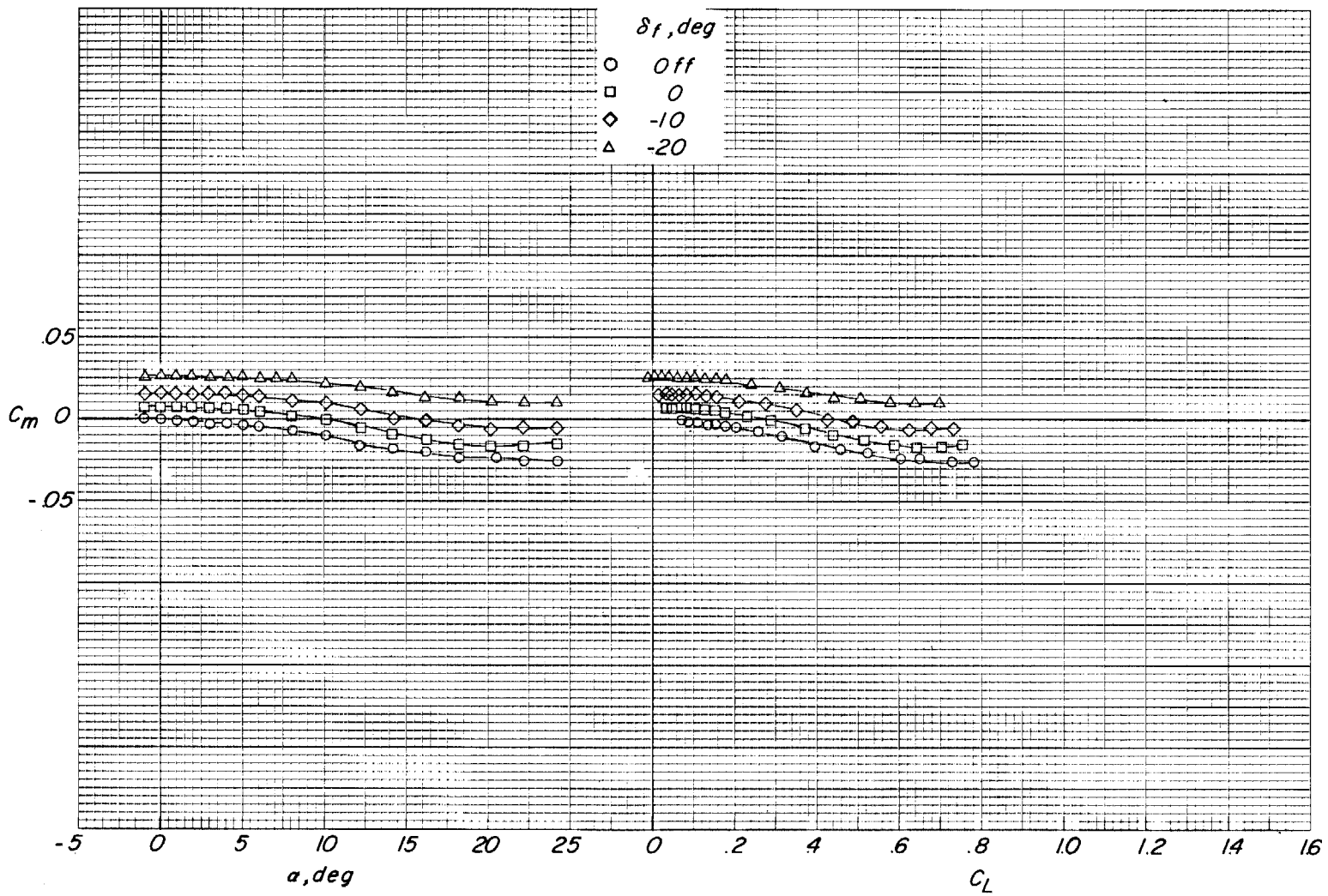

Figure 12.- Concluded.

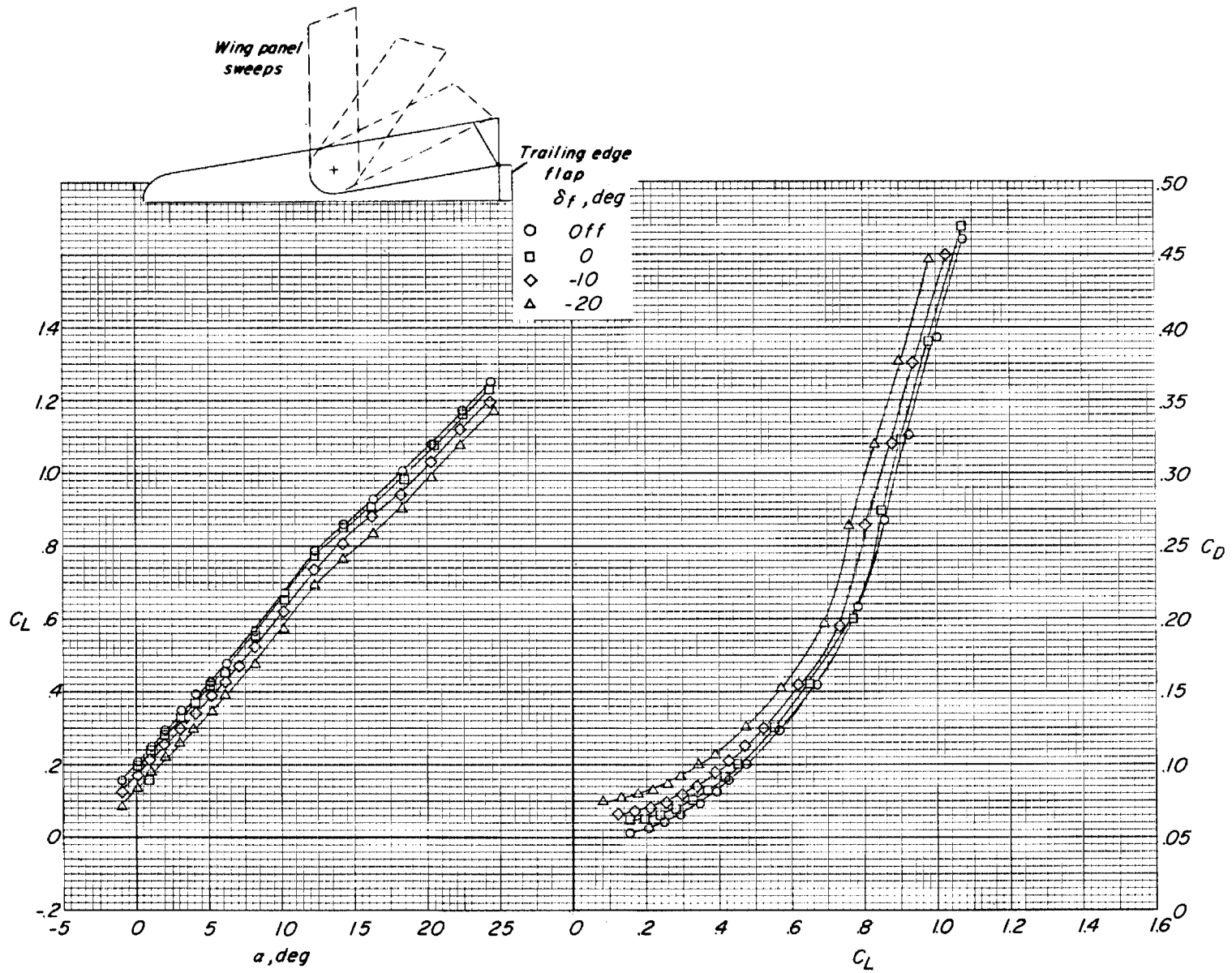

Figure 13.- The effects of the addition and deflection of a trailing-edge flap located at the base of the basic configuration on the longitudinal aerodynamic characteristics of the configuration having the wing panel swept back 40°. i_t = -0°; M = 0.40.

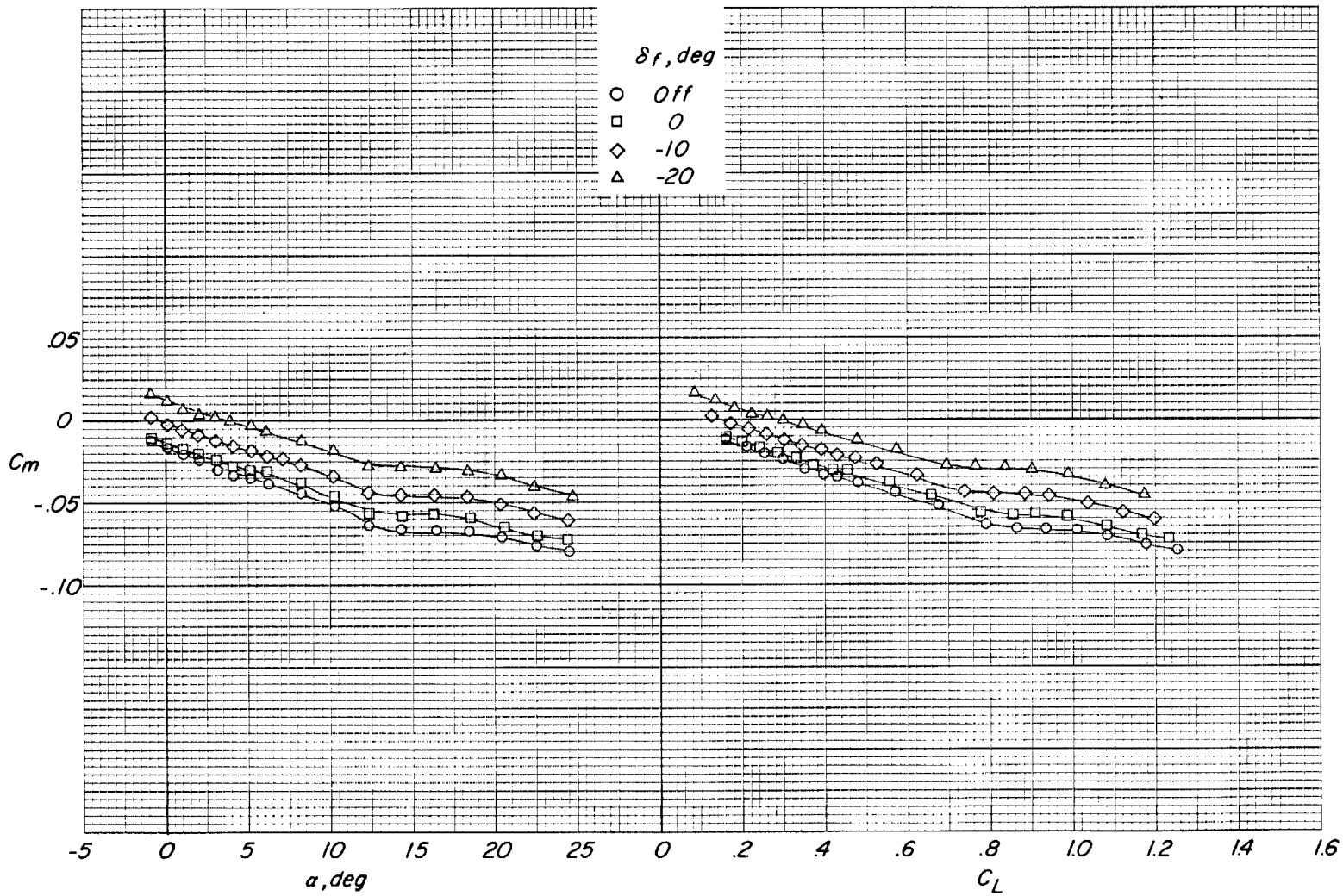

Figure 13.- Concluded.

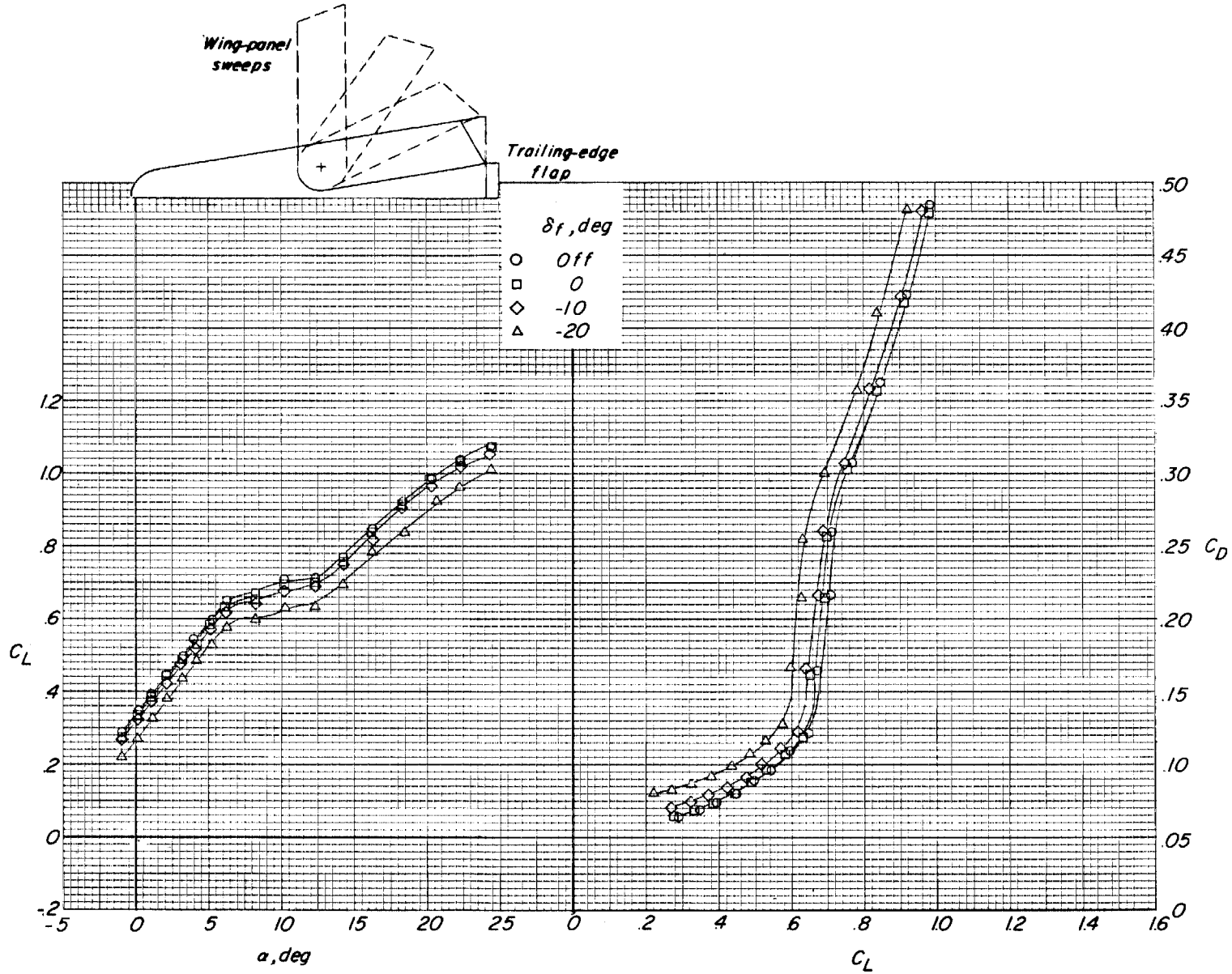

Figure 14.- The effects of the addition and deflection of a trailing-edge flap located at the base of the basic configuration on the longitudinal aerodynamic characteristics of the configuration having the wing panel at 0° of sweep. $i_t = 0°$; M = 0.40.

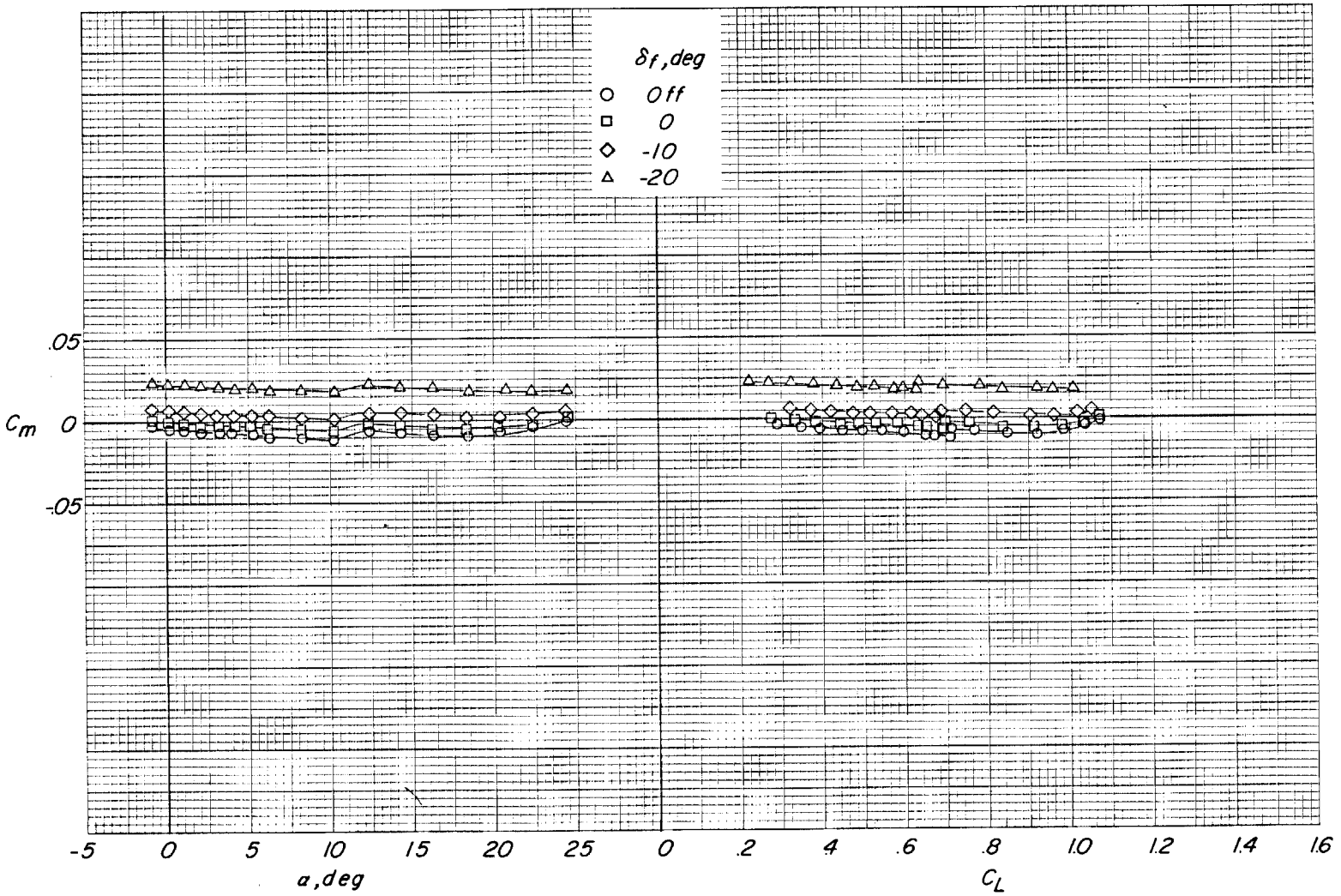

Figure 14.- Concluded.

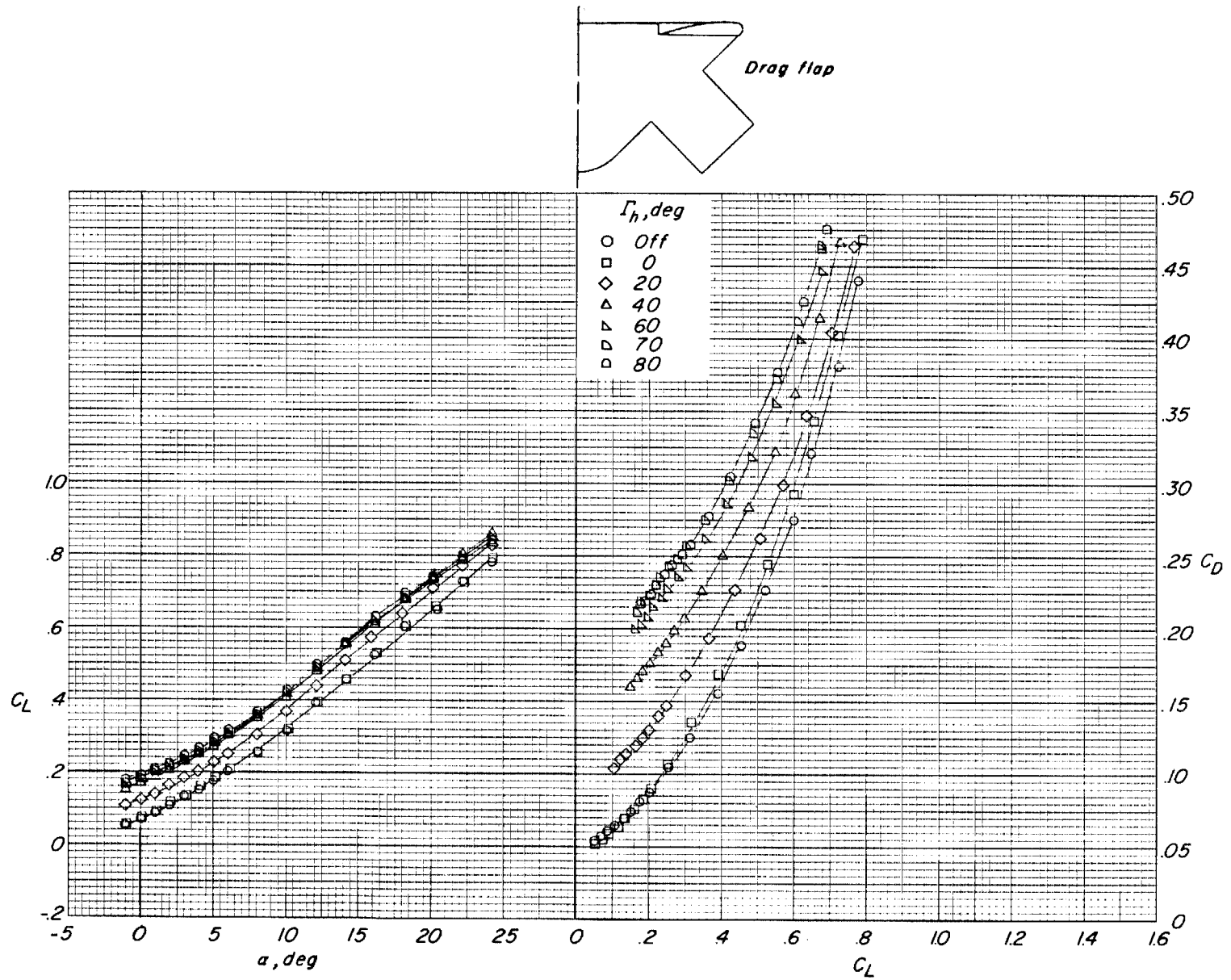

Figure 15.- The effects of the addition and deflection of flaps located on the underside of the basic configuration on the longitudinal aerodynamic characteristics of the basic configuration. $i_t = 0^o$; $\delta_f = 0^o$; $\Lambda_{LE} = 80^o$; M = 0.40.

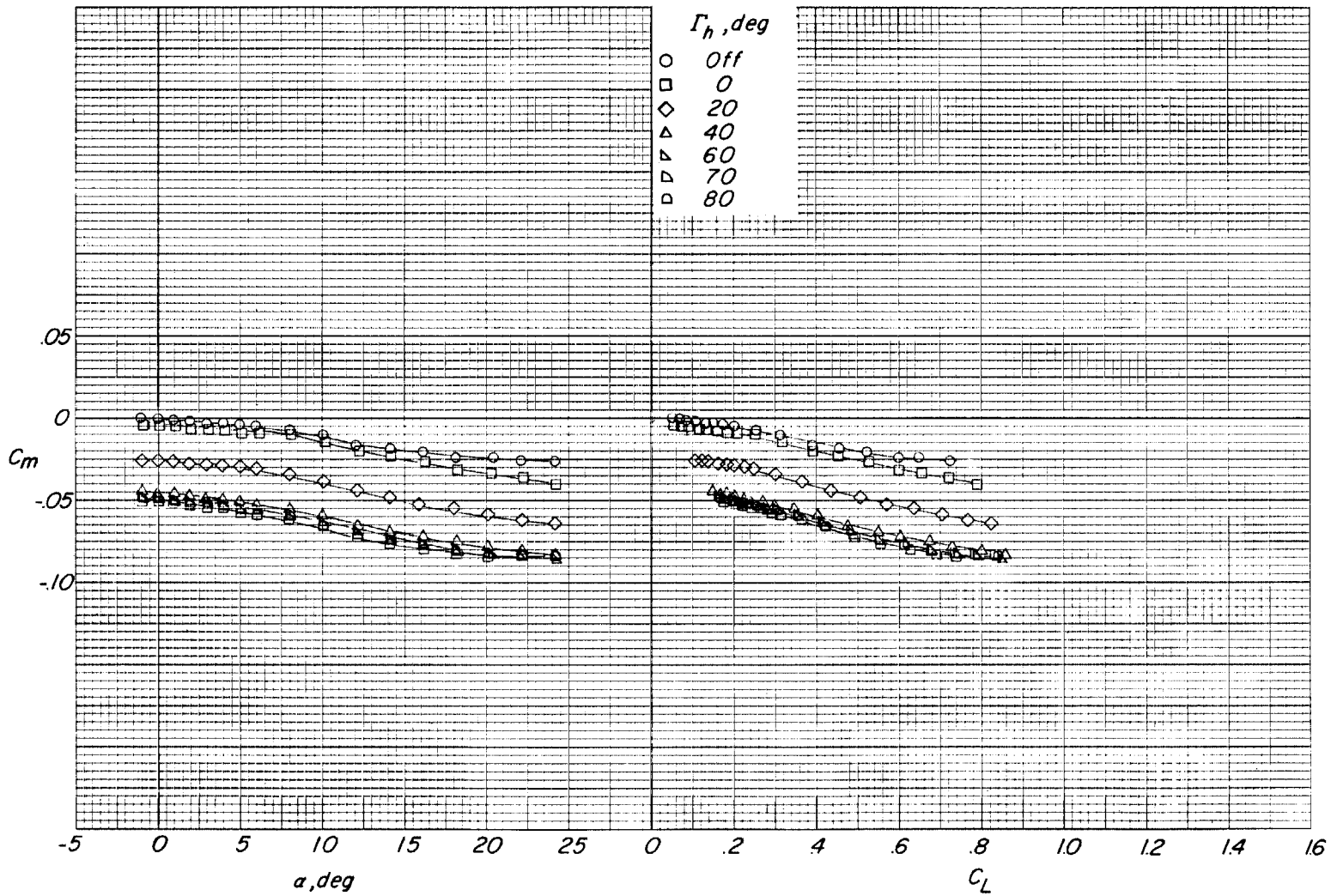

Figure 15.- Concluded.

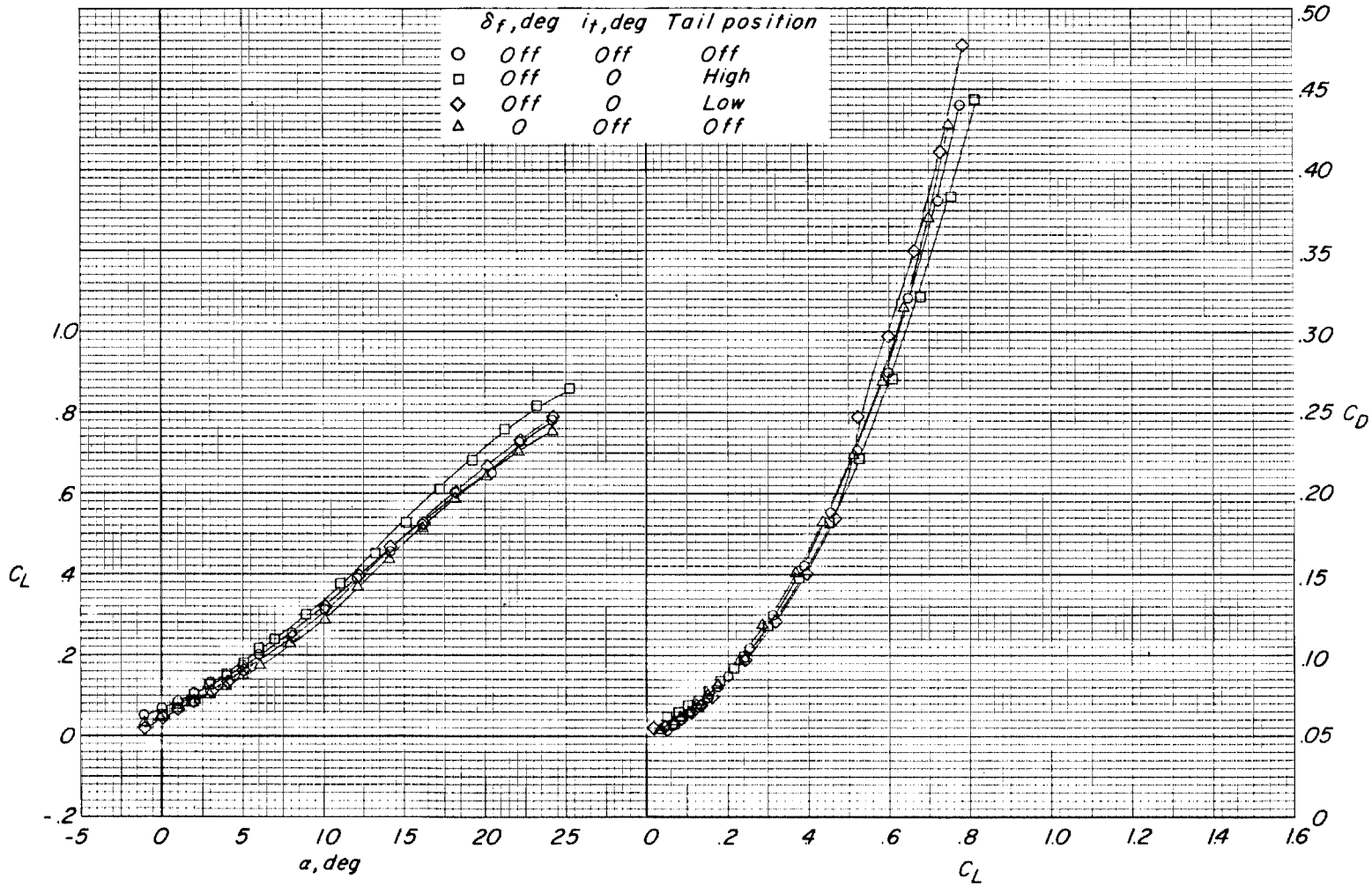

Figure 16.- A comparison of the effects of various longitudinal controls on the longitudinal aerodynamic characteristics of the basic configuration. $\Lambda_{LE} = 80^\circ$; M = 0.40.

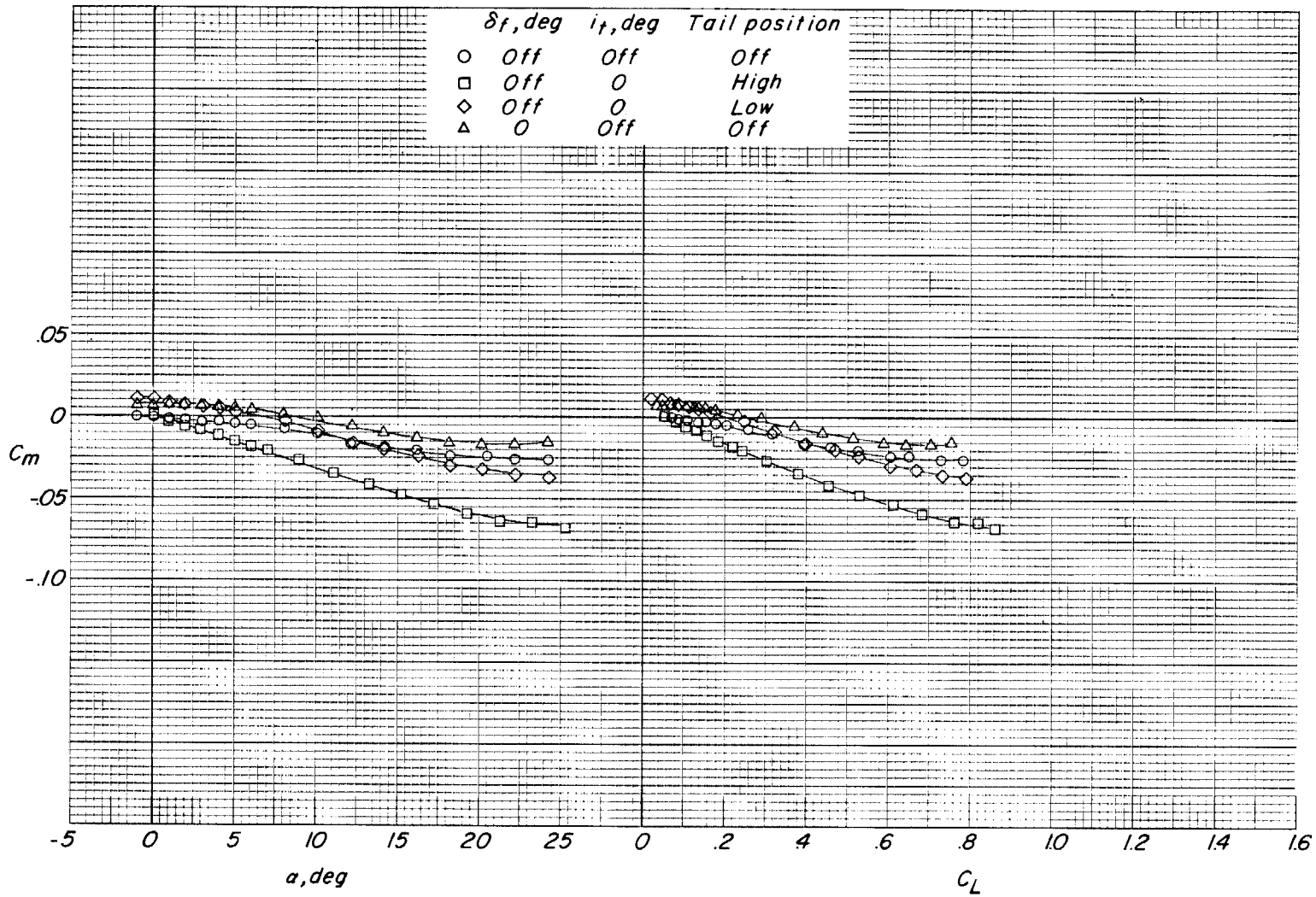

Figure 16.- Concluded.

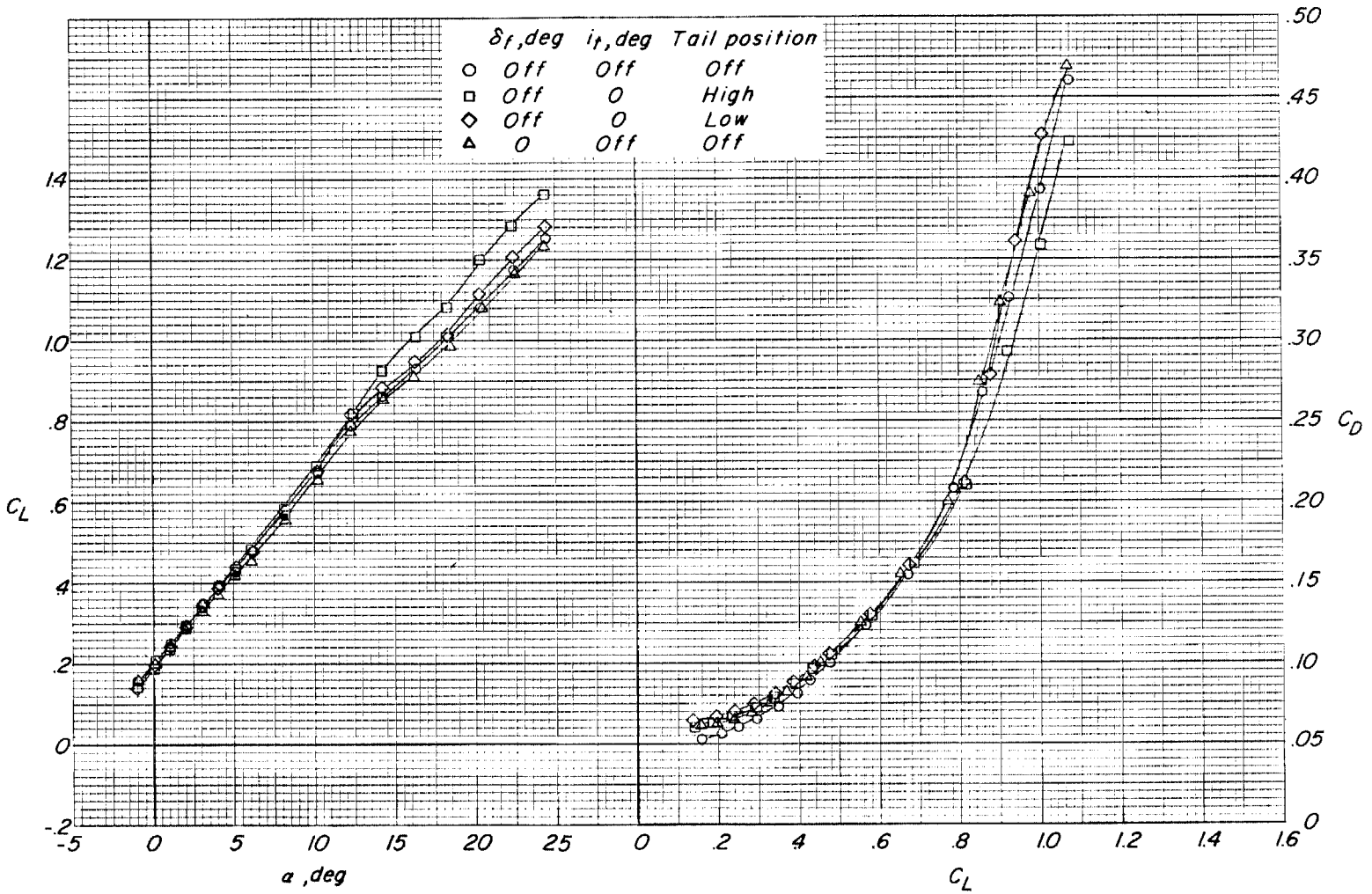

Figure 17.- A comparison of the effects of various longitudinal controls on the longitudinal aerodynamic characteristics of the configuration having the wing panel swept back 40°. M = 0.40.

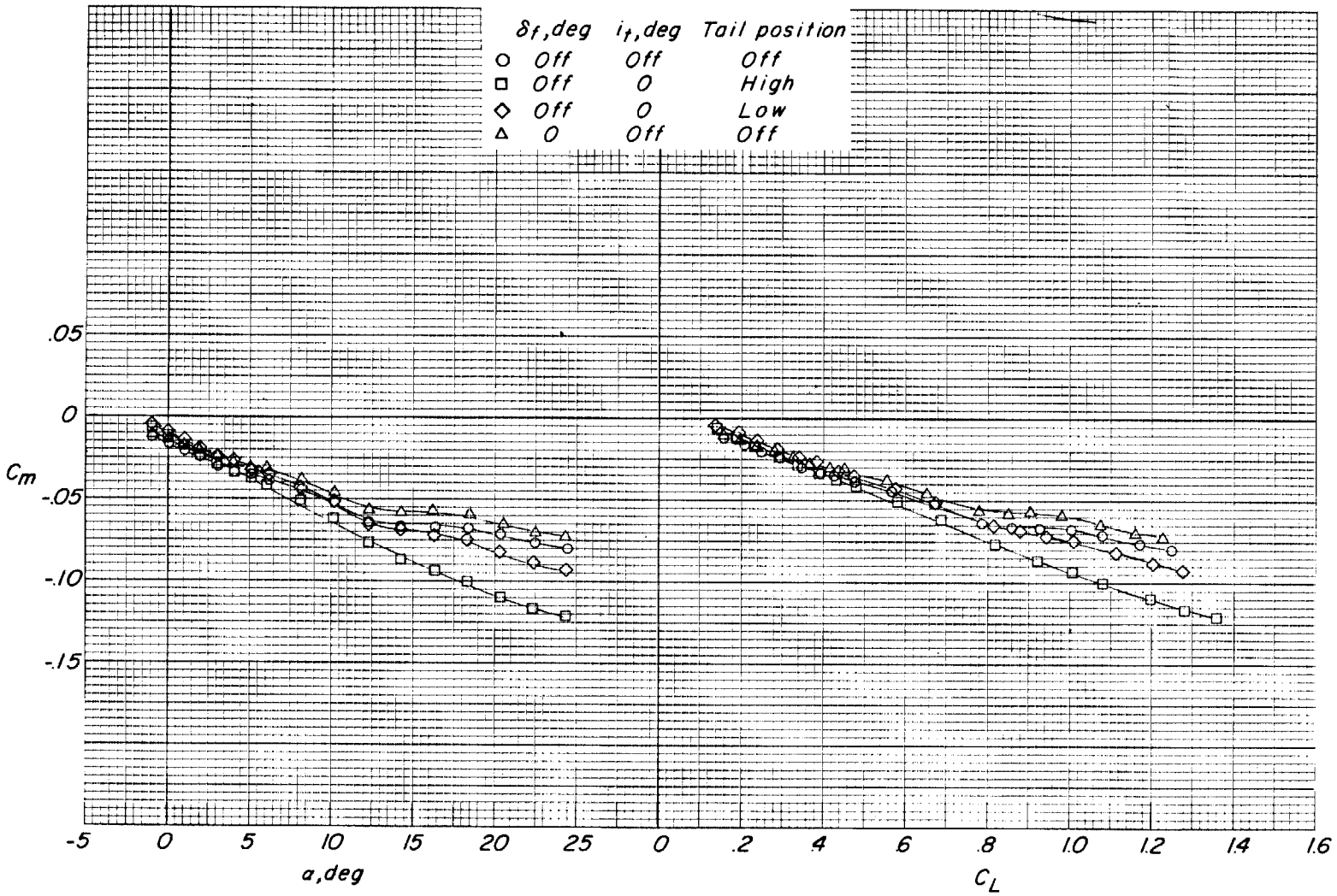

Figure 17.- Concluded.

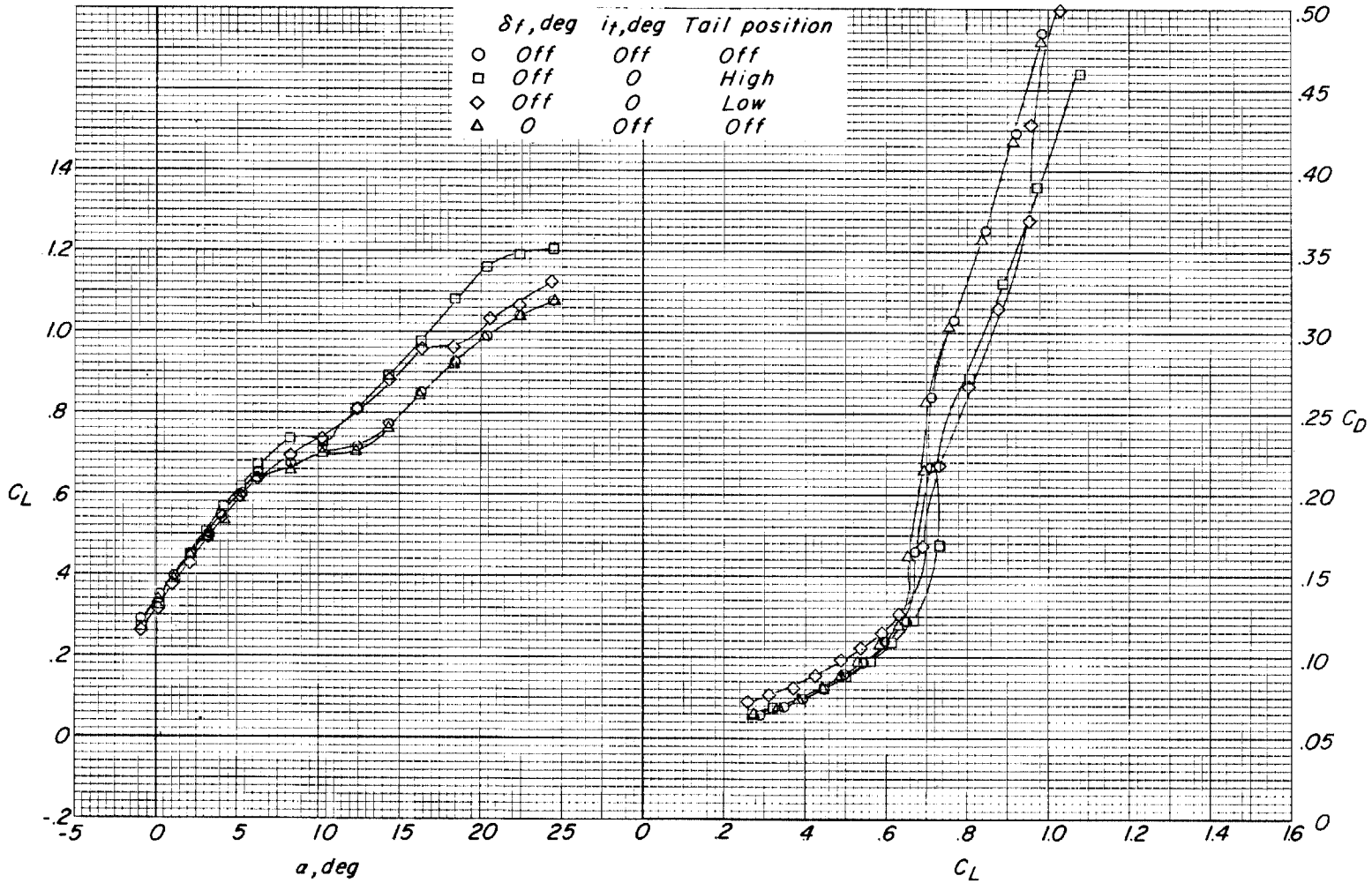

Figure 18.- A comparison of the effects of various longitudinal controls on the longitudinal aerodynamic characteristics of the configuration having the wing panel at 0° of sweep. M = 0.40.

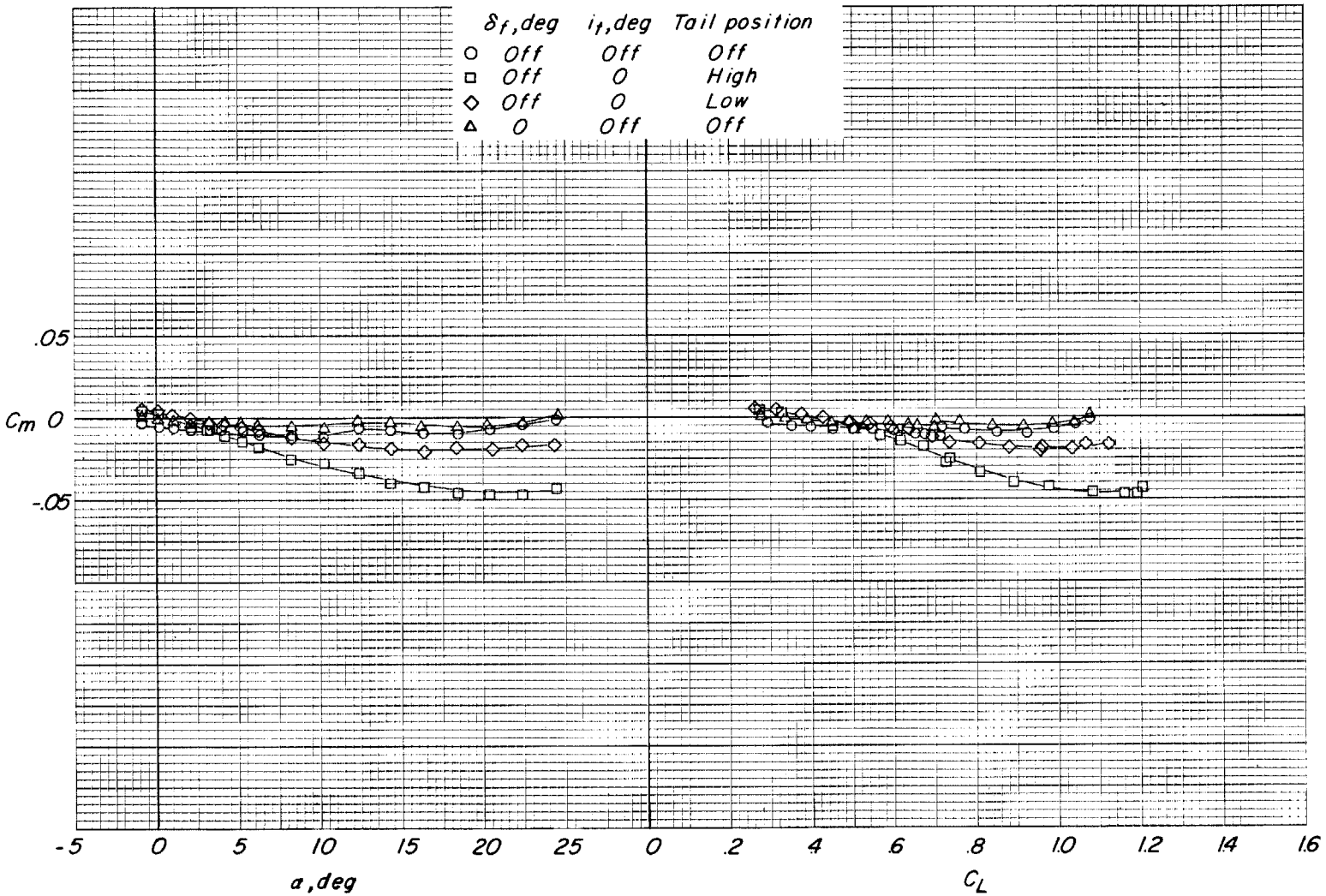

Figure 18.- Concluded.

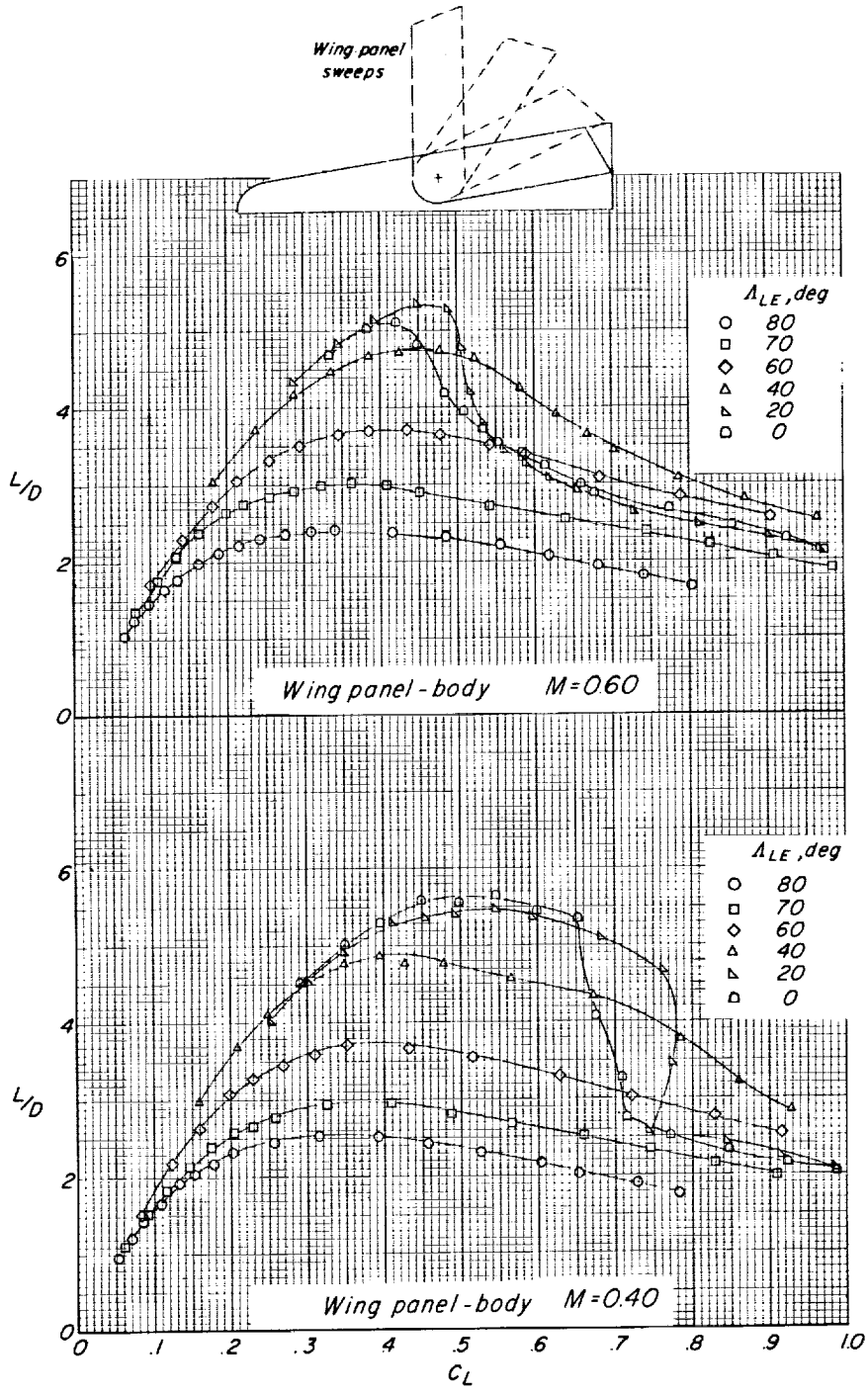

(a) M = 0.40 and 0.60.

Figure 19.- Lift-drag ratios for various wing-panel sweeps at various Mach numbers. All longitudinal controls off.

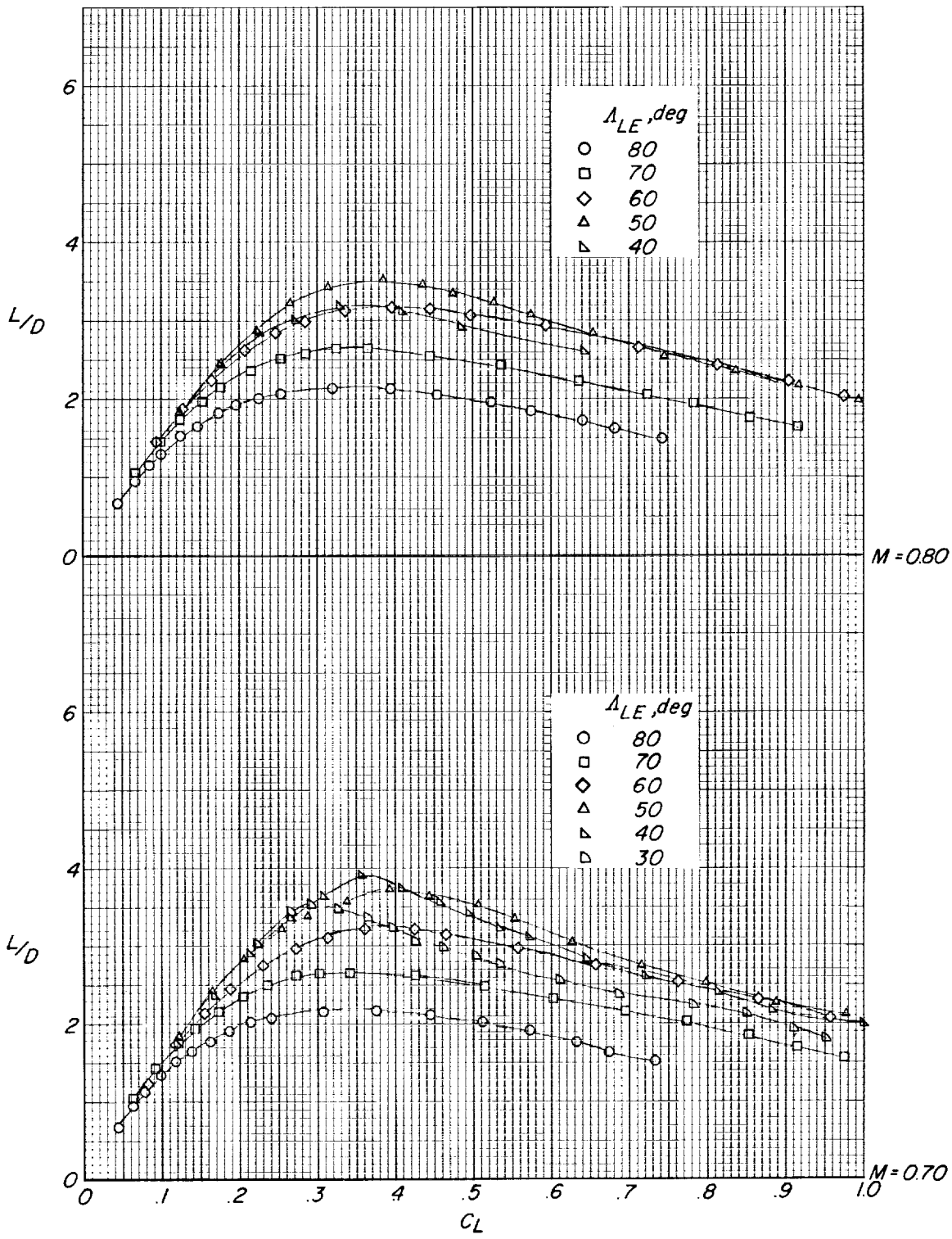

(b) M = 0.70 and 0.80.

Figure 19.- Continued.

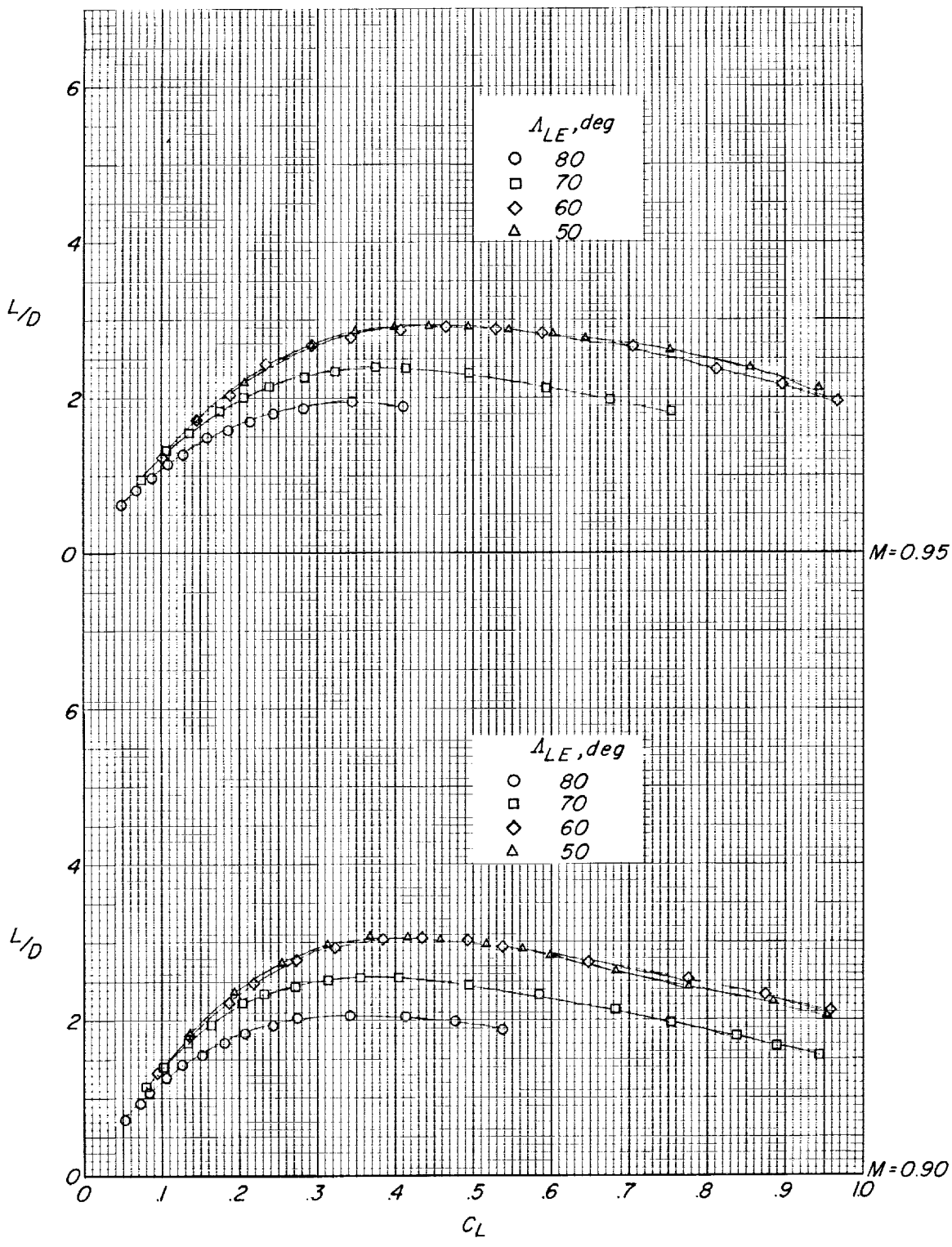

(c) M = 0.90 and 0.95.

Figure 19.- Concluded.

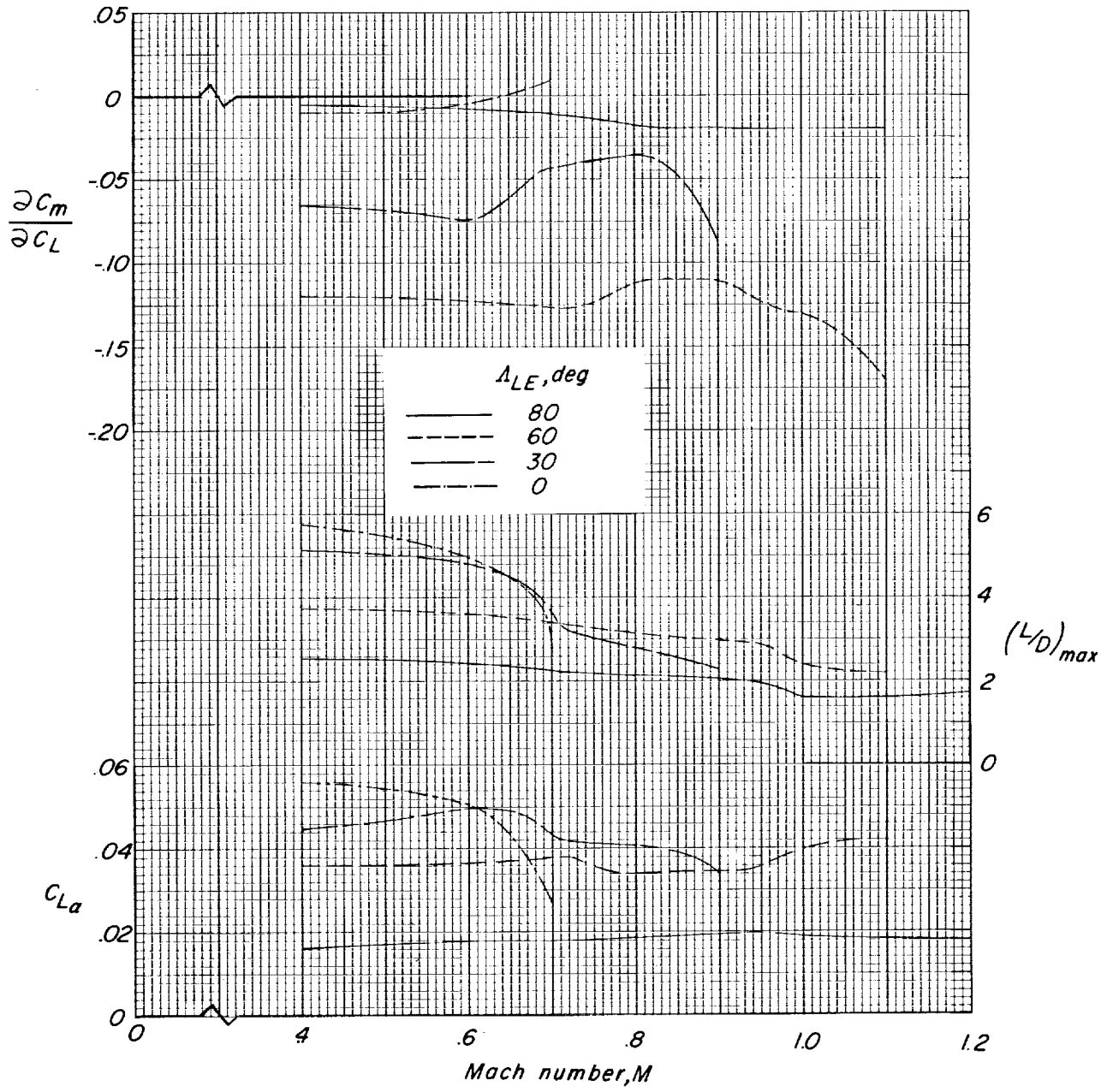

Figure 20.- Summary of the effects of increasing Mach number on the longitudinal aerodynamic parameters C_{L_α}, $(L/D)_{max}$, and $\partial C_m/\partial C_L$ for the range of wing-panel sweeps. All controls off.

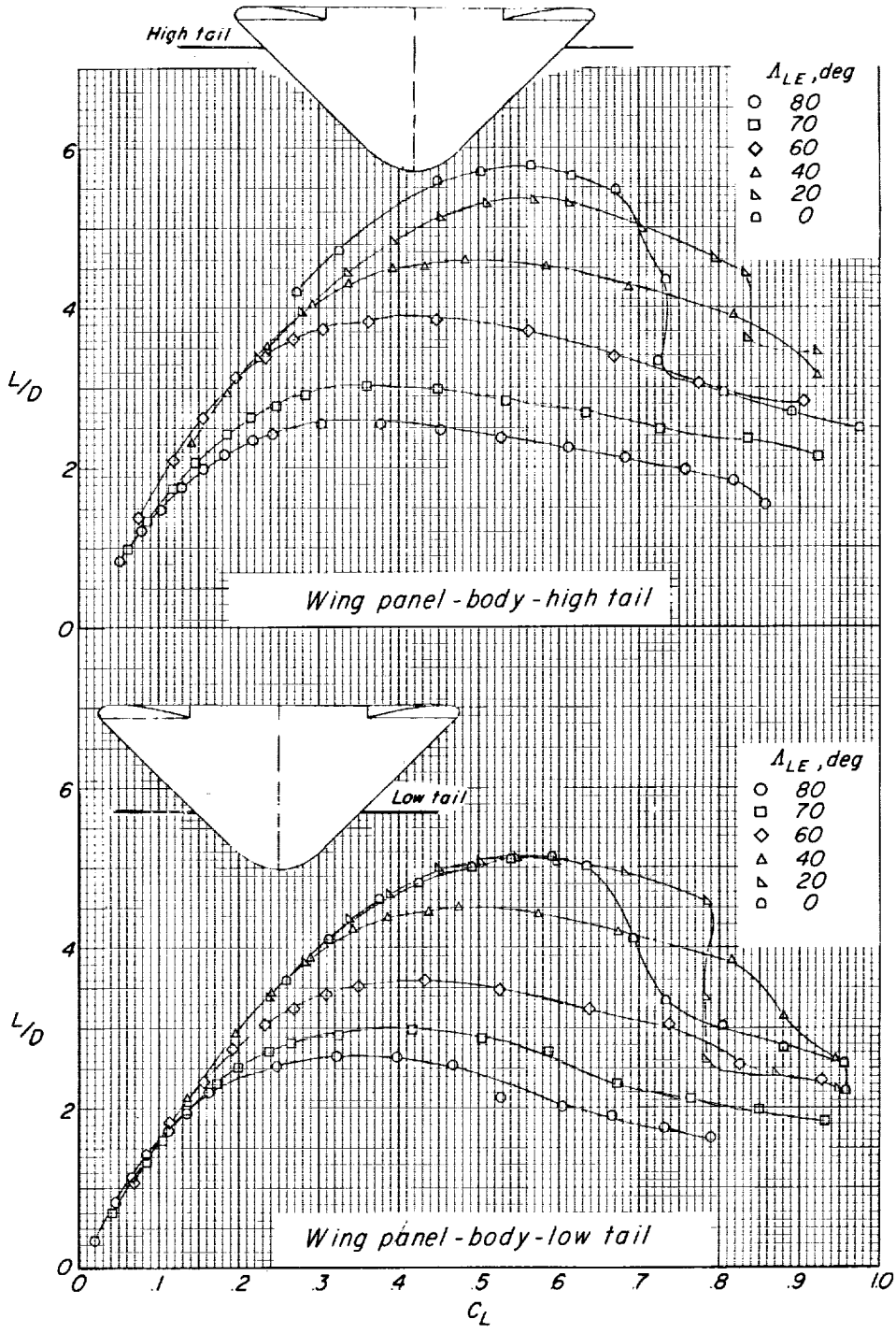

Figure 21.- Lift-drag ratios for various wing-panel sweeps and the configurations having low or high horizontal tails. $i_t = 0^o$; δ_f = Off; M = 0.40.

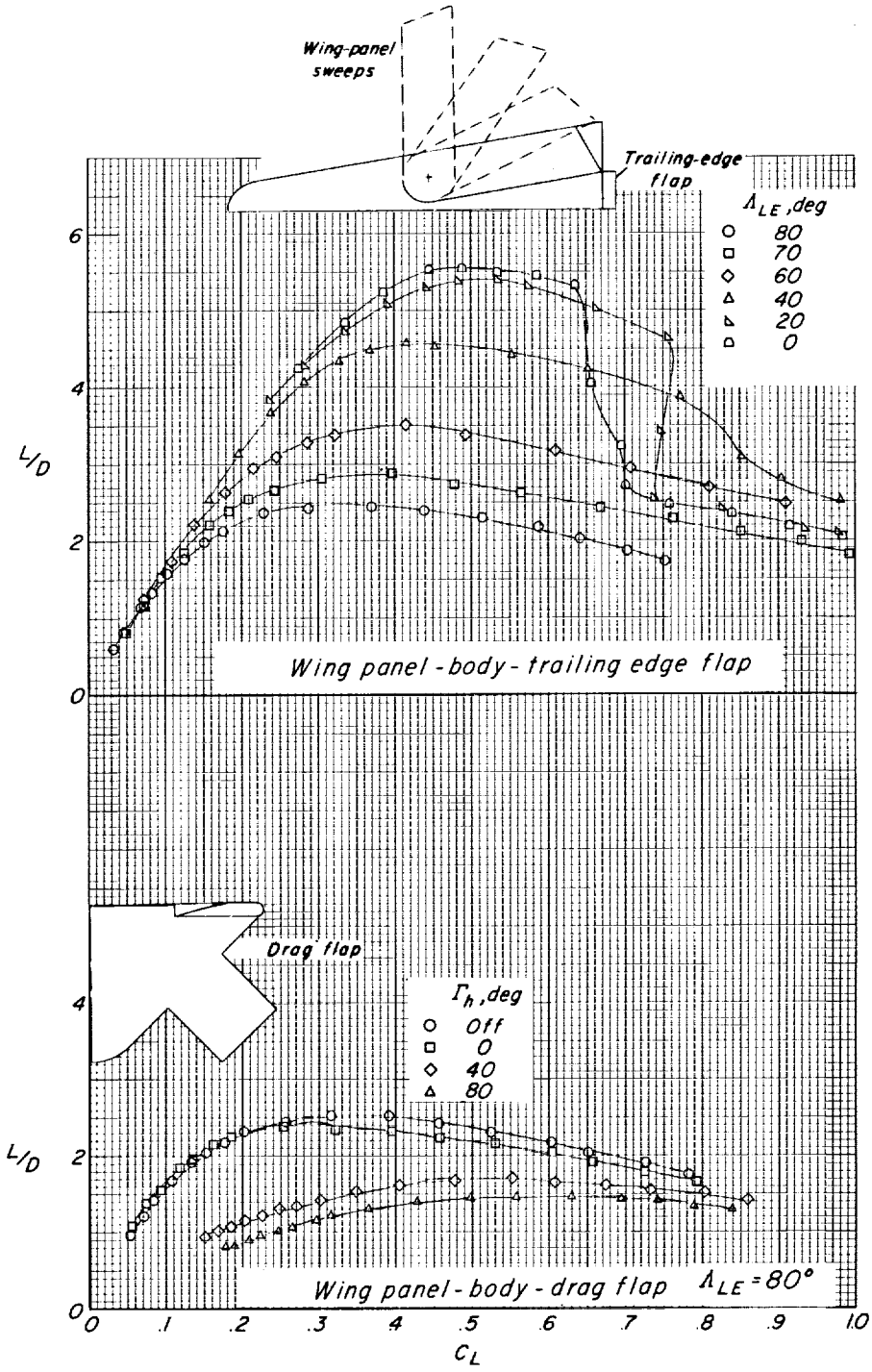

Figure 22.- Lift-drag ratios associated with the configurations having a trailing-edge flap or a drag flap located at the model base. $i_t = 0^o$; M = 0.40.

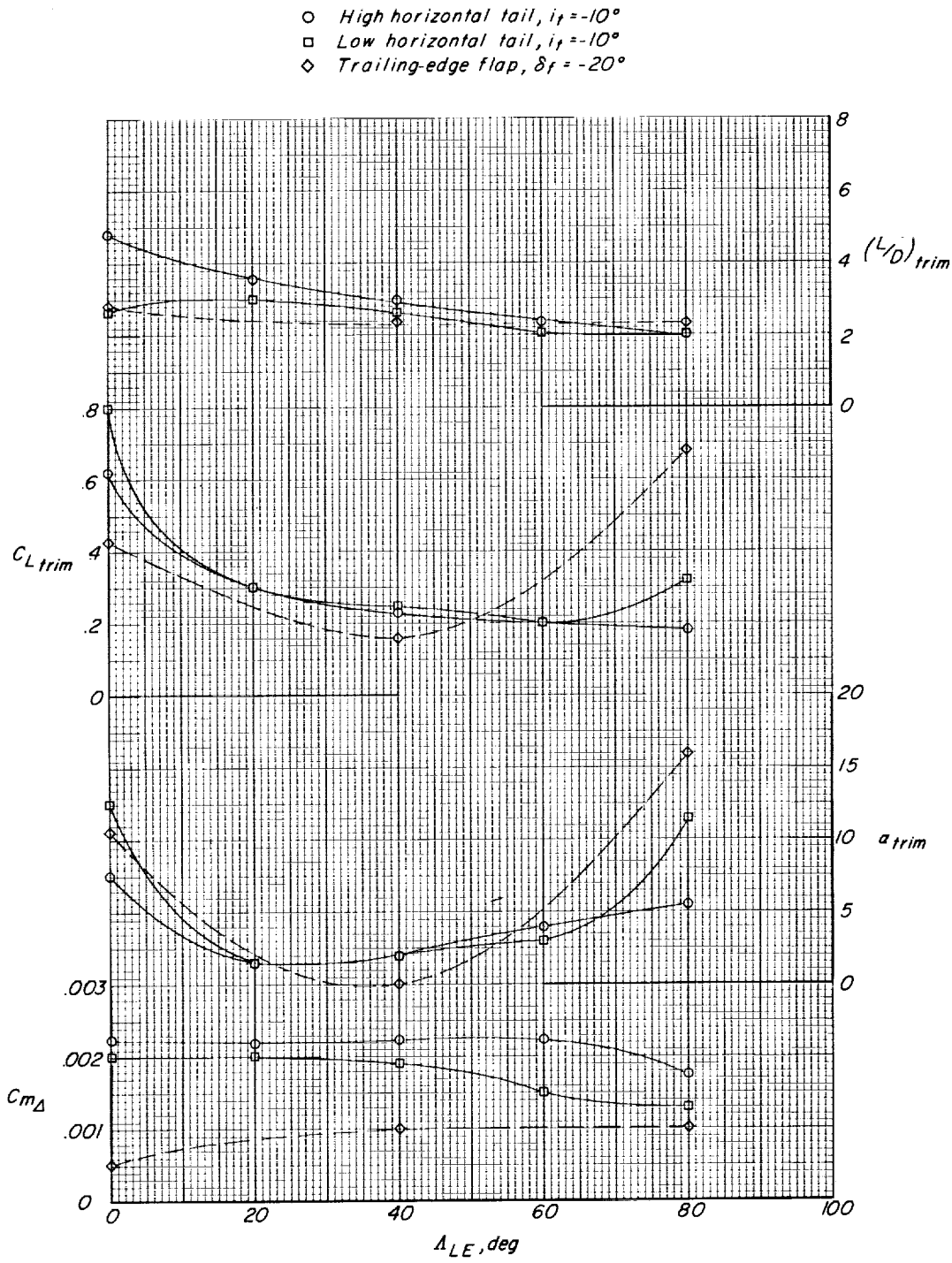

Figure 23.- Variation of longitudinal control parameters associated with the high and low horizontal tails and trailing-edge flap control for various wing-panel sweeps. M = 0.40.

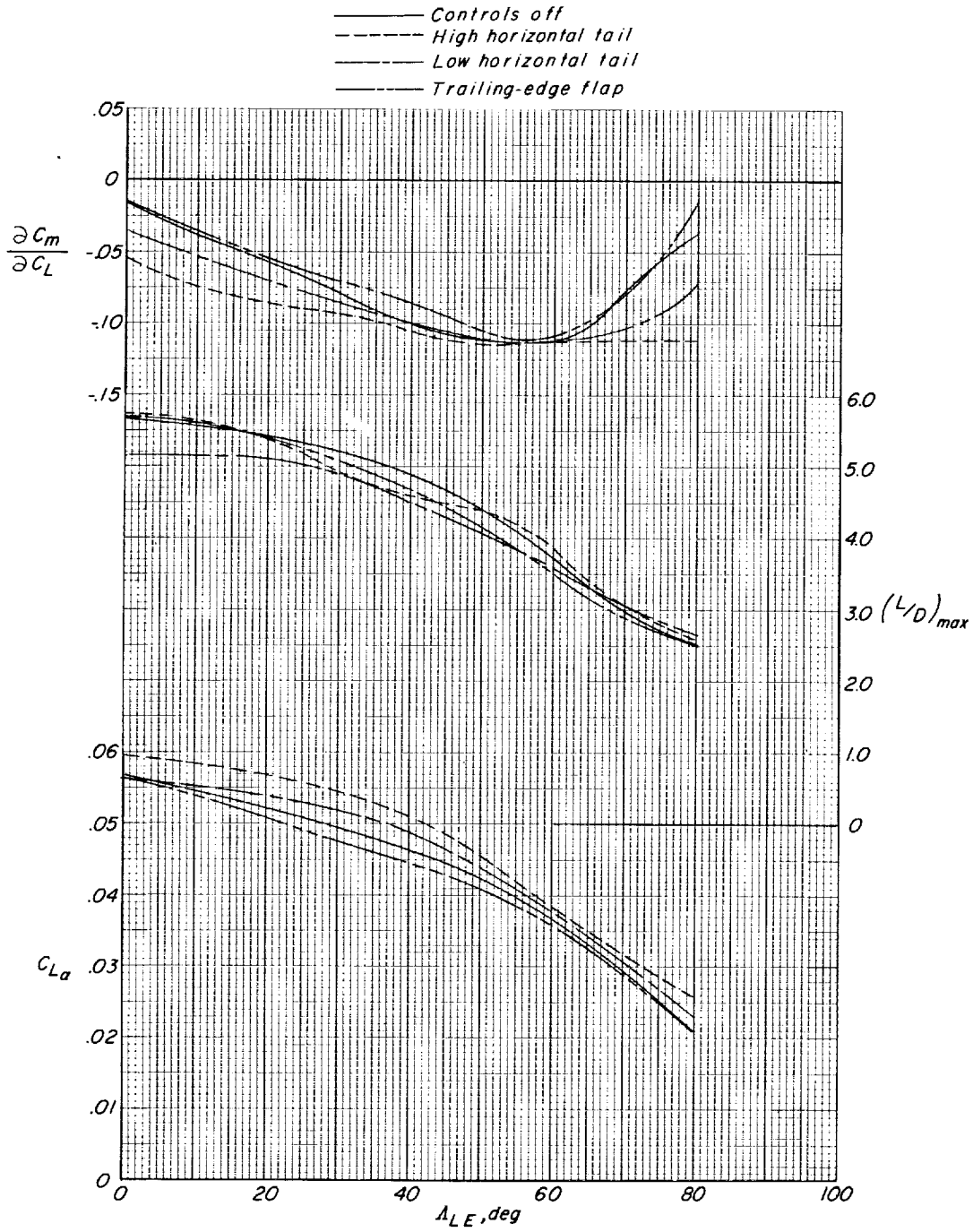

Figure 24.- Summary of the longitudinal aerodynamic parameters C_{L_α}, $(L/D)_{max}$, and $\partial C_m/\partial C_L$ for each wing-panel sweep and for various longitudinal controls. All control surfaces at zero deflection; M = 0.40.